

LOW COMPLEXITY ITERATIVE RECEIVER DESIGN FOR OFDM SYSTEMS

by

VAMADEVAN NAMBOODIRI

A Dissertation submitted to the
Graduate School—New Brunswick
Rutgers, The State University of New Jersey
in partial fulfillment of the requirements

for the degree of

Doctor of Philosophy

Graduate Program in Electrical and Computer Engineering

written under the direction of

Prof. Predrag Spasojević

and approved by

New Brunswick, New Jersey

May, 2012

© 2012

Vamadevan Namboodiri

ALL RIGHTS RESERVED

ABSTRACT OF THE DISSERTATION

Low Complexity Iterative Receiver Design for OFDM Systems

By Vamadevan Namboodiri

Advisor: Prof. Predrag Spasojević

Single Input Single Output (SISO) Orthogonal Frequency Division Multiplexing (OFDM) systems have been adopted in many of the recent wireless communication standards such as European terrestrial broadcast systems based on DVB-H, DVB-T, DVB-T2. For OFDM systems, cyclic prefix of sufficient length makes the receiver design simple in frequency-selective multipath environments. Wireless communication based on Multiple Input Multiple Output (MIMO) systems has also gained popularity due to the potential capacity increases it can provide. MIMO-OFDM based transmission systems can thus provide very high data rates with a relatively simple receiver design and are now adopted widely in recent wireless communication standards such as Long Term Evolution(LTE), LTE Advanced, WiMAX and WiFi. Modern wireless communication applications, both SISO and MIMO, require high data rates in a limited bandwidth at high carrier frequencies and at high levels of mobility. This results in less intercarrier spacing and severe time-varying frequency-selective multipath fading, which breaks the orthogonality of subcarriers and causes intercarrier interference (ICI) in the received signal thus severely impacting the BER performance of the receiver. In the trend of adopting higher carrier frequencies, higher bandwidth and higher mobility, ICI is expected to be more of a limiting factor in mobile OFDM systems. Therefore efficient

receiver design which is fundamental to any communication system is ever more relevant.

Turbo iterative receivers (IR) are based on the observation that performance of the system can be significantly improved if detection and decoding are combined together. They, in general, are found to have superior performance compared to other solutions. However turbo IRs usually suffer from high computational complexity which makes their implementation expensive, requiring a significant amount of silicon area and/or high clock speeds, and may result in high battery power consumption, a scarce resource in mobile applications. Thus the adoption of existing turbo equalization (TE) techniques in single and multiple antenna OFDM systems will act very much against the very same principles which made OFDM popular. Such practical application challenges motivate us, in this dissertation, to propose a new, low complexity IR for SISO and MIMO OFDM systems under time varying frequency selective channel conditions.

Motivated by the classical TE, we first propose a sub-optimal, successive interference cancellation and MAP decoding (SIC-MAP) algorithm for SISO systems wherein we avoid the explicit equalization stage. In SIC-MAP, copies of the received signal on the same and adjacent subcarriers are carefully combined to take advantage of the frequency diversity (on account of the time variations of the channel) while eliminating the interference from the other transmit symbols leveraging the feedback information from the decoder. The resulting system matrix becomes a single column vector which allows an easy MAP decoding. BER performance, computation complexity and convergence behavior of the proposed scheme has been contrasted with two other similar schemes. It has been found that SIC-MAP, while having near identical performance to the competing schemes, can be implemented approximately with only a third of their computational complexity.

Channel estimation and equalization are two crucial components in any coherent receiver. A low complexity Least Squares (LS) based iterative channel estimation scheme using soft feedback information has also been proposed. The proposed scheme is especially suitable when the number of significant channel taps are higher than the number of pilots, a phenomenon that is often encountered in practical receivers.

Subsequent to this, we extend the above detection idea, SIC-MAP, to MIMO systems (SIC-MAP-MIMO). Unlike single antenna systems, even under static multipath channel conditions, the received signal in a MIMO receiver is corrupted by the co-antenna interference (CAI), thus making the detection task more challenging. Extrinsic Information Transfer (EXIT) chart analysis supplemented with numerical simulation results show, as in the case of SISO, that SIC-MAP-MIMO algorithm achieves comparable BER performance to the competing equalization schemes but with even more computational savings than SISO. Besides low complexity, another distinctive advantage of the proposed schemes is their flexibility to trade between performance and implementation complexity. This feature can be handy in mobile applications where the available battery power and system performance can be adjusted dynamically.

Acknowledgements

Thesis Advisors: The work presented in this dissertation started quite accidentally. I was working with my colleagues at our lab tuning the performance of a HDTV receiver. Our office was by the side of highway I-95. While tuning the performance, we often observed blips in the demodulated video stream when trucks passed by. This turned out to be an interesting topic to investigate which finally resulted in this thesis.

Dr. Hong Liu (Iris Liu) is my colleague at Broadcom Yardley PA. It was from her that I got to know about Turbo Equalization. Our initial casual talks on the topic finally fascinated me to look at iterative receivers to solve the above problem. In the past four or five years, we had numerous discussions on this topic, all generally after office hours. I do not remember Iris postponing a discussion because she was tired. Iris never gets tired or irritated, is always positive, allows no compromise in the quality of presentation and is very brilliant. She is remarkable. I sincerely thank her.

It has been a good experience working with Professor Predrag Spasojević. Being a part-time student, I was away from WINLAB most of the time and it was hard for any Professor to accommodate such a student. Prof. Spasojević was always accommodative with his friendly attitude and was very encouraging at times of distress. In our not-so-often but long discussions I have often felt sparks of brilliance in his questions which certainly influenced my thought process. Doubtless to say, his suggestions helped me to improve my writing skills.

Loving Family: Starting from a part-time Masters program, the slow but steady journey of mine for the past 11 years towards PhD is coming to an end at last! My heartfelt thanks goes to my loving wife Suja who was with me all along this journey and the little ones, Sudev, Suvida and Sreevas who joined this journey of mine at various times. Had it not been for my wife's constant support and encouragement at times of distress,

which by the way is part and parcel of a PhD program, I would have long abandoned my studies. An item in the evening prayers for my children was let their dad finish “his PhD”. To them PhD is something that makes their dad out of reach for playing! Their innocent remark “We’ll never ever do a PhD whatever that is!” is thought provoking. I know I owe a great deal to my family for their patience and support.

Friends and Colleagues: Special thanks goes to my friend from WINLAB, Chandrasekharan Raman for his help and encouragement at all levels of my study. He was my point of contact for all these years for any issues starting from LaTeX installation. His ‘always at your service’ attitude and counseling skills are truly amazing.

I am greatly thankful to Troy Schaffer, Associate Technical Director, Broadcom Corporation, USA, for his constant support and encouragement all along my studies and granting permission to publish my work. Vineet Srivastava and Krishna Sankar Madhavan Pillai from Broadcom India need special mention for their support and suggestions at the final stages of this thesis.

Dedication

To Suja, Sudev, Suvida and Sreevas

Table of Contents

Abstract	ii
Acknowledgements	v
Dedication	vii
List of Tables	xi
List of Figures	xii
List of Abbreviations	xiv
1. Introduction	1
1.1. Thesis Outline and Contributions	4
2. Notations and Background	5
2.1. Notations	5
2.2. Background	5
2.2.1. Modeling Doubly Selective Channels for OFDM Systems	5
2.2.2. OFDM Single Input Single Output (SISO) System Model	7
2.2.3. OFDM Multiple Input Multiple Output (MIMO) System Model	10
2.2.4. Symbol Estimation	13
LMMSE Estimator	14
LMMSE Estimator for SISO	14
LMMSE Estimator for MIMO	16
MAP and ML Estimators	17
2.2.5. Channel Estimation	18
2.2.6. Soft Decoding	19
2.2.7. Iterative Equalization/Turbo Equalization	20

2.2.8. Extrinsic Information Transfer (EXIT) Charts	22
3. A Low Complexity Iterative Detection and Decoding Scheme for Single Antenna Mobile OFDM Systems	26
3.1. Introduction	26
3.2. Related Work	27
3.3. System Model	29
3.4. Successive Interference Cancellation Based MAP Receiver (SIC-MAP) .	31
3.5. Creating EXIT Charts	36
3.6. Computational Complexity	37
3.7. Simulation Results	40
3.8. Conclusion	41
3.9. Appendix	42
3.9.1. Derivation of (3.8)	42
3.9.2. Detailed Complexity Computation	45
4. Channel Estimation–SISO Systems	49
4.1. Introduction	49
4.2. Related Work	50
4.3. System Model	53
4.4. Channel Estimation Algorithm	53
4.4.1. The Proposed IR with SIC-MAP	58
4.5. Computational Complexity	59
4.6. Simulation Results	60
4.7. Conclusion	61
5. Low Complexity Turbo Equalization Scheme for Multi Antenna OFDM Systems	63
5.1. Introduction	63
5.2. Related Work	64

5.3. System Model	66
5.4. Successive Interference Cancellation Based MAP Receiver: MIMO (SIC- MAP-MIMO)	68
5.4.1. Formulation of the Proposed MAP Receiver	68
5.4.2. Example	72
5.4.3. Receiver Operation	72
5.4.4. Computation of Residual ICI and CAI	73
5.5. Convergence Analysis Using EXIT Charts	74
5.6. Computational Complexity	75
5.7. Simulation Results	78
5.8. Conclusion	86
5.9. Appendix	87
5.9.1. Derivation of (5.8)	87
5.9.2. Detailed Complexity Computation	88
6. Conclusion and Possible Future Work	94
Delay Mitigation	94
A Complete Receiver	95
EXIT Chart Modifications	95
MIMO Channel Estimation	96
References	97
Curriculum Vitae	106

List of Tables

3.1. Complexity Comparison - Channel Equalization	39
3.2. QPSK Alphabet	44
3.3. TE-MMSE-OND2 – An Efficient Implementation	46
3.4. Complexity - TE-MMSE-OND2	47
3.5. MMSE-OND2 – An Efficient Implementation	48
3.6. Complexity - MMSE-OND2	48
3.7. Complexity - SIC-MAP	48
4.1. Complexity Computation - Channel Estimation.	59
5.1. Complexity Comparison	77
5.2. QPSK Alphabet	87
5.3. TE-MMSE-OND2-MIMO - An Efficient Implementation	89
5.4. Complexity - TE-MMSE-OND2-MIMO	90
5.5. MMSE-OND2-MIMO - An Efficient Implementation	91
5.6. Complexity - MMSE-OND2-MIMO	92
5.7. Complexity - SIC-MAP-MIMO	93

List of Figures

2.1. OFDM Transceiver Block Diagram.	8
2.2. Cyclic Prefix in OFDM.	9
2.3. MIMO OFDM Transceiver.	24
2.4. Iterative Equalization.	25
3.1. OFDM Transceiver.	30
3.2. OFDM Channel Structure.	31
3.3. EXIT Chart Set Up - Decoder	36
3.4. EXIT Chart Set Up - SISO Equalizer	36
3.5. BER Plots- TE-MMSE-OND2, SIC-MAP and TE-BLK2 ($f_d T_s N = 0.2$, $N = 256$, $L = 1$, $\#iter = 1, 3$, $N_h = 30$).	42
3.6. BER Plots - SIC-MAP ($L = 3$), TE-MMSE-OND2 ($L = 1$) and TE- BLK2 ($L = 1$).($f_d T_s N = 0.2$, $N = 256$, $\#iter = 1, 3$, $N_h = 30$).	43
3.7. BER Plots - SIC-MAP, TE-MMSE-OND2 and SIC-MAP($f_d T_s N = 0.1$, $N = 256$, $L = 1$, $\#iter = 1, 6$, $N_h = 30$).	44
3.8. EXIT Charts - TE-MMSE-OND2 and SIC-MAP ($f_d T_s N = 0.2$, $N = 256$, $L = 1$, $\#iter = 3$, $N_h = 30$).	45
4.1. BER Plots - TE-MMSE-OND2 and SIC-MAP Based IRs With Channel Estimation ($N_h \leq P$). ($f_d T_s N = 0.2$, $N = 256$, $L = 1$, $\#iter = 3$, $P = 32$, $N_h = 30$).	61
4.2. BER Plots - TE-MMSE-OND2 and SIC-MAP Based IRs With Channel Estimation ($N_h > P$). ($f_d T_s N = 0.2$, $N = 256$, $L = 1$, $\#iter = 3$, $P = 32$, $N_h = 40$).	61
4.3. Slopes $\alpha_{pre}^j(l)$ and $\alpha_{post}^j(l)$ in Channel Estimation.	62
5.1. MIMO OFDM Transceiver.	67

5.2. MIMO OFDM Channel Structure.	68
5.3. Interference Power (ICI and CAI) across Iterations.	78
5.4. EXIT Curves - I_E vs I_A . ($E_b/N_0 = 10$, $n_T = 2$, $n_R = 2$, $N = 256$, $N_h = 6$, $f_d T_s N = 0.12$, QPSK).	79
5.5. EXIT Curves for Different E_b/N_0 . ($n_T = 2$, $n_R = 2$, $N = 256$, $N_h = 9$, $f_d T_s N = 0.1$, QPSK)	80
5.6. BER Plots - Different # Iterations. SIC-MAP-MIMO (# iter 3, 6), TE- MMSE-OND2-MIMO (# iter 1, 2) and TE-BLK2-MIMO (# iter 1, 2). ($n_T = 2$, $n_R = 2$, $N = 256$, $N_h = 6$, $f_d T_s N = 0.12$, QPSK).	81
5.7. BER Plots. ($f_d T_s N = 0.23$, $n_T = 2$, $n_R = 2$, $N = 256$, $N_h = 6$, # iter = 6, QPSK).	82
5.8. BER Plots. ($f_d T_s N = 0$ (static) $n_T = 2$, $n_R = 2$, $N = 256$, $N_h = 9$, # iter = 8 (SIC-MAP-MIMO), # iter = 4 (TE-MMSE-OND2-MIMO), QPSK).	83
5.9. BER Plots. ($f_d T_s N = 0.1$, $n_T = 2$, $n_R = 2$, $N = 256$, $N_h = 9$, # iter = 8 (SIC-MAP-MIMO), # iter = 4 (TE-MMSE-OND2-MIMO), QPSK). . .	84
5.10. BER Plots. ($f_d T_s N = 0.23$, $n_T = 3$, $n_R = 3$, $N = 256$, $N_h = 6$, # iter = 6, QPSK).	85
5.11. BER Plots. ($f_d T_s N = 0.3$, $n_T = 2$, $n_R = 2$, $N = 256$, $N_h = 9$, # iter = 8 (SIC-MAP-MIMO), # iter = 4 (TE-MMSE-OND2-MIMO), QPSK). .	86

List of Abbreviations

A/D	Analog to Digital Converter
ADSL	Asymmetric digital subscriber Line
ARMA	Auto Regressive Moving Average
AWGN	Additive White Gaussian Noise
BCJR	Bahl, Cocke, Jelinek and Raviv
BEM	Basis Expansion Model
BER	Bit Error Rate
BI/BDI	Bit Interleaver/Deinterleaver
BLUE	Best Linear Unbiased Estimator
BPSK	Binary Phase Shift Keying
CAI	Co-antenna Interference
CCI	Co-Channel Interference
CDMA	Code Division Multiple Access
CFO	Carrier Frequency Offset
CP	Cyclic Prefix
CSI	Channel State Information
D/A	Digital to Analog Converter
DF	Decision Feedback
DFE	DF Equalizer
DFT	Discrete Fourier Transform
DMB-T/H	Digital Multimedia Broadcast-Terrestrial/Handheld
DTV	Digital Television
DVB-T/H	Digital Video Broadcast — Terrestrial/Hand held
EM	Expectation Maximization
EXIT	Extrinsic Information Transfer
FDI	Frequency De-interleaver
FE	Frequency Equalization
FFT	Fast Fourier Transform
FI	Frequency Interleaver
GSM	Global Systems for Mobile Communications
HDTV	High Definition Television
ICI	Inter-Carrier Interference
ICS	Inter Carrier Spacing
IDFT	Inverse Discrete Fourier Transform
IFFT	Inverse Fast Fourier Transform
iid	independent and identically distributed
ISDB-T	Integrated Services Digital Broadcasting-Terrestrial
ISI	Inter-Symbol Interference

LDPC	Low Density Parity Check
LLR	Log Likelihood Ratio
LMMSE	Linear MMSE
LS	Least Squares
LTE	Long Term Evolution
LTI	Linear Time Invariant
LTV	Linear Time Varying
MAI	Multiple access interference
MAP	Maximum A-posteriori Probability
MC	Multicarrier
MCMC	Markov chain Monte Carlo
MIMO	Multiple Input Multiple Output
ML	Maximum Likelihood
MLD	Maximum Likelihood Decoding
MMSE	Minimum MSE
MPEG	Moving Photographic Experts Group
MSE	Mean Square Error
NLMS/LMS	Normalized Least Mean Squares
OFDM	Orthogonal Frequency Division Multiplexing
OFDMA	OFDM Access
PA	Power Amplifier
PAPR	Peak to Average Power Ratio
PDF/pdf	Probability Density Function
PDP	Power Delay Profile
PDSL	power line digital subscriber line
PLC	Power line carrier
QAM	Quadrature Amplitude Modulation
QPSK	Quadrature Phase Shift Keying
RLS	Recursive Least Squares
SC	Single Carrier
SI/SDI	Symbol Inerleaver/Deinterleaver
SIC	Successive Interference Cancellation
SISO	Single Input Single Output/Soft Input Soft Output
SNR	Signal to Noise Ratio
SOVA	Soft Output Viterbi Algorithm
STTrC	Space Time Trellis Codes
TE	Turbo Equalization
TE-BLK2	TE Algorithm Proposed in [1]
TE-MMSE-OND2	TE Algorithm Proposed in [2]
TR-STBC	Time Reversal Space Time Block Codes
VDSL	Very-high-bit-rate digital subscriber line
V-BLAST	Vertical Bell Laboratories Layered Space-Time
WLAN	Wireless Local Area Network
WSS	Wide Sense Stationary
ZF	Zero Forcing
4G	Fourth Generation
2D	Two Dimentional

Chapter 1

Introduction

In this dissertation, we describe the design of a low complexity iterative receiver for coherent Orthogonal Frequency Division Multiplexed (OFDM) systems under time varying frequency selective channels.

At high transmission rates, as the transmitted symbol duration reduces, the dispersive fading of the wireless channel exacerbates inter symbol interference (ISI) if single carrier (SC) modulation such as in Global Systems for Mobile Communications (GSM) is used. In OFDM systems the entire channel is divided into many narrow band sub-channels and symbols are transmitted in these sub-channels in parallel to maintain high-data rate and at the same time to increase the symbol duration to combat ISI. Thus OFDM technology is deployed in many of the modern communication systems that require very high data rates. A detailed survey of OFDM and its wireless applications is given in [3]. OFDM is a special form of Multi Carrier (MC) modulation that dates back to 1960s. Authors of [4, 5], studied the performance and complexity of Multi Carrier modulations and [4] concluded as long back as 1990 that the time for MC has come.

As a result of reflection, diffraction and scattering, the transmitted wireless signal arrives at the receiver via multiple propagation paths with different delays. This gives rise to frequency selectivity (static fading) of the channel. For SC systems, the received signal is the convolution of the transmitted symbols and the impulse response of the channel (in addition to Additive White Gaussian Noise(AWGN)). However, by virtue of Cyclic Prefix (CP) of sufficient length and transform domain processing, the impact of the channel is only a multiplicative distortion at each subcarrier at the receiver for OFDM systems in static channel scenarios. This makes the receiver design for OFDM

systems simple (one-tap equalizer) and is one of the major reasons why OFDM is popular. A practical SISO OFDM receiver design taking various impairments into account is described in [6]. Besides, the flexibility of OFDM provides additional opportunities to use advanced techniques such as adaptive modulation on each subcarrier based on the SNR in accordance with the *water filling* principle [7] to improve transmission efficiency.

The first generation Digital Television (DTV) standard, DVB-T [8] (Digital Video Broadcast - Terrestrial), issued by the consortium DVB, is devised for the broadcast transmission of digital terrestrial television in Europe over 8MHz channels. It employs single antenna OFDM systems. These systems transmit compressed digital audio, video and other data in an MPEG transport stream. The actual transported data rate can range from about 5 to 32 Mbit/s depending on a number of coding and modulation parameters. DVB-T has been further developed into newer standards, all OFDM based, such as DVB-H (DVB - Handheld), now in operation, and DVB-T2, which was recently finalized. DVB-H is a technical specification for bringing broadcast services to mobile handsets. DVB-T2 is an abbreviation for Digital Video Broadcasting Second Generation Terrestrial. ISDB-T (Integrated Services Digital Broadcasting-Terrestrial) system [9] deployed in Japan is yet another example for OFDM based DTV transmission systems. DMB-T/H (Digital Multimedia Broadcast-Terrestrial/Handheld) is China's new DTV standard. It has both SC and OFDM options. Asymmetric digital subscriber line (ADSL), very-high-bit-rate digital subscriber line (VDSL) and power line carrier (PLC) also known as power line digital subscriber line (PDSL) are some of the examples for OFDM deployment over wired media.

OFDM systems are more sensitive to time varying impairments. It can come from either the carrier frequency offset(CFO) caused by the mismatches of frequencies between the oscillators at the transmitter and the receiver or from the Doppler spread at the receiver signal. Changes in the relative positions of different objects in the environment, the transmitter and/or the receiver with time give rise to Doppler spread. The effect of CFO is relatively easy to counteract. However, in time and frequency selective or doubly selective fading due to Doppler spread, even with perfect synchronization,

the orthogonality of different subcarriers in OFDM signal is lost and this leads to inter-carrier interference (ICI). ICI makes the symbol detection difficult and thus adversely affect the performance of OFDM systems. At relatively low data rate mobile applications, time selectivity of the channel due to Doppler spread can be ignored making the OFDM receiver design simple. Future wireless applications are expected to operate at high carrier frequencies, at high levels of mobility and at high data rates where special detectors have to be designed to counteract the doubly selective nature of the channel. Battery life is one of the prime considerations in mobile communication systems. Efficient detector design which use less silicon area and power is always a challenging problem.

Wireless communication based on MIMO systems has gained popularity due to the potential capacity increases it can provide [10, 11, 12, 13] . It is proved in [14] that, compared with a single input single output (SISO) system, a MIMO system can improve the capacity by a factor of the minimum number of the transmit and receive antennas for flat fading or narrow-band channels. MIMO-OFDM based transmission systems can thus provide very high data rates with a relatively simple receiver design and are now adopted widely in recent wireless communication standards [15] such as Long Term Evolution(LTE), LTE Advanced [16, 17, 18], WiMAX [19, 20, 21] and WiFi [22, 23]. An overview of MIMO wireless technology covering channel models, performance limits, coding and transceiver design is given in [24, 13]. In single user mobile MIMO systems, in addition to ICI, the received signal is corrupted by Co Antenna Interference (CAI). CAI is relatively high compared to ICI even under high Doppler spread. Efficient MIMO detector design is thus harder to tackle.

Turbo equalization (TE) based iterative detection schemes, where the detection process takes advantage of the soft feedback information obtained from the decoder have been found to perform better compared to the non-iterative detection schemes in general. However, these schemes are saddled with high computational complexity. We first propose a new low complexity iterative detection scheme based on successive interference cancellation and MAP decoding (SIC-MAP) algorithm for SISO OFDM systems and later extend it to MIMO systems. In SIC-MAP, copies of the received signal on

the same and adjacent subcarriers are carefully combined to take advantage of the frequency diversity (on account of the time variations of the channel) while eliminating the interference from the other transmit symbols leveraging the feedback information from the decoder. BER performance, computation complexity and convergence behavior of the proposed scheme has been contrasted with other similar schemes. The computational complexity of the proposed scheme is comparable to non-iterative schemes, yet, the performance has been found to be on par with iterative schemes. Channel estimation and equalization are two crucial components in any coherent receiver. A low complexity Least Squares (LS) based iterative channel estimation method using soft feedback information has thus also been proposed.

1.1 Thesis Outline and Contributions

Notations used in this dissertation and the required background material are introduced in Chapter 2. The proposed detector is mathematically formulated at first for SISO systems in Chapter 3, its performance and computational complexity are compared with two similar iterative schemes. We briefly introduce EXIT chart based convergence analysis of the proposed scheme, however, a detailed discussion on the topic is postponed until Chapter 5. In Chapter 4, we propose a low complexity iterative channel estimation scheme that suites the proposed detection technique for SISO systems. The channel estimator performance is compared with different detection schemes. In Chapter 5, we extend the detector design to MIMO systems. Convergence characteristics of the proposed detector is discussed in detail. In each chapter, we provide a survey of the recent research on the topic. Finally in Chapter 6, we discuss the possible future direction to enhance the proposed iterative receiver to a commercially viable receiver.

Chapter 2

Notations and Background

2.1 Notations

We use the following notations in our formulation throughout this thesis. $(\cdot)^t$ denotes transpose; $(\cdot)^H$ denotes conjugate transpose (Hermitian); \otimes is the Kronecker product; $\{a\}$ denotes a set with elements $\{a(0), a(1), \dots\}$; \mathbf{F} for normalized N point Discrete Fourier Transform (DFT), where $\mathbf{F}_{k,l} := (1/\sqrt{N})e^{-j2\pi kl/N}$; \mathbf{I} is the identity matrix; \mathbf{i}_k is the k^{th} column of \mathbf{I} ; $\mathbf{0}_{n_R \times n_T}$ is the null matrix of size $n_R \times n_T$; $*$ denotes convolution; $\|\cdot\|$ for l_2 -norm; $\lceil \cdot \rceil$ is the ceiling of a function; modulo- N is denoted by $\langle \cdot \rangle_N$; $Re(\cdot)$ and $Im(\cdot)$ for the real and imaginary parts. $diag(\boldsymbol{\nu}_{\mathbf{x}})$ is the diagonal matrix with vector $\boldsymbol{\nu}_{\mathbf{x}}$ in the main diagonal. Expectation is denoted by $E\{\cdot\}$. Both \times and \cdot are used to denote multiplication. Bold lower case letters, e.g., \mathbf{x} , denote vectors, or continuous random variables (RV) as the case may be and bold upper case letters, e.g., \mathbf{X} , denote matrices or discrete RVs. Covariance is denoted by either $\text{cov}(\mathbf{b}, \mathbf{c})$ or $\boldsymbol{\Sigma}_{bc}$ and is defined as $E\{\mathbf{b}\mathbf{c}^H\} - E\{\mathbf{b}\}E\{\mathbf{c}^H\}$.

2.2 Background

Before we delve into the design of the proposed iterative receiver, we introduce the major components of an iterative receiver, the knowledge of which is critical in understanding the proposed receiver design.

2.2.1 Modeling Doubly Selective Channels for OFDM Systems

Let the linear time varying (LTV) channel taps in the discrete time domain be represented as $h(i, l)$. $h(i, l)$ is the l^{th} time-varying multipath coefficient at the i^{th} time

instant. Fading coefficients for different paths are assumed to be statistically independent. The l^{th} channel tap can be characterized as a band limited wide-sense stationary random process with a time autocorrelation function (wide-sense stationary uncorrelated scattering model) given by [25],

$$E\{h(m, l)h(n, l)^*\} = \alpha_l \mathcal{J}_0(2\pi(m - n)f_d T_s) \quad (2.1)$$

where α_l is the average power of the l^{th} path given by $E\{|h(i, l)|^2\}$ (expectation is taken across the time index i), $\mathcal{J}_0(\cdot)$ is the zeroth-order Bessel function of the first kind, m and n are integers, T_s is the sampling interval and f_d is the maximum Doppler frequency given by

$$f_d = \frac{v}{c} f_c \cos(\theta_d). \quad (2.2)$$

Here v is the vehicle speed, c is the velocity of light, f_c is the carrier frequency and θ_d is the scattering angle. When a sinusoidal tone of frequency f_c is transmitted, the received signal spectrum, called the Doppler spectrum, will have components in the range $f_c - f_d$ to $f_c + f_d$. The amount of spectral broadening depends on f_d . Inverse of the Doppler shift is proportional to coherence time [26]. It is a measure of the time duration over which the channel impulse response is essentially invariant, in other words, it is the time duration over which two received signals have a strong potential for amplitude correlation.

The discrete time delay spread of a wireless channel is defined as

$$\tau_{spread} = \sqrt{\frac{\sum_{l=0}^{N_h-1} |\sigma_l|^2 (\tau_l - \bar{\tau})^2}{\sum_{l=0}^{N_h-1} |\sigma_l|^2}} \quad (2.3)$$

where N_h is the number of separately resolvable multipath components in the sampled domain, $\tau_l = l \times T_s$ is the delay of the l^{th} multipath in the sampled domain,

$$|\sigma_l|^2 = E\{|h(i, l)|^2\} \quad (2.4)$$

($E\{h(i, l)\} = 0$) and

$$\bar{\tau} = \frac{\sum_{l=0}^{N_h-1} |\sigma_l|^2 \tau_l}{\sum_{l=0}^{N_h-1} |\sigma_l|^2}. \quad (2.5)$$

Coherence bandwidth is the range of frequencies over which the channel passes all the spectral components with approximately equal gain. It is inversely proportional to the delay spread [26].

2.2.2 OFDM Single Input Single Output (SISO) System Model

The front end of an OFDM transceiver model is described in Fig. 2.1. A set of N QAM “frequency domain” symbols coming from the symbol mapper $\{x_n(k)\}$ is collected together to form the n^{th} OFDM symbol. This is converted into “discrete time-domain” samples that are ready for digital to analog (D/A) conversion and subsequent transmission, $\{z_n(i)\}$, by a) performing an N point inverse discrete Fourier transform (IDFT), b) converting to a serial stream and c) pre-pending a cyclic prefix (CP) which is also called guard interval of length N_p . Note that we consider only baseband transmission here. As shown in Fig. 2.2 and explained in the sequel, CP is critical for OFDM systems to avoid intersymbol interference (ISI) caused by the delay spread of the channel. With the CP, the length of the OFDM symbol is $N_p + N$. A D/A converts these digital samples into analog waveform, $z_n(t)$, of duration $T = T_g + T_s$ where T_g is the duration of the CP and T_s is the OFDM symbol duration. The analog signal $z_n(t)$ can be represented as,

$$z_n(t) = \sum_{k=0}^{N-1} x_n(k) e^{j2\pi k \Delta f t}, -T_g \leq t \leq T_s \quad (2.6)$$

where Δf is the subcarrier spacing. It is obvious that $z_n(t) = z_n(t + T_s)$ for $-T_g \leq t \leq 0$. In order to demodulate the OFDM signal, the symbol duration should be long enough such that $T_s \Delta f = 1$. This is called the orthogonal condition since it ensures that $e^{j2\pi k \Delta f t}$ are orthogonal to each other for different k . Note that $z_n(i)$ can be expressed mathematically as a sampled sequence of $z_n(t)$ at T_s/N intervals as below.

$$\begin{aligned} z_n(i) = z_n\left(i \frac{T_s}{N}\right) &= \sum_{k=0}^{N-1} x_n(k) e^{j2\pi k \Delta f i \frac{T_s}{N}} \\ &= \sum_{k=0}^{N-1} x_n(k) e^{j \frac{2\pi i k}{N}} \end{aligned} \quad (2.7)$$

which, as observed earlier, is the N point IDFT of the transmitted signal.

In this thesis, unless otherwise mentioned, we assume the maximum delay spread in sampled domain $N_h = \tau_{max}/T_s$ to be such that $N_h \leq N_p$, the length of the CP. Note that τ_{max} is the maximum delay spread in the continuous time domain. Therefore for any given OFDM symbol, ISI due to the contributions from the past or future OFDM symbols is absent. At any given time, we deal only with the present OFDM symbol

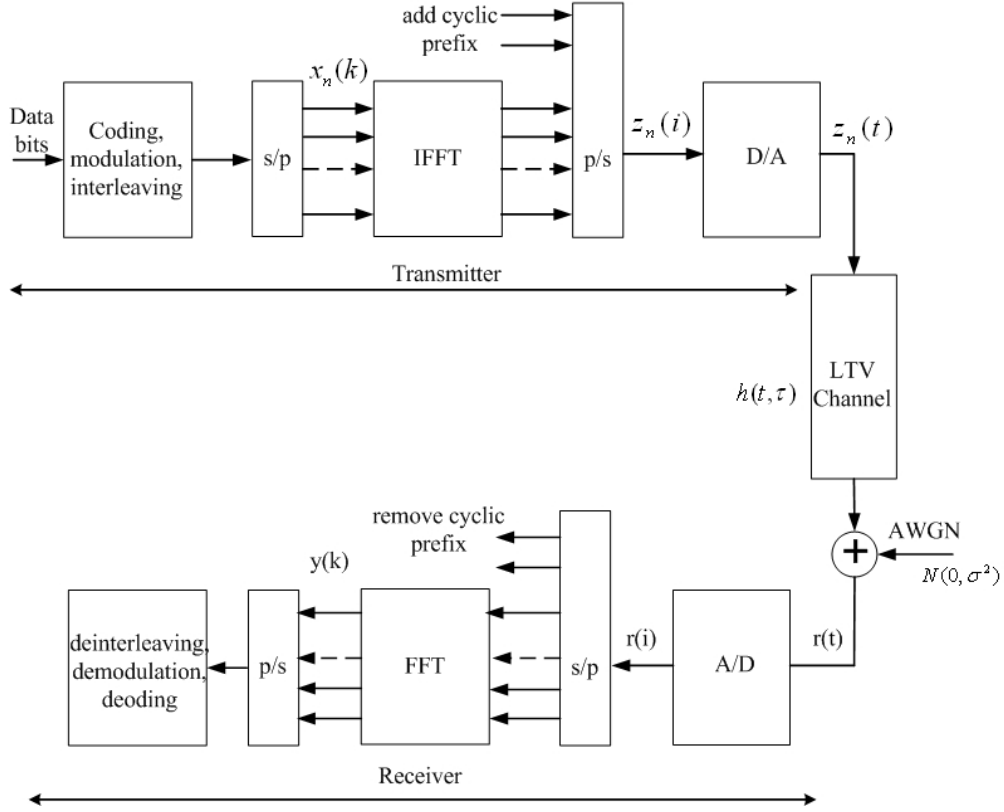


Figure 2.1: OFDM Transceiver Block Diagram.

and can therefore discard the subscript n that denote the OFDM symbol index in the discussions below. The received signal at the input to the analog to digital converter (A/D) is $r(t)$. As demonstrated in Fig. 2.2, $r(t)$ consists only the signal component from the n^{th} OFDM block when $\tau_l \leq t \leq \tau_u$, where $\tau_l = -T_g + \tau_M$, $\tau_u = T_s + \tau_m$, $\tau_M = \max_l \{\tau_l\}$ and $\tau_m = \min_l \{\tau_l\}$; otherwise $r(t)$ will contain signals from other OFDM blocks.

We assume perfect carrier, symbol and sample synchronization at the receiver. The received samples after digitization can be represented as,

$$r(i) = \sum_{l=0}^{N_h-1} h(i, l)z(i-l) + n(i), 0 \leq i < N, \quad (2.8)$$

where $\{n(i)\}$ are samples of AWGN with zero mean and variance σ^2 .

After the CP removal, N of these samples that belong to the same OFDM symbol are collected together to form the received vector \mathbf{r} , corresponding to a single OFDM

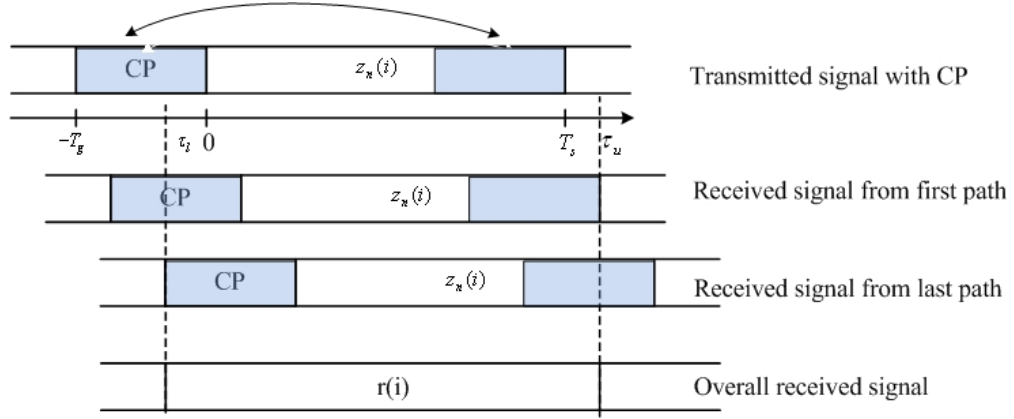


Figure 2.2: Cyclic Prefix in OFDM.

symbol. Defining $\mathbf{r} := [r(0), r(1), \dots, r(N-1)]^t$, it can be written as,

$$\mathbf{r} = \mathbf{\Xi} \mathbf{z} + \boldsymbol{\psi} \quad (2.9)$$

where $\mathbf{\Xi}$ is the time varying system matrix determined by the channel estimator and is given in (2.10). $\boldsymbol{\psi} := [n(0), n(1), \dots, n(N-1)]^t$. The circulant like (A matrix is circulant if the $(n+1)^{th}$ row is a right circular shift of the n^{th} row. The term ‘circulant like’ is used here because the channel taps do not change significantly between the n^{th} and $(n+1)^{th}$ instants) form of the $\mathbf{\Xi}$ is resulted from the CP in the system.

$$\mathbf{\Xi} := \begin{bmatrix} h(0,0) & \dots & h(0, N_h - 1) & \dots & h(0,1) \\ h(1,1) & h(1,0) & \dots & \dots & h(1,2) \\ \dots & \dots & \dots & \dots & \dots \\ 0 & \dots & h(N-1, N_h - 1) & \dots & h(N-1, 0) \end{bmatrix} \quad (2.10)$$

These “time domain” samples are presented to a DFT processor which, in turn, outputs N “frequency domain” samples, $\{y(k)\}$. Taking DFT on both sides of (2.9),

$$\begin{aligned} \mathbf{y} &= \mathbf{F} \mathbf{r} \\ &= \mathbf{F} \mathbf{\Xi} \mathbf{z} + \mathbf{F} \boldsymbol{\psi} \\ &= \mathbf{F} \mathbf{\Xi} \mathbf{F}^H \mathbf{x} + \mathbf{w} \\ &= \mathbf{H} \mathbf{x} + \mathbf{w} \end{aligned} \quad (2.11)$$

where

$$\mathbf{H} := \mathbf{F}\mathbf{\Xi}\mathbf{F}^H,$$

$$\mathbf{y} := [y(0), y(1), \dots, y(N-1)]^t,$$

$$\mathbf{x} := [x(0), x(1), \dots, x(N-1)]^t,$$

and

$$\mathbf{w} = \mathbf{F}\boldsymbol{\psi}.$$

Note that \mathbf{w} is wide sense stationary (WSS) with mean and Covariance same as that of $\boldsymbol{\psi}$ as \mathbf{F} is unitary. Here \mathbf{x} is the transmitted OFDM symbol, \mathbf{H} is the channel matrix in frequency domain and \mathbf{y} is the received OFDM symbol.

2.2.3 OFDM Multiple Input Multiple Output (MIMO) System Model

The front end of a MIMO OFDM transceiver system with n_T transmit and n_R receive antennas used in this thesis is given in Fig. 2.3. We assume that $n_T \leq n_R$. As in the case of SISO, the symbol mapper modulates the input bits into QAM symbols. A set of N of these coded QAM “frequency domain” symbols is collected to form an OFDM symbol. The demultiplexer collects n_T OFDM symbols (an OFDM symbol frame) and sends each symbol, $\{\mathbf{x}_q\}$, to one of the n_T transmit paths. They are then converted into “discrete time-domain” samples, $\{\mathbf{z}_q\}$, by performing N point IDFT. Cyclic prefix (CP) of length $N_p \leq N$, is added to each of these symbols. They are then simultaneously transmitted from n_T transmit antennas. For brevity, no A/D or D/A are shown in the figure and no equations in the analog domain are presented here. Transmit and receive antennas are assumed to be placed sufficiently far apart so that the $n_T \cdot n_R$ multipath channels are independent. Further, these channels are assumed to be both frequency and time selective and are modeled as a linear time varying (LTV) system with a discrete impulse response $h_{pq}(i, l)$ which is defined as the time i response to an impulse at time $i - l$ for the wireless channel from the q^{th} transmit antenna to the p^{th} receive antenna. Static multipath channel conditions are treated as a special case of the above general formulation. At the receiver, the CP removed OFDM data from each receive antenna is converted back to the “frequency domain” by performing N point

DFT. Assuming that maximum channel delay spread in sampled domain $N_h \leq N_p$, the received samples on any of the p receive antennas in base band under perfect carrier, symbol and sample synchronization can be represented as

$$r_p(i) = \sum_{q=1}^{q=n_T} \sum_{l=0}^{l=N_h-1} h_{pq}(i, l) z_q(i - l) + n_p(i), 0 \leq i < N, \quad (2.12)$$

where $\{n_p(i)\}$ are noise (AWGN) samples on the p^{th} receive antenna with zero mean and variance σ^2 (we assume equal noise power on all receive antennas). The condition $N_h \leq N_p$ ensures that $r_p(i)$ contains contributions only from the currently transmitted OFDM symbol frame.

Signal at the input to the MIMO receiver at the i^{th} time instant,

$$\mathbf{r}^{(\mathbf{m})}(i) := [r_1(i), r_2(i), \dots, r_{n_R}(i)]^t,$$

can be expressed as

$$\mathbf{r}^{(\mathbf{m})}(i) = \sum_{l=0}^{l=N_h-1} \mathcal{H}^{(m)}(i, l) \mathbf{z}^{(\mathbf{m})}(i - l) + \mathbf{n}^{(\mathbf{m})}(i), 0 \leq i < N, \quad (2.13)$$

where

$$\mathcal{H}^{(m)}(i, l) := \begin{bmatrix} h_{11}(i, l) & h_{12}(i, l) & \dots & h_{1n_T}(i, l) \\ h_{21}(i, l) & h_{22}(i, l) & \dots & h_{2n_T}(i, l) \\ \dots & \dots & \dots & \dots \\ h_{n_R1}(i, l) & h_{n_R2}(i, l) & \dots & h_{n_Rn_T}(i, l) \end{bmatrix},$$

$$\mathbf{z}^{(\mathbf{m})}(i) := [z_1(i), z_2(i), \dots, z_{n_T}(i)]^t$$

and

$$\mathbf{n}^{(\mathbf{m})}(i) := [n_1(i), n_2(i), \dots, n_{n_R}(i)]^t.$$

Over a time window of N sample duration, (2.13) can be expressed in matrix form as

$$\mathbf{r}^{(\mathbf{m})} = \mathbf{\Xi}^{(\mathbf{m})} \mathbf{z}^{(\mathbf{m})} + \mathbf{\psi}^{(\mathbf{m})}, \quad (2.14)$$

where

$$\mathbf{r}^{(\mathbf{m})} := [\mathbf{r}^{(\mathbf{m})^t}(0), \mathbf{r}^{(\mathbf{m})^t}(1), \dots, \mathbf{r}^{(\mathbf{m})^t}(N-1)]^t \in \mathcal{C}^{N \cdot n_R},$$

$$\mathbf{z}^{(\mathbf{m})} := [\mathbf{z}^{(\mathbf{m})^t}(0), \mathbf{z}^{(\mathbf{m})^t}(1), \dots, \mathbf{z}^{(\mathbf{m})^t}(N-1)]^t \in \mathcal{C}^{N \cdot n_T},$$

$$\boldsymbol{\psi}^{(m)} := [\mathbf{n}^{(\mathbf{m})^t}(0), \mathbf{n}^{(\mathbf{m})^t}(1), \dots, \mathbf{n}^{(\mathbf{m})^t}(N-1)]^t \in \mathcal{C}^{N \cdot n_R}$$

and

$$\boldsymbol{\Xi}^{(\mathbf{m})} \in \mathcal{C}^{N \cdot n_R \times N \cdot n_T}$$

is the time varying system matrix given in (2.15).

$$\boldsymbol{\Xi}^{(\mathbf{m})} := \begin{bmatrix} \mathcal{H}^{(m)}(0,0) & \mathbf{0}_{n_R \times n_T} & \dots & \mathcal{H}^{(m)}(0, N_h - 1) & \dots & \mathcal{H}^{(m)}(0,1) \\ \mathcal{H}^{(m)}(1,1) & \mathcal{H}^{(m)}(1,0) & \mathbf{0}_{n_R \times n_T} & \dots & \dots & \mathcal{H}^{(m)}(1,2) \\ \dots & \dots & \dots & \dots & \dots & \dots \\ \mathbf{0}_{n_R \times n_T} & \dots & \mathcal{H}^{(m)}(N-1, N_h - 1) & \dots & \dots & \mathcal{H}^{(m)}(N-1,0) \end{bmatrix} \quad (2.15)$$

N samples from the same OFDM symbol from each of the n_R receive antennas (a total of $N \cdot n_R$ samples) are presented to a FFT processor. It performs N point FFT on each of the n_R group of samples (n_R FFTs of size N) and outputs $N \cdot n_R$ “frequency domain” samples. This operation can be represented mathematically as follows:

$$\begin{aligned} \mathbf{y}^{(\mathbf{m})} &= \mathbf{Q}^{(Rx)} \mathbf{r}^{(\mathbf{m})} = \mathbf{Q}^{(Rx)} \boldsymbol{\Xi}^{(\mathbf{m})} \mathbf{z}^{(\mathbf{m})} + \mathbf{Q}^{(Rx)} \boldsymbol{\psi}^{(m)} \\ &= \mathbf{Q}^{(Rx)} \boldsymbol{\Xi}^{(\mathbf{m})} (\mathbf{Q}^{(Tx)})^H \mathbf{x}^{(\mathbf{m})} + \mathbf{w}^{(\mathbf{m})} \\ &= \mathbf{H}^{(\mathbf{m})} \mathbf{x}^{(\mathbf{m})} + \mathbf{w}^{(\mathbf{m})}, \end{aligned} \quad (2.16)$$

where

$$\mathbf{Q}^{(Tx)} = \mathbf{F} \otimes \mathbf{I}_{n_T},$$

$$\mathbf{Q}^{(Rx)} = \mathbf{F} \otimes \mathbf{I}_{n_R},$$

$$\mathbf{H}^{(\mathbf{m})} = \mathbf{Q}^{(Rx)} \boldsymbol{\Xi}^{(\mathbf{m})} \mathbf{Q}^{(Tx)H},$$

$$\mathbf{z}^{(\mathbf{m})} = \mathbf{Q}^{(Tx)H} \mathbf{x}^{(\mathbf{m})},$$

$$\mathbf{y}^{(\mathbf{m})} := [(\mathbf{y}^{(\mathbf{m})})^t(0), (\mathbf{y}^{(\mathbf{m})})^t(1), \dots, (\mathbf{y}^{(\mathbf{m})})^t(N-1)]^t, \mathbf{y}^{(\mathbf{m})}(k) := [y_1(k), y_2(k), \dots, y_{n_R}(k)]^t,$$

$$\mathbf{x}^{(\mathbf{m})} := [\mathbf{x}^{(\mathbf{m})^t}(0), \mathbf{x}^{(\mathbf{m})^t}(1), \dots, \mathbf{x}^{(\mathbf{m})^t}(N-1)]^t,$$

$$\mathbf{x}^{(\mathbf{m})}(k) := [x_1(k), x_2(k), \dots, x_{n_T}(k)]^t$$

and

$$\mathbf{w}^{(\mathbf{m})} = \mathbf{Q}^{(Rx)} \boldsymbol{\psi}^{(m)}.$$

Note that each element of $\mathbf{H}^{(\mathbf{m})}$ is matrix with entries as below.

$$\mathbf{H}^{(\mathbf{m})}(m, n) := \begin{bmatrix} H_{11}(m, n) & H_{12}(m, n) & \dots & H_{1n_T}(m, n) \\ H_{21}(m, n) & H_{22}(m, n) & \dots & H_{2n_T}(m, n) \\ \dots & \dots & \dots & \dots \\ H_{n_R1}(m, n) & H_{n_R2}(m, n) & \dots & H_{n_Rn_T}(m, n) \end{bmatrix}$$

and each of those elements can be written as,

$$H_{pq}(n, n) = \frac{1}{N} \sum_{i=0}^{N-1} \sum_{l=0}^{N_h-1} h_{pq}(i, l) e^{-j2\pi ln/N} \quad (2.17)$$

and

$$H_{pq}(m, n) = \frac{1}{N} \sum_{l=0}^{N_h-1} \sum_{i=0}^{N-1} h_{pq}(i, l) e^{-j2\pi(m-n)i/N} e^{-j2\pi ln/N}, m \neq n. \quad (2.18)$$

$\mathbf{w}^{(\mathbf{m})}$ is wide sense stationary (WSS) with same mean and covariance as that of $\boldsymbol{\psi}^{(m)}$, since \mathbf{F} is unitary. The channel is assumed to be not known at the transmitter. Therefore, transmit symbols are selected from an independent and identically distributed (iid) ensemble and transmitted with equal power to achieve maximum rate [27]. Total transmit power is assumed to be unity; thus, each antenna transmits at a power of $1/n_T$.

2.2.4 Symbol Estimation

In this section we derive Linear MMSE Estimator and MAP estimator from the common frame work of Bayesian estimation. Bayesian estimation assumes that the observations \mathbf{y} are drawn according to the conditional probability density function (pdf) $p(\mathbf{y}|\mathbf{x} = x)$ and the parameter x is the realization of a random variable \mathbf{x} with the prior distribution $p(x)$. We assume that $C(a, x)$ is the cost of estimating a true value of x as a . Given such a function C , we can then associate with an estimator $\hat{x}(y)$ a conditional risk or cost averaged over \mathbf{y} for all the values of x ; i.e., we define

$$C(\hat{x}(y), x) := E_x\{C(\hat{x}(\mathbf{y}), x)\}.$$

The design goal is to find an estimator that minimizes this cost, given the observations \mathbf{y} . This is the Bayes estimate of x [28]. Two different cost functions $C(\hat{x}, x)$, in general,

are applied to construct two different estimator functions. The first in the sequel corresponds to the MMSE estimator and second corresponds to the MAP estimator.

LMMSE Estimator

Here the cost function is the squared euclidean distance between the estimate \hat{x} and x , i.e.,

$$C(\hat{x}, x) = |x - \hat{x}|^2.$$

Taking the expectation with respect to $p(\mathbf{x}|\mathbf{y} = y)$ yields the posterior cost; i.e.,

$$C_{post}(\hat{x}(\mathbf{y}), x) = E(|\mathbf{x} - \hat{x}(\mathbf{y})|^2 | \mathbf{y}).$$

Let $\hat{x} := h(\mathbf{y})$ be the estimator that minimizes this. After some algebra [28], we get \hat{x} , the least mean square estimator of \mathbf{x} given \mathbf{y} , as the conditional expectation of \mathbf{x} given \mathbf{y} . i.e.,

$$\begin{aligned} \hat{x} := h(\mathbf{y}) &= E\{\mathbf{x}|\mathbf{y} = y\} \\ &= \int_{S_x} x f_{\mathbf{x}|\mathbf{y}}(x|y) dx \end{aligned} \quad (2.19)$$

where S_x denotes the domain of the random variable \mathbf{x} . Such conditional expectations are generally hard to evaluate in closed form. Due to the difficulty in evaluating $E(\mathbf{x}|\mathbf{y})$, it is common practice to restrict the choice of $h(\cdot)$ to the sub class of *affine* functions of \mathbf{y} , i.e., to the functions of the form

$$h(\mathbf{y}) = \mathbf{K}\mathbf{y} + \mathbf{b}$$

for some matrix \mathbf{K} and some vector \mathbf{b} . The affine estimator/Linear MMSE estimator can be computed to be [29]

$$\hat{x} = h(\mathbf{y}) = E(\mathbf{x}) + \text{cov}(\mathbf{x}, \mathbf{y})\text{cov}(\mathbf{y}, \mathbf{y})^{-1} \{\mathbf{y} - E(\mathbf{y})\} \quad (2.20)$$

LMMSE Estimator for SISO

For the SISO system described by (2.11), $\hat{x}(k)$, the MMSE linear estimate of $x(k)$ given \mathbf{y} is

$$\hat{x}(k) = E\{x(k)\} + \text{cov}(x(k), \mathbf{y})\text{cov}(\mathbf{y}, \mathbf{y})^{-1}(\mathbf{y} - E\{\mathbf{y}\}) \quad (2.21)$$

Here,

$$\begin{aligned}\text{cov}(\mathbf{y}, \mathbf{y}) = \mathbf{\Sigma}_{yy} = E\{\mathbf{y}\mathbf{y}^H\} &= E\{(\mathbf{H}\mathbf{x} + \mathbf{w})(\mathbf{H}\mathbf{x} + \mathbf{w})^H\} \\ &= \mathbf{H}\mathbf{\Sigma}_{xx}\mathbf{H}^H + \mathbf{R}_w\end{aligned}\quad (2.22)$$

and

$$\begin{aligned}\text{cov}(x(k), \mathbf{y}) = E\{x(k)\mathbf{y}^H\} &= E\{x(k)(\mathbf{H}\mathbf{x} + \mathbf{w})^H\} \\ &= \nu_x(k)i_k^t\mathbf{H}^H\end{aligned}\quad (2.23)$$

where

$$\nu_x(k) = \text{cov}(x(k), x(k)).$$

Note that $x(k)$ s are independent and identically distributed (IID), therefore,

$$\text{cov}(x(k), \mathbf{y}) = \nu_x(k)i_k^t\mathbf{H}^H.$$

Define

$$\boldsymbol{\mu}_x := [\mu_x(0), \mu_x(1), \dots, \mu_x(N-1)]^t$$

where

$$\mu_x(k) := E\{x(k)\},$$

$$\boldsymbol{\mu}_y := [\mu_y(0), \mu_y(1), \dots, \mu_y(N-1)]^t$$

where

$$\mu_y(k) := E\{y(k)\}.$$

Using (2.23), (2.20) can be written as,

$$\hat{x}(k) = \mu_x(k) + \nu_x(k)i_k^t\mathbf{H}^H\mathbf{\Sigma}_{yy}^{-1}(\mathbf{y} - \mathbf{H}\boldsymbol{\mu}_x)\quad (2.24)$$

Since the elements of \mathbf{x} are independent,

$$\mathbf{\Sigma}_{xx} = \text{diag}(\boldsymbol{\nu}_x)$$

where

$$\boldsymbol{\nu}_x = [\nu_x(0), \nu_x(1), \dots, \nu_x(N-1)]^t.$$

Knowing $\boldsymbol{\nu}_x$ and substituting for $\boldsymbol{\Sigma}_{yy}$ from (2.22), $\hat{x}(k)$ can be estimated using (2.21).

In a conventional non-iterative MMSE based symbol estimator [29], all transmitted symbols are assumed to be uniformly distributed and have zero mean. In this case, the LMMSE estimator is obtained by substituting $\boldsymbol{\mu}_x = \mathbf{0}$ and $\boldsymbol{\Sigma}_{xx} = \mathbf{I}_N$ in (2.24) as,

$$\hat{x}(k) = i_k^t \mathbf{H}^H (\sigma^2 \mathbf{I}_N + \mathbf{H} \mathbf{H}^H)^{-1} \mathbf{y} \quad (2.25)$$

Further, if the channel is linear time invariant (LTI), \mathbf{H} becomes diagonal ($\boldsymbol{\Xi}$ in (2.10) becomes circulant) and (2.25) reduces to,

$$\hat{x}(k) = f(k)y(k) \quad (2.26)$$

where

$$f(k) = H^*(k, k) / (\sigma^2 + |H(k, k)|^2) \quad (2.27)$$

LMMSE Estimator for MIMO

Let

$$\boldsymbol{\Sigma}_{\mathbf{xx}}(k) := \text{cov}(\mathbf{x}(k), \mathbf{x}(k)) \in \mathcal{R}^{n_T \times n_T}.$$

Since $\mathbf{x}(k)$ s are iid,

$$\text{cov}(\mathbf{x}(k), \mathbf{y}) = \boldsymbol{\Sigma}_{\mathbf{xx}}(k) [\mathbf{i}_{k.n_T}, \mathbf{i}_{k.n_T+1}, \dots, \mathbf{i}_{(k+1).n_T-1}]^t \mathbf{H}^H.$$

Define

$$\boldsymbol{\mu}_{\mathbf{x}} := [\boldsymbol{\mu}_{\mathbf{x}}^t(0), \boldsymbol{\mu}_{\mathbf{x}}^t(1), \dots, \boldsymbol{\mu}_{\mathbf{x}}^t(N-1)]^t$$

where

$$\boldsymbol{\mu}_{\mathbf{x}}(k) := E\{\mathbf{x}(k)\} := [E\{x_1(k)\}, E\{x_2(k)\}, \dots, E\{x_{n_T}(k)\}]^t,$$

$$\boldsymbol{\mu}_{\mathbf{y}} := [\boldsymbol{\mu}_{\mathbf{y}}^t(0), \boldsymbol{\mu}_{\mathbf{y}}^t(1), \dots, \boldsymbol{\mu}_{\mathbf{y}}^t(N-1)]^t$$

where

$$\boldsymbol{\mu}_{\mathbf{y}}(k) := E\{\mathbf{y}(k)\} := [E\{y_1(k)\}, E\{y_2(k)\}, \dots, E\{y_{n_R}(k)\}]^t.$$

Using the above, (2.20), for MIMO can be written as,

$$\hat{\mathbf{x}}(k) = \boldsymbol{\mu}_{\mathbf{x}}(k) + \frac{1}{n_T} \boldsymbol{\Sigma}_{\mathbf{xx}}(k) [\mathbf{i}_{k.n_T}, \mathbf{i}_{k.n_T+1}, \dots, \mathbf{i}_{(k+1).n_T-1}]^t \mathbf{H}^H \boldsymbol{\Sigma}_{\mathbf{yy}}^{-1} (\mathbf{y} - \boldsymbol{\mu}_{\mathbf{y}}) \quad (2.28)$$

where

$$\mathbf{\Sigma}_{\mathbf{y}\mathbf{y}} := \sigma^2 \mathbf{I}_{N.n_R} + \frac{1}{n_T} \mathbf{H} \mathbf{\Sigma}_{\mathbf{x}\mathbf{x}} \mathbf{H}^H. \quad (2.29)$$

Since the elements of \mathbf{x} are independent,

$$\mathbf{\Sigma}_{\mathbf{x}\mathbf{x}} := \text{diag}(\boldsymbol{\nu}_{\mathbf{x}})$$

where $\boldsymbol{\nu}_{\mathbf{x}}$ is the conditional variance vector (conditioned on the observation vector \mathbf{y}) given as,

$$\boldsymbol{\nu}_{\mathbf{x}} := [\nu_{x_1}(0), \dots, \nu_{x_{n_T}}(0), \nu_{x_1}(1), \dots, \nu_{x_{n_T}}(N-1)]^t.$$

Knowing $\boldsymbol{\mu}_{\mathbf{x}}$, $\boldsymbol{\nu}_{\mathbf{x}}$, σ and \mathbf{H} , $\hat{\mathbf{x}}(k)$ can be estimated in principle using (2.28).

In a conventional noniterative MMSE based symbol estimator [29], all transmitted symbols are assumed to be uniformly distributed and are having zero mean. In this case, therefore, (2.28) simplifies to

$$\hat{\mathbf{x}}(k) = \frac{1}{n_T} [\mathbf{i}_{k.n_T}, \mathbf{i}_{k.n_T+1}, \dots, \mathbf{i}_{(k+1).n_T-1}]^t \mathbf{H}^H (\sigma^2 \mathbf{I}_{N.n_R} + \frac{1}{n_T} \times \mathbf{H} \mathbf{H}^H)^{-1} \mathbf{y}. \quad (2.30)$$

MAP and ML Estimators

The cost function considered is given by [28]

$$\begin{aligned} C(\hat{x}(\mathbf{y}), x) &= 1, \hat{x} \neq x \\ &= 0, \hat{x} = x. \end{aligned} \quad (2.31)$$

With the above choice of cost function, $C_{post}(\hat{x}(\mathbf{y}), x)$ (for discrete x) becomes

$$\begin{aligned} C_{post}(\hat{x}(\mathbf{y}), x) &= \sum_{\mathbf{x} \in S_x} C(\hat{x}(\mathbf{y}), x) p(\mathbf{x}|\mathbf{y}) \\ &= 1 - p(\hat{x}(\mathbf{y}) = x) \end{aligned} \quad (2.32)$$

$C_{post}(\hat{x}(\mathbf{y}), x)$ is minimized if \hat{x} is set to the maximum of $p(\mathbf{x}|\mathbf{y})$. This is the maximum a-posteriori probability (MAP) estimator. Thus a MAP estimator is optimal with respect to minimizing the error ($\hat{x} \neq x$) probability. If the prior distribution $P(\mathbf{x})$ is uniform, it can be neglected in the minimization problem (2.32) above, yielding a maximum likelihood (ML) estimator, given as,

$$\hat{x}(\mathbf{y}) = \arg \max_{x \in S_x} p(\mathbf{y}|\mathbf{x}) \quad (2.33)$$

2.2.5 Channel Estimation

Channel estimation is a challenging problem in wireless systems. The radio channel is highly dynamic. Transmitted signals are typically reflected and scattered, arriving at receivers along multiple paths. Due to the mobility of transmitters, receivers or the scattering objects in the path, channel response can be changing rapidly over time. Multipath propagation, mobility and scattering cause the signal to be spread in time, frequency and angle. Channel estimation performance is directly related to these statistics. Different techniques are proposed to exploit these statistics for better channel estimates.

Channel estimation for OFDM systems basically falls into two categories. Blind and non-blind. The blind channel estimation method, where training signals are absent, require a large amount of data and thus suffer severe performance degradation in fast fading channels and are not considered here. The non-blind channel estimation falls further in two categories, Pilot/Data aided and decision directed. In pilot aided channel estimation, a complete OFDM symbol as in the case of WLAN systems, or a portion of a symbol, as in the case of DVB systems, which is known at the receiver is transmitted so that the receiver can estimate the radio channel by demodulating the received samples. Estimation accuracy can be improved by increasing the pilot density, which, however causes more overheads and thus reduces the spectral efficiency. When pilot tones are assigned to all sub-carriers of a particular OFDM symbol, it is called a training symbol. This type of pilot arrangement is considered when the channel variation is known to be slow and burst type data transmission schemes such as WLAN systems. When the channel varies between consecutive OFDM symbols, as is common in DVB systems, pilots are inserted regularly within each OFDM symbol. In decision directed methods, to estimate the current OFDM symbol, channel estimates from the previous OFDM symbols are generally used. Channel corresponding to the current symbol is then estimated by using the updated symbol estimates information.

Performance of channel estimation is greatly affected by how the pilots are placed within an OFDM symbol. Spacing of pilot tones within an OFDM symbol is determined

by the coherence bandwidth, a measure of the frequency selectivity, of the channel whereas the spacing of pilot tones across OFDM symbols is determined by the coherence time, a measure of channel variability. It has been observed that in a static channel scenario, the minimum MSE from Least Square(LS) estimation is obtained when the pilots are equispaced with maximum distance. In the case of time varying channels, it has been shown that the pilots should be all grouped for optimum elimination of ICI [30, 31, 32, 33]. Therefore, in the case of doubly selective channels, the optimum pilot placement strategy would be to place a group (cluster) of pilots equi-spaced across the OFDM symbol. This has been validated in [34] via. simulations.

2.2.6 Soft Decoding

Maximum likelihood decoding (MLD) such as Viterbi decoding [35] minimizes the sequence error probability. (It however, does not necessarily minimize the bit error probability.) MLD delivers hard decoded bits (hard outputs) without providing their reliability values. In many error control coding schemes such as Turbo decoding, LDPC decoding etc. and TE schemes, it is desirable to provide both decoded bits and their reliability information (also called soft outputs) for further processing to improve the system performance.

A decoding algorithm that processes soft-decision inputs and produces soft-decision outputs is called a soft-in/soft-out (SISO) decoding algorithm. A well known SISO algorithm is the MAP (Maximum a posteriori probability) decoding algorithm that was devised by Bahl, Cocke, Jelinek and Raviv [35, 36]. This algorithm, called the BCJR algorithm, is devised to minimize the bit-error probability and to provide reliability values of the decoded bits. The soft Viterbi algorithm (SOVA) [35] is another example of a SISO decoding algorithm for convolutional codes. Message passing algorithm [37] employed in decoding LDPC codes is yet another example of SISO. In this thesis we use a BCJR based SISO decoder for turbo equalization.

2.2.7 Iterative Equalization/Turbo Equalization

The job of the receiver is to estimate the transmitted data from the observations of the received data. To do this optimally in terms of minimizing the bit error rate (BER), as we saw in sec. 2.2.4, the receiver must try to fit all probable sequences of transmitted bits to the received data and select the one for which the BER is minimum. But the complexity of this task grows exponentially with the length of the bit sequence to decode. So most practical receivers perform the symbol estimation at first where the received observations is treated to account for the effects of the channel impairments based on a performance criteria such as MSE. Once these symbols are estimated they are demapped into their associated code bits, deinterleaved and decoded using a BER optimal outer decoder. In this separate equalization and decoding process, it is usual for the equalizer to make hard decisions on the symbol estimates before mapping them into their constituent binary code bits. The process of making hard decisions discards information pertaining to how likely each of the possible channel symbols might have been. This “soft” information can be converted into probabilities that each of the received code bits takes on the value of zero or one that, after deinterleaving, is precisely the form of information that can be exploited by a BER optimal decoding algorithm [38].

The remarkable performance of turbo codes makes it clear that the soft information need not only flow in one direction. Once the error control decoding algorithm processes the soft information it can, in turn, generate its own soft information (on account of the coding gain of the underlying error control code) indicating the relative likelihood of each of the transmitted bits. This soft information from the decoder could be taken into account in the equalization process, creating a feedback loop between the equalizer and decoder. In this framework, each of the constituent algorithms communicates its beliefs about the relative likelihood that each given bit takes on a particular value (ref. Fig. 2.4). The ‘ping-pong’ process generally results in the *amplification* of information over iterations. This essentially is the process of iterative equalization.

The following terms are employed throughout this thesis. They are explained below

and depicted in Fig. 2.4.

A-priori: The a-priori information associated with a bit is the information known about it before the equalization or decoding starts. It is also often referred to as the intrinsic information.

Extrinsic: The extrinsic information associated with a bit a_n is the information provided by the equalizer or decoder based on a) the received sequence and b) the a-priori information of all bits *with the exception of the received and a-priori information explicitly related to a_n* . When processing soft information as an input to the equalizer or decoder it is assumed that the soft information about each bit is an independent piece of information. If the decoder formulates its soft information about a given bit based on soft information provided to it from the equalizer about exactly the same bit, then the equalizer cannot consider this information to be independent of its channel observations. In effect this would create a feedback loop in the over all process of length two: The equalizer informs the decoder about a given bit, and then the decoder simply re informs the equalizer what it already knows. To avoid such short cycles in the feedback , when soft information is passed between constituent algorithms, such information is never formed based on the information passed into the algorithm concerning the same bit. This amounts to the equalizer only telling the decoder new information about a given bit based on information it gathered from distinct parts of the received signal - thanks to the interleaver. Similarly the decoder only tells the equalizer information it gathered on distinct parts of the encoded bit stream. As a result the iterative equalization and decoding process can continue for many iterations before cycles are introduced, which eventually limits further improvements. This process of only passing “extrinsic information” between constituent decoders is essential to the performance of turbo decoding algorithms.

A-posteriori: It is the information that the SISO algorithm provides about a bit taking into account all available information contained in the received signal.

In the original TE proposed by Douillard *et al.*, [39], data is convolutionally encoded and the channel with a finite memory is considered as a rate one encoder. Receiver consists of two trellis based detectors: one for the channel (the equalizer) and one for

the code (the decoder). The detection-decoding process can then be associated to the turbo-decoding of serial concatenated codes. This architecture has achieved tremendous improvement in bit rate compared to independent detection decoding based receiver architecture, however, at the cost of exponential computational complexity. A modified, MMSE based TE scheme has since been suggested in [40, 41, 42] with polynomial complexity. Numerous articles have appeared on the topic since then and they attempted to a) bring down the computational complexity, b) improve the performance, c) analyze the convergence behavior of the scheme or d) enhance the scheme to several different application scenarios etc.

2.2.8 Extrinsic Information Transfer (EXIT) Charts

EXIT charts, originally proposed by Stephan ten Brink in [43] for the convergence analysis of Turbo codes (parallel concatenated codes) is a simulation based technique that can be extended for analyzing the convergence behavior of iterative equalization [44, 45], which in the coding paradigm is an example of serially concatenated codes. At the input to a SISO decoder, a stream of soft bits that has a certain mutual information with the transmitted stream, is presented. The SISO decoder generates an output stream that in general will have a higher mutual information (with the transmitted bit stream). The same is true for a SISO equalizer as well. Thus, both the SISO equalizer and decoder can be considered as mutual information transformers. The trajectory of the mutual information exchange between detector and decoder is traced using simulation. This can be used to get good insights into the behavior of the iterative schemes [45, 44, 46, 47, 48, 49].

Let $B \in \{1, 0\}$ and $B' \in \{1, -1\}$ be two discrete random variables (RV) and L_B, L'_B be the Log likelihood ratios (LLR) of B and B' respectively. Note that L_B and L'_B are continuous RV. B and B' can be thought to be the outputs of a convolutional encoder and BPSK mapper respectively if there is a one to one relation between B and B' . The mutual information, $I(B; L_B)$ is defined [7] as,

$$I(B; L_B) = \sum_{b=1,0} \int_{-\infty}^{+\infty} p(l_b|b) P(b) \ln \frac{p(l_b|b)}{p(l_b)} dl_b \quad (2.34)$$

where $p(l_b|b) = p(\text{LLR}(b(n))|b(n) = b)$.

Maximal mutual information is achieved for equally likely inputs b as,

$$I(B; L_B) = \frac{1}{2} \sum_{b=1,0} \int_{-\infty}^{+\infty} p(l_b|b) \ln \frac{p(l_b|b)}{p(l_b)} dl_b \quad (2.35)$$

It is clear that L_B is equivalent to L'_B . Therefore,

$$p(l_b) = \frac{1}{2} (p(l'_b|b' = +1) + p(l'_b|b' = -1)) \quad (2.36)$$

Therefore, Mutual information $I(B; L_B)$ between transmitted bits b and their LLR values is as given in (2.37).

$$I(B; L_B) = \frac{1}{2} \sum_{b' \in \{-1, +1\}} \int_{-\infty}^{\infty} p(l_{b'}|b') \ln \frac{2p(l_{b'}|b')}{p(l_{b'}|b' = +1) + p(l_{b'}|b' = -1)} dl_{b'} \quad (2.37)$$

The extrinsic LLRs of $b(n)$ at the output of the equalizer/soft demapper is denoted as $\text{LLR}_{\text{ext}}(b(n))$. Let $I_E = I(b(n); \text{LLR}_{\text{ext}}(b(n)))$ be the mutual information between $b(n)$ and LLR_{ext} at the output of the equalizer and $I_D = I(b(n); \text{LLR}'_{\text{ext}}(b(n)))$ be the mutual information at the output of the decoder. I_D and I_E can be found by calculating (2.37) numerically. Since equalizer and decoder are connected serially, the *a priori* mutual information, I_A , at the equalizer input is I_D and at the decoder input is I_E . A plot of I_E vs. I_D , called the EXIT chart, as described in the sequel, can give good insights into the convergence behavior of the iterative system [50].

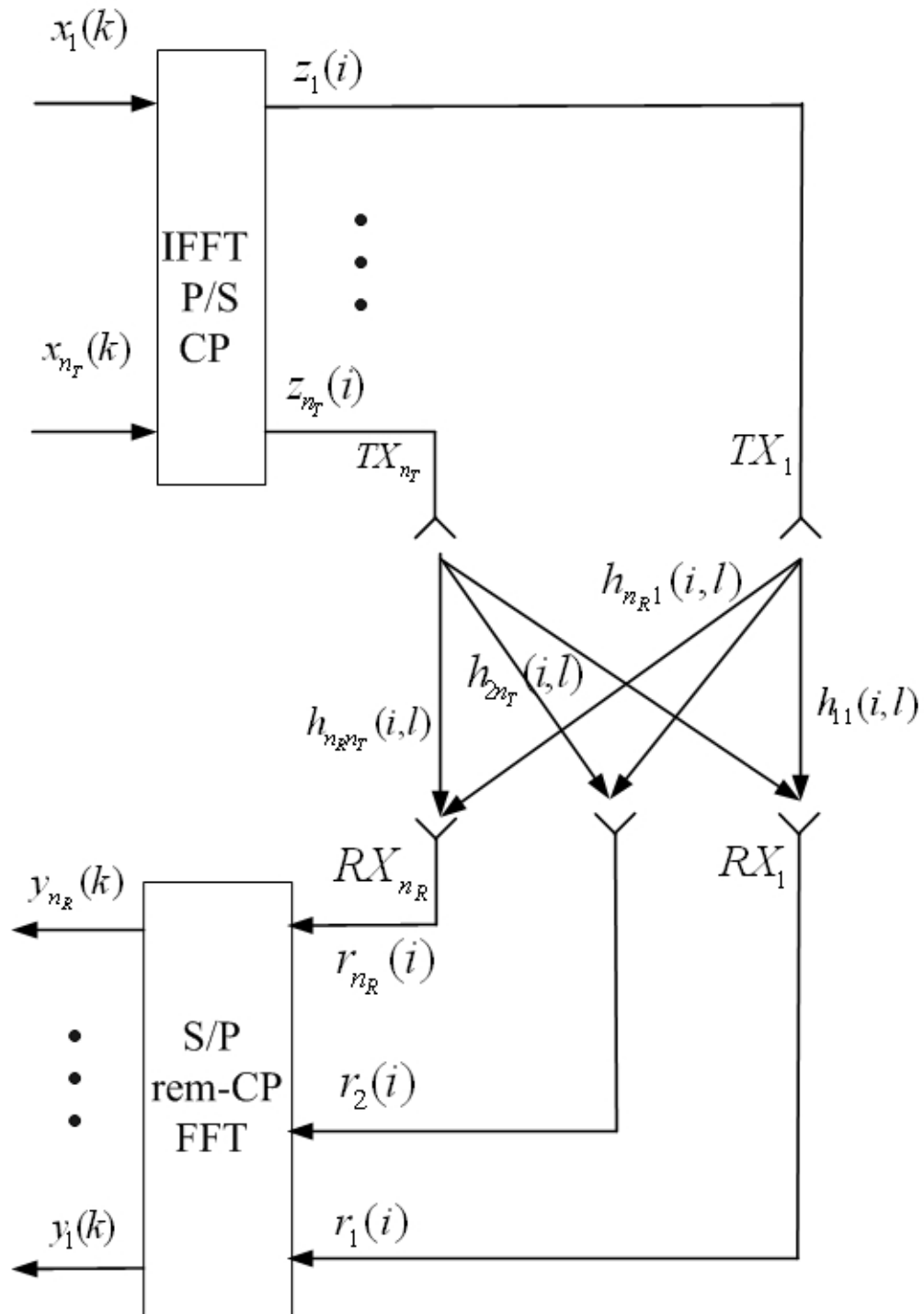


Figure 2.3: MIMO OFDM Transceiver.

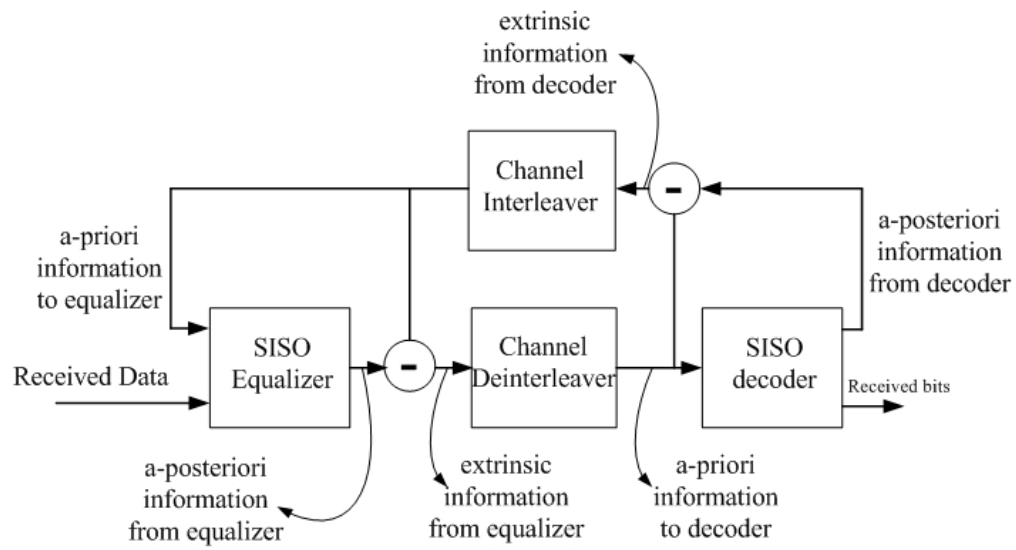


Figure 2.4: Iterative Equalization.

Chapter 3

A Low Complexity Iterative Detection and Decoding Scheme for Single Antenna Mobile OFDM Systems

3.1 Introduction

Advantages of OFDM compared to SC systems have been discussed in Chapter 1. We also saw in Chapter 1 that OFDM based systems have been adopted in many of the recent wireless communication standards. However, modern wireless communication applications require high data rates at high carrier frequencies and at high levels of mobility. This results in less intercarrier spacing and severe time-varying frequency-selective multipath fading, which breaks the orthogonality of subcarriers and leads to intercarrier interference thus severely impacting the receiver BER performance. In DVB-H, for e.g., the inter-carrier spacing (ICS) could be as low as approximately 1KHz and the expected maximum receiver Doppler frequency is of the order of $10 - 20\%$ of the ICS. In such scenarios, efficient receiver design is a challenging practical problem.

Even with the help of reduced complexity MMSE based TE schemes [40, 41], one of the major disadvantages of iterative detection is high computational complexity arising from channel covariance matrix inversion per iteration per tone as demonstrated in (2.19). Motivated by the classical MMSE TE, in this Chapter we propose a sub-optimal, successive interference cancellation and MAP decoding (SIC-MAP) wherein we avoid the explicit equalization stage.

Doubly-selective channels can offer large joint multipath Doppler/frequency diversity gains when coherent demodulation and decoding are employed in the receiver. In SIC-MAP, copies of the received signal on the same and adjacent subcarriers are carefully separated to take advantage of this frequency diversity. We eliminate the

interference from other transmit symbols which are estimated using the feedback information from the decoder. This results in multiple receiver observations for the same transmit symbol as in the case of a diversity system. The resulting system matrix becomes a single column matrix. It is easy to implement MAP decoding in such systems [51].

As in references [52, 2, 1], we also exploit the banded nature of the system matrix (\mathbf{H} in (2.9)) in SIC-MAP. The performance and computational complexity of the proposed scheme are compared with that of TE-MMSE-OND2 suggested in [2] and TE-BLK2, the best performing equalizer in a group of three [1]. In [2, 1], windowing technique is used to make the energy more concentrated along the diagonal. Windowing mentioned in those papers will work as good in our proposed scheme as well. We incorporate channel coding in [2, 1] to render a fair comparison. It has been found that SIC-MAP provides comparable performance to TE-MMSE-OND2 and TE-BLK2 but with significantly less computational complexity. Such a receiver, compared to their counterparts, will take only a fraction of the silicon area (or the cost) and battery power, a scarce resource in mobile applications, thus making it especially suitable for mobile applications with large symbol length such as [20, 8].

3.2 Related Work

Vast majority of schemes proposed in the literature for symbol detection fall in three categories: a) independent equalization and decoding [53, 54, 55, 56, 57]. Ref. [53] proposes a MMSE filter that takes not only amplitudes but also the derivatives of subcarrier amplitudes while computing the transmitted symbol estimate. Ref. [54] proposes MMSE detection in time domain where the time varying nature of the channel is exploited as a provider of time diversity. In [55], a pre-equalizer to mitigate the ICI in large sized symbol systems such as DVB-T2 where the symbol is divided into smaller sizes and a compensating pre-equalizer based on minimizing the interfering power and a single tap equalizer to compensate for channel selectivity is proposed. In [56], an iterative decision feedback equalizer (DFE) is proposed to perform ICI cancellation such that the modified system matrix becomes diagonal in the frequency domain and consequently

the equalizer becomes single tap. In [57], the received signal is split into small segments such that the channel remains approximately static during each small segment. Suitable signal processing is performed on each of these segments such that the resulting channel matrix is made diagonal. b) successive cancellation of the interference [58, 59, 60] . Ref. [58, 59], propose ICI (due to insufficient CP or mobility) removal in time domain. The signal is then converted to frequency domain thus resulting in a diagonal frequency domain system matrix. Hard decisions are made on the equalized signal following which it is converted back to time domain and the time-frequency iterations are repeated. In [60], mean value of the transmit symbol is computed using the LLR values from the decoder, which then is used to remove the ICI from the received symbol, resulting in a diagonal system matrix. A modified low-complexity MMSE equalizer that takes the decision error into account is now derived. The symbol error probability is computed using LLRs and is used in the MMSE equalizer for estimation of the transmit symbol. These estimates are used for computing the LLRs which are sent for decoding and c) turbo like iterative equalization [39, 42, 40, 61, 62, 63, 64]. Authors of [40] propose MMSE based reduced complexity TE where the computational complexity is $O(N^3)$ or $O(N^2)$ whereas the original TE proposed by [39] has exponential complexity. In [42], multiple access interference (MAI) and inter symbol Interference (ISI) in a static multipath environment are removed in a code-division-multipath-access (CDMA) system using a combination of soft iterative interference cancellation and Linear MMSE filtering. Authors of [64] propose a modified LMMSE equalizer based on a scheme that provides a more accurate modeling of the statistics of the two quadrature components of the transmitted symbol and is claimed to have better performance compared to [40]. Ref. [65] extends MMSE-TE to higher order modulations. Authors of [61] proposes an iterative equalization with a channel estimation scheme for rapidly varying channels for communication systems that operate under water. The channel that is assumed to follow a three parameter model is estimated using convex optimization techniques in an iterative fashion. Three equalizer structures based on MAP, MMSE and ZF criteria are proposed. Iterations are performed for several parameter combinations in a systematic manner until a decoder success is observed. In [62] a low complexity MAP decoding

for doubly selective OFDM systems is proposed. Proposed algorithm successively estimates the transmit symbols and remove the interference due to these symbols from the observation thus bringing down the search space progressively, thus significantly reducing the decoding complexity. The successive symbol search is made in a computationally efficient manner by making use of the Markov chain Monte Carlo(MCMC) with Gibbs sampling method. In [63], an iterative technique for the inversion of a linear system of equations called “operator-perturbation technique” is made use of to cancel ICI iteratively.

Turbo like iterative schemes, in general are found to have superior performance among the above. However turbo schemes above are saddled in general with high computational complexity (quadratic or sometimes cubic in the number of sub carriers). Such practical application challenges motivate us to come up with a new scheme with better trade off between performance and implementation complexity [66, 51].

Encouraged by the MMSE based turbo equalization [42, 40], a large number of low complexity iterative OFDM equalization schemes have been proposed [67, 2, 1, 68]. They exploit the banded nature of the frequency domain channel matrix to bring down the equalization complexity to linear in the number of sub-carriers. The references above propose, in general, either a new technique for iterative MMSE linear equalization using priors on the banded sub matrix around the main diagonal or a new technique to compute the soft information from the symbol estimates.

3.3 System Model

The OFDM transceiver model is described in Fig 3.1. The front end of this is identical to the system described in 2.2.2 in Chapter 2. At the transmitter, information bits ($\{a(n)\}$) are convolutionally encoded ($\{b(n)\}$) and passed through a bit interleaver (BI) ($\{c(n)\}$). The symbol mapper modulates them into QAM symbols ($\{s(k)\}$). A set of N of these QAM “frequency domain” symbols is collected to form an OFDM symbol. A symbol interleaver (SI) interleaves them (\mathbf{x}). The OFDM symbol is converted into “discrete time-domain” samples, $\{z(i)\}$, by performing an N point IDFT.

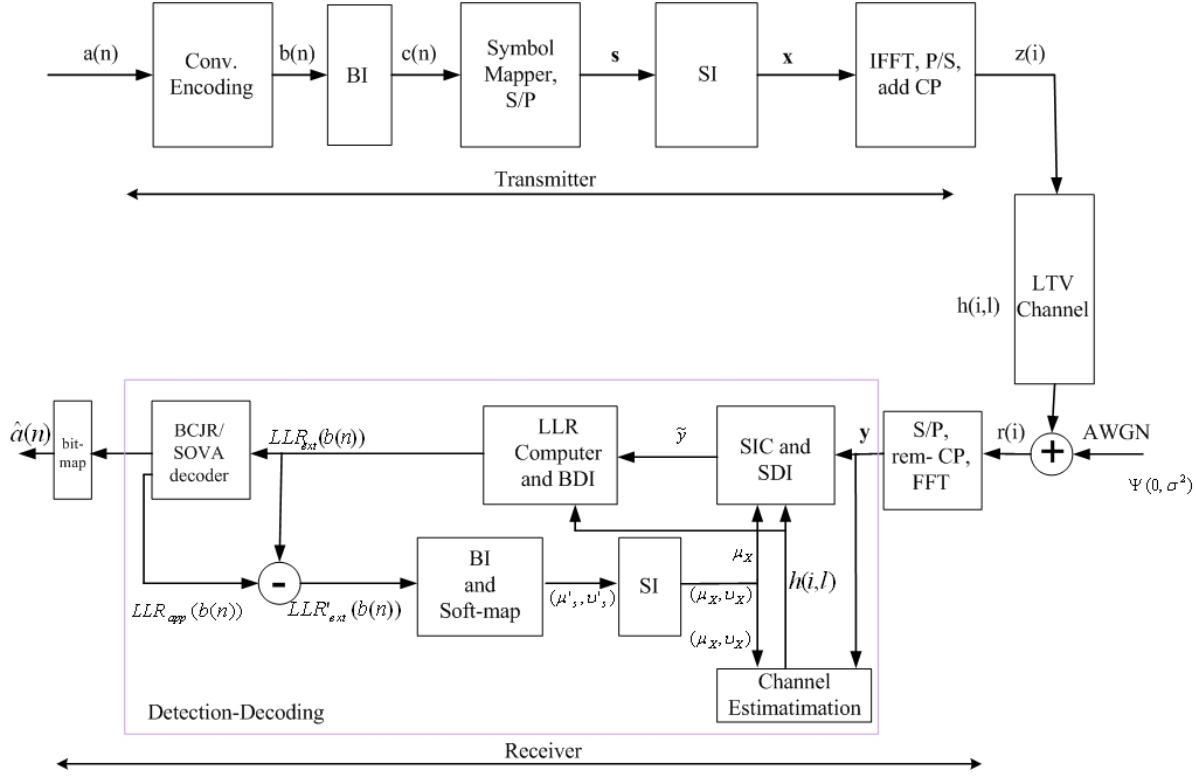


Figure 3.1: OFDM Transceiver.

CP is added to each of these symbols. These samples are then transmitted from the transmit antenna. The multipath channel is modeled as a linear time varying (LTV) system with discrete impulse response $h(i, l)$. At the receiver, the CP removed data is converted back to “frequency domain” by performing an N point DFT and passed to the symbol Detection-Decoding block. It comprises Successive Interference Canceled (SIC), Channel Estimator, Symbol and Bit Interleaver/de-interleaver, LLR Computer and BCJR or SOVA based decoder [35]. We assume perfect carrier, symbol and sample synchronization at the receiver. Mathematical modeling of this system has been described in 2.2.2.

The structure of the \mathbf{H} matrix is given in Fig. 3.2. In the case of time varying Rayleigh fading channels [25], for SISO systems, it has been shown that \mathbf{H} in (2.11) will be a banded matrix with significant coefficients concentrated in a banded structure with width D along the diagonal. D is a measure of the Doppler spread and is typically

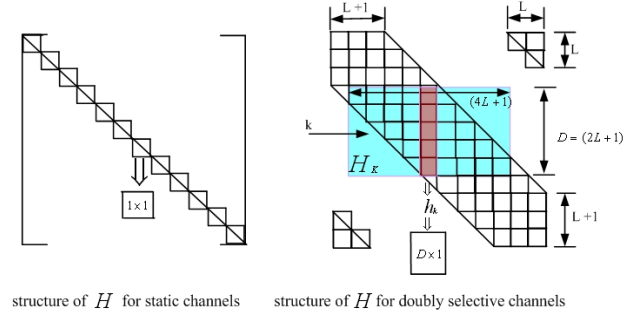


Figure 3.2: OFDM Channel Structure.

chosen as

$$D = 2L + 1 \quad (3.1)$$

where

$$L = \lceil f_d T_s N \rceil. \quad (3.2)$$

Different structures for \mathbf{H} are shown in Fig 3.2 [2]. If the channel is static, \mathbf{H} will be a diagonal matrix.

3.4 Successive Interference Cancellation Based MAP Receiver (SIC-MAP)

In this section, we present a low complexity iterative receiver that implements successive interference cancellation followed by maximum *a posteriori* probability (MAP) decoding. The proposed scheme, at first, simplify the system matrix to a single column vector by selectively removing the ICI interference from the received symbols using the feedback symbol mean values. Soft information can be computed directly from this modified model. These are fed to a MAP bit decoder.

The following observations are key in formulating the proposed scheme:

1. The relative magnitude of each sub diagonal and super diagonal element of the doubly selective Rayleigh fading channel matrix \mathbf{H} decreases significantly as we move away from the main diagonal. We can thus ignore all elements that are

far away from the main diagonal [52, 2, 1] without significantly impacting performance. Note that these elements are absent for a static multipath channel.

2. As the *extrinsic* information becomes more accurate over multiple iterations, the conditional mean, $\mu_x(k) \rightarrow x(k)$, which is the true symbol value and the conditional variance, $\nu_x(k) \rightarrow 0$. Therefore in each new iteration, we can use $\mu_x(k)$ from the previous iteration to selectively remove ICI from the received symbol such that the resulting system matrix is turned into a single column vector. We compute LLRs $\left(\ln \left(\frac{P(b(n)=0)}{P(b(n)=1)}\right)\right)$ from the modified system directly thus avoiding MMSE symbol estimation and the associated matrix inversion.

Based on observation one, (2.11) can be approximated as,

$$\begin{aligned} \mathbf{y}_{\mathbf{k}} &:= [y(\langle k-L \rangle_N), \dots, y(\langle k+L \rangle_N)]^t \\ &= \mathbf{H}_{\mathbf{k}} \mathbf{x}_{\mathbf{k}} + \mathbf{w}_{\mathbf{k}} \end{aligned} \quad (3.3)$$

where

$$\begin{aligned} \mathbf{x}_{\mathbf{k}} &:= [x(\langle k-2L \rangle_N), \dots, x(\langle k+2L \rangle_N)]^t, \\ \mathbf{w}_{\mathbf{k}} &:= [w(\langle k-L \rangle_N), \dots, w(\langle k+L \rangle_N)]^t \end{aligned}$$

and $\mathbf{H}_{\mathbf{k}}$ is the shaded (green) section of \mathbf{H} in Fig. 3.2 (right) given by (3.4). Note that modulo-N ($\langle \rangle_N$) operation is used in the equation above; thanks to the CP in the system. For simplicity of notation, the modulo operation ($\langle \rangle_N$) is omitted in the sequel.

$$\mathbf{H}_{\mathbf{k}} := \begin{bmatrix} h(\langle k-L \rangle_N, \langle k-2L \rangle_N) & \dots & h(\langle k-L \rangle_N, \langle k+2L \rangle_N) \\ h(\langle k-L+1 \rangle_N, \langle k-2L \rangle_N) & \dots & h(\langle k-L+1 \rangle_N, \langle k+2L \rangle_N) \\ \dots & \dots & \dots \\ h(\langle k+L \rangle_N, \langle k-2L \rangle_N) & \dots & h(\langle k+L \rangle_N, \langle k+2L \rangle_N) \end{bmatrix} \quad (3.4)$$

Now,

$$\mathbf{x}_{\mathbf{k}} = \boldsymbol{\mu}_{\mathbf{x}_{\mathbf{k}}} + \boldsymbol{\delta}_{\mathbf{x}_{\mathbf{k}}}$$

where $\boldsymbol{\delta}_{\mathbf{x}_{\mathbf{k}}}$ is the residual error which approaches $\mathbf{0}_{4L+1}$ as the extrinsic LLR becomes more reliable over multiple iterations. Substituting for $\mathbf{x}_{\mathbf{k}}$ in (3.3) and rearranging

yields (3.5). $\tilde{\mathbf{w}}_{\mathbf{k}}$, the new noise, contains the ICI from the residual error $\delta_{\mathbf{x}_{\mathbf{k}}}$. $\tilde{\mu}_{\mathbf{x}_{\mathbf{k}}}$ is a vector as defined in (3.5).

$$\mathbf{y}_{\mathbf{k}} = \mathbf{h}_{\mathbf{k}}x(k) + \mathbf{H}_{\mathbf{k}} \underbrace{\begin{bmatrix} \mu_x(k-2L) \\ \vdots \\ 0 \\ \vdots \\ \mu_x(k+2L) \end{bmatrix}}_{\tilde{\mu}_{\mathbf{x}_{\mathbf{k}}}} + \mathbf{H}_{\mathbf{k}} \underbrace{\begin{bmatrix} \delta_x(k-2L) \\ \vdots \\ \mathbf{0} \\ \vdots \\ \delta_x(k+2L) \end{bmatrix}}_{\tilde{\mathbf{w}}_{\mathbf{k}}} + \mathbf{w}_{\mathbf{k}} \quad (3.5)$$

Let

$$\begin{aligned} \tilde{\mathbf{y}}_{\mathbf{k}} &:= \mathbf{y}_{\mathbf{k}} - \mathbf{H}_{\mathbf{k}}\tilde{\mu}_{\mathbf{x}_{\mathbf{k}}} \\ &= \mathbf{h}_{\mathbf{k}}x(k) + \tilde{\mathbf{w}}_{\mathbf{k}}. \end{aligned} \quad (3.6)$$

$\mathbf{h}_{\mathbf{k}}$ is shown in red in Fig. 3.2 (right). It is a column vector of size $D \times 1$. We also approximate that $\tilde{\mathbf{w}}_{\mathbf{k}}$ and $\mathbf{w}_{\mathbf{k}}$ has identical covariance as the noise due to residual ICI is small and decreasing over multiple iterations. This approximation is validated with simulations in Chapter 5.

The LLR Computer calculates the *extrinsic* LLR, $\text{LLR}_{\text{ext}}(c(n))$ which represents information about $c(n)$ contained in $\tilde{\mathbf{y}}_{\mathbf{k}}$ and $P(c(l))$ for all $l \neq n$. These are passed to a MAP decoder where they are used as *a priori* LLRs. $\text{LLR}_{\text{ext}}(c(n))$ is calculated from the modified system using (3.7), where $0 \leq u \leq Q-1$,

$$\mathbf{m} = [m_0, m_1, \cdot, m_{Q-1}]^t,$$

$$\{\eta\} = \text{map}(\mathbf{m})$$

is the signal constellation and F_2 is binary Galois Field. Q denotes the number of bits

per symbol. For e.g., for BPSK $Q = 1$, for QPSK $Q = 2$ and so on.

$$\begin{aligned}
\text{LLR}_{\text{ext}}(c(Qk + u)) &= \text{LLR}_{\text{app}}(c(Qk + u)) - \text{LLR}(c(Qk + u)) \\
&= \ln \frac{P((c(Qk + u) = 0)|\tilde{\mathbf{y}}_{\mathbf{k}})}{P((c(Qk + u) = 1)|\tilde{\mathbf{y}}_{\mathbf{k}})} - \text{LLR}(c(Qk + u)) \\
&= \ln \frac{p(\tilde{\mathbf{y}}_{\mathbf{k}}|(c(Qk + u) = 0))P(c(Qk + u) = 0)}{p(\tilde{\mathbf{y}}_{\mathbf{k}}|(c(Qk + u) = 1))P(c(Qk + u) = 1)} - \text{LLR}(c(Qk + u)) \\
&= \left(\ln \frac{p(\tilde{\mathbf{y}}_{\mathbf{k}}|(c(Qk + u) = 0))}{p(\tilde{\mathbf{y}}_{\mathbf{k}}|(c(Qk + u) = 1))} + \text{LLR}(c(Qk + u)) \right) - \text{LLR}(c(Qk + u)) \\
&= \ln \frac{\sum_{\mathbf{m} \in F_2: \mathbf{m}_u = 0} p(\tilde{\mathbf{y}}_{\mathbf{k}}|(x(k) = \text{map}(\mathbf{m}))) \prod_{j=0: j \neq u}^{Q-1} P(m_j)}{\sum_{\mathbf{m} \in F_2: \mathbf{m}_u = 1} p(\tilde{\mathbf{y}}_{\mathbf{k}}|(x(k) = \text{map}(\mathbf{m}))) \prod_{j=0: j \neq u}^{Q-1} P(m_j)} \quad (3.7)
\end{aligned}$$

As shown in Appendix 3.9.1, for QPSK, the above expression can be simplified as

$$\text{LLR}_{\text{ext}}(c_q(2k)) = \frac{\sqrt{8} \text{Re}(\tilde{\mathbf{y}}_{\mathbf{k}}^H \mathbf{h}_{\mathbf{k}})}{\sigma^2} \quad (3.8)$$

$$\text{LLR}_{\text{ext}}(c_q(2k + 1)) = \frac{\sqrt{8} \text{Im}(\tilde{\mathbf{y}}_{\mathbf{k}}^H \mathbf{h}_{\mathbf{k}})}{\sigma^2}. \quad (3.9)$$

A closer look at the derivation in 3.9.1 reveals that this expression is applicable, within a scale factor, to any constant-modulus constellations. Observe that the *extrinsic LLR* of $c(n)$ is conditioned only on $\tilde{\mathbf{y}}_{\mathbf{k}}$ and in the simplified system model, $\tilde{\mathbf{y}}_{\mathbf{k}}$ depends only on the present symbol $x(k)$. This makes the evaluation of $\text{LLR}_{\text{ext}}(c(n))$ easy. (Extrinsic LLR is computed by imposing the iid assumption on the transmit symbol $x(k)$.)

The MAP decoder computes soft outputs, $\text{LLR}_{\text{app}}(b(n))$ —the *a posteriori* reliability information of each coded bit—in LLR form by minimizing the bit error probability (BEP) [35]. i.e.,

$$\hat{b}(n) = \underset{b \in F_2}{\text{argmax}} P(b(n) = b|\tilde{\mathbf{y}}_{\mathbf{k}}) \quad (3.10)$$

for $n = 0, 1, \dots, K - 1$ where K is the number of data bits being encoded in a block. The posterior probabilities $P(b(n)|\tilde{\mathbf{y}}_{\mathbf{k}})$ is obtained by marginalizing $b(n)$ in $P(\{b\}|\tilde{\mathbf{y}}_{\mathbf{k}})$. Finally, taking LLR and using the iid assumption on the bits $b(n)$ we get,

$$\begin{aligned}
\text{LLR}_{\text{app}}(b(n)|\tilde{\mathbf{y}}_{\mathbf{k}}) &= \ln \frac{\sum_{\{b: b(n)=0\}} \prod_{l=0: l \neq n} P(b(l))}{\sum_{\{b: b(n)=1\}} \prod_{l=0: l \neq n} P(b(l))} \\
&\quad + \ln \frac{P(b(n) = 0)}{P(b(n) = 1)} \\
&= \text{LLR}_{\text{ext}}(b(n)|\tilde{\mathbf{y}}_{\mathbf{k}}) + \text{LLR}(b(n))
\end{aligned}$$

$\text{LLR}_{\text{ext}}(b(n)|\tilde{\mathbf{y}}_{\mathbf{k}})$ represents information about $b(n)$ contained in $\tilde{\mathbf{y}}_{\mathbf{k}}$ and $P(b(l))$ for all $l \neq n$. This is called the *extrinsic* LLR. It is the additional information produced by the decoder from $\text{LLR}(b(n))$, the input *a prioary* LLR.

The input *a priori* LLR to the decoder is subtracted from $\text{LLR}_{\text{app}}(b(n))$ to obtain the *extrinsic* reliability information $\text{LLR}'_{\text{ext}}(b(n))$. It is passed through a bit interleaver and is used in the soft-mapper to compute mean $\boldsymbol{\mu}'_s$ and variance $\boldsymbol{\nu}'_s$. These are symbol interleaved to produce $\boldsymbol{\mu}_x$ and $\boldsymbol{\nu}_x$. $\boldsymbol{\mu}_x$ is used to remove the ICI interference as described in (3.6), whereas $\boldsymbol{\nu}_x$ is used in the channel estimator (Chapter 4) to determine the reliability of $\boldsymbol{\mu}_x$. The ICI removed data is fed to the LLR Computer to generate more reliable LLRs to further improve the output bit estimate. This process is repeated until further gains are insignificant. $\text{LLR}_{\text{app}}(b(n))$ are then hard-sliced at the bit-map block and information bit estimates $\hat{a}(n)$ are retrieved from the received data bit estimates $\hat{b}(n)$. Mapping $\text{LLR}'_{\text{ext}}(c(n))$ s to $\mu'_s(k)$ and $\nu'_s(k)$ is described in [42, 40]. For QPSK modulation,

$$\mu'_s(k) = \tanh(\text{LLR}'_{\text{ext}}(c(2n))/2) + i \tanh(\text{LLR}'_{\text{ext}}(c(2n+1))/2), \quad (3.11)$$

$$\nu'_s(k) = 1 - |\mu'_s(k)|^2. \quad (3.12)$$

Notice that the approximation in (3.6), may not be valid for a generic system matrix $\mathbf{H}_{\mathbf{k}}$. However it fits the scenario of doubly selective OFDM channels, where the magnitude of the off-diagonal elements in the frequency domain are significantly smaller than that of the main-diagonal elements. This gives raise only to a relatively small residual ICI power (ICI after cancellation) even with a moderate value of $\delta_{\mathbf{x}_{\mathbf{k}}}$ in the early iterations and as the iterations proceed the approximation becomes progressively more accurate. (This is elaborately investigated in Chapter 5.)

Another low complexity SISO detector has been proposed in [66]. However, its performance is inferior compared to the proposed scheme above. [66] is based on the diagonalization of channel matrix.

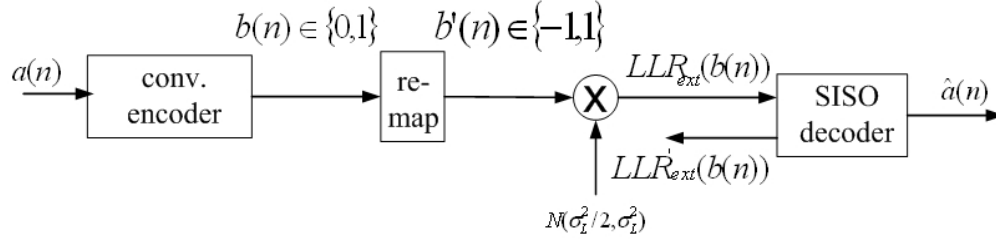


Figure 3.3: EXIT Chart Set Up - Decoder

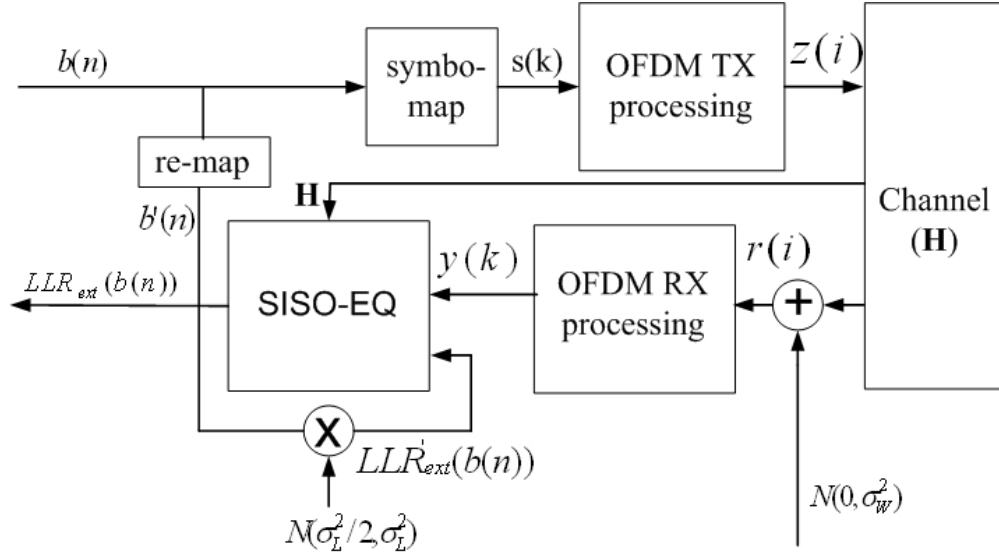


Figure 3.4: EXIT Chart Set Up - SISO Equalizer

3.5 Creating EXIT Charts

Simulation set up for generating EXIT charts for decoder is described in Fig. 3.3. A block of information bits $\{a(n)\}$ is convolutionally encoded to generate $\{b(n)\}$ which are BPSK modulated to obtain $\{b'(n)\}$. Input LLRs to the decoder are generated independently from a Gaussian distribution with a mean $\sigma_L^2/2$ and variance σ_L^2 . Relation between mean and variance arises from consistency conditions that is satisfied by the symmetric LLR distribution [43, 45]. Relationship between σ_L^2 and $I(B; L_B)$ is monotonically increasing. In order to obtain an EXIT chart with approximately equally

spaced inputs, we use the relation

$$\sigma_L = f^{-1}(I)$$

described in [69] or [46]. A number of blocks are simulated for different values of input *a priori* mutual information, I_A (or σ_L). Output mutual information, I_D , is computed using (2.37). Mean I_A is plotted along the x-axis and mean I_D along the y-axis. This is the EXIT curve for the decoder.

Simulation setup for EXIT charts for iterative detector is given in Fig. 3.4. Frames of OFDM symbols generated from iid input bits ($\{b(n)\}$) are passed through the transmitter, channel and receiver front end. The received data, \mathbf{y} , is fed to the equalizer. Other inputs to the equalizer are the *a priori* LLRs, $\text{LLR}'_{\text{ext}}(b(n))$, and the channel matrix, \mathbf{H} . *A priori* LLRs are generated as in the earlier setup. Symbol mean values are computed within the detector from input LLRs using (3.11). The extrinsic LLRs are computed using (3.8) and (3.9).

Convergence behavior of the equalizer is a function of E_b/N_0 . Keeping noise power (σ_w) as a parameter, σ_L (or equivalently the input *a priori* mutual information I_A) is varied, and the output mutual information I_E is computed each time, as was done in the decoder. The experiment is repeated for different snapshots of the channel, and the average I_E is computed. This ensures that several fades are taken into account while creating the EXIT chart. Alternatively, the symbol frame can be made very long for the same purpose. The plot I_A vs. I_E corresponds to an EXIT curve for the equalizer for a given σ_w . The experiment is repeated for different values of σ_w , to obtain different EXIT curves.

3.6 Computational Complexity

In this section, the computational complexity of SIC-MAP is compared with the iterative equalization schemes TE-MMSE-OND2 [2] and TE-BLK2 [1]. Complexity of the non-iterative MMSE scheme [70] that is popularly used in practical receivers, referred to as MMSE-OND2 in this paper, is also computed. MMSE-OND2 is based on a section of \mathbf{H} ($\mathbf{H}_{\mathbf{k}}$ in Fig. 3.2 (right)) given in (3.4).

MMSE-OND2 schemes, turbo or not, involve the inversion of a matrix of size D . Matrix inversion, generally, has cubic complexity. However, it has been shown that MMSE-OND2 or TE-MMSE-OND2 can be performed with approximately $O(N \cdot D^2)$ operations [71]. Table 3.1 tabulates the total number of arithmetic operations (\times, \div) required at the receiver for different schemes. Details of this computation are given in Appendix 3.9.2.

Computations involved in BCJR are identical across all these schemes and so are not considered. (The cost of adders is significantly lower than that of multipliers. *tanh* operation can be performed using a small look-up table. These two operations are thus not tabulated in table 3.1. Although not differentiated here, the cost of a divider, in practice, is higher than that of a multiplier).

For a typical set of parameters ($L = 1$), it is clear from table 3.1 that TE-BLK2 and TE-MMSE-OND2 require approximately 3.3 and 4.5 times more computations than SIC-MAP per iteration, while the channel estimation efforts are the same. The non-iterative scheme, MMSE-OND2, requires 3.0 times more computations than SIC-MAP per iteration.

	TE-BLK2 per sample per iter	MMSE-OND2 per sample	TE-MMSE-OND2 per sample per iter.	SIC-MAP per sample per iter.
Total \times	$12L^2 + 24L + 17$	$(2L + 1)(14L + 4)$	$(2L + 1)(20L + 7) + 2$	$2(2L + 1)^2 + 1$
Total \div	$2L + 7$	$2L + 1$	$(2L + 1) + 1$	–
Total Oper.	$12L^2 + 26L + 24$	$2L + 1 + (2L + 1) \times (14L + 4)$	$(2L + 1) + (2L + 1) \times (20L + 7) + 2 + 1$	$2(2L + 1)^2 + 1$
Normalized Complexity (L=1)	3.3	3.0	4.5	1

Table 3.1: Complexity Comparison - Channel Equalization

3.7 Simulation Results

Here we evaluate SIC-MAP by comparing its performance with two other iterative schemes described in section 3.6. For this purpose we assume that CSI is known at the receiver. We consider an OFDM system with $N = 256$, $N_h = 30$ and $N_p = N/4$. A 1/2 rate convolutional code with generator polynomial (7, 5) is used. Symbols are QPSK modulated with unit variance and AWGN with a circular variance of $(E_b/N_0)^{-1}$. Both bit and symbol interleaving are performed with S-random interleavers [72] with $S = 22$ and $S = 5$ respectively. Each channel path is Rayleigh fading characterized by Jakes Doppler Spectrum (exponentially decaying power delay profile) with a frequency spread of $f_d = 900\text{Hz}$. With the DVB-T sampling rate of $T_s^{-1} = 9.14\text{MHz}$, this corresponds to a normalized Doppler spread of 20% of the sub-carrier spacing.

Fig 3.5 shows the BER performance of all the three schemes. Although windowing employed in [2, 1] can improve the performance in all the three schemes, no windowing is employed in our study as it will increase the computation burden significantly. SIC-MAP performs poorly in the first iteration as no interference is canceled before computing the LLRs. However the incremental BER gain between the first and second iterations of SIC-MAP is very significant. Therefore TE-MMSE-OND2 and SIC-MAP perform more or less identically within three iterations. Note that the computational complexity of SIC-MAP is approximately only 33% that of TE-MMSE-OND2. It was shown in [1] that the performance of TE-BLK2 is superior to TE-MMSE-OND2 [2]. This can be seen from Fig 3.5; however, the performance difference is not significant in a system where error correction coding (convolutional coding in this case) is incorporated which is the case with most of the practical receivers. SIC-MAP scheme can be implemented with only a thrid of the computations required that for TE-BLK2. (Entries corresponding to TE-BLK2 in Table 3.1 are obtained from [1].)

BER performance of the non-iterative MMSE-OND2 [70] is that corresponding to the first iteration of TE-MMSE-OND2. We can note from Table 3.1 that complexity of MMSE-OND2 is approximately 3.0 times higher than SIC-MAP and from Fig 3.5 we observe that SIC-MAP converges sufficiently in three iterations and outperforms

MMSE-OND2 significantly. Thus we conclude that SIC-MAP has all the performance benefits of any iterative scheme, yet, the total computational complexity of it is even far less even than that of a commonly used non-iterative scheme namely MMSE-OND2.

If we set $L = 3$ for SIC-MAP but $L = 1$ for the other two iterative schemes, all three schemes will approximately have the same computational cost. The performance of such a system is given in Fig. 3.6. As can be seen, for the same computational cost, SIC-MAP clearly outperforms TE-MMSE-OND2 and TE-BLK2. This illustrates the excellent complexity-performance tradeoff capabilities of the proposed scheme.

Fig. 3.7 illustrates the BER performance at low Doppler. A few observations can be made from this plot. a) SIC-MAP in the first iteration can be thought of as a simple detector ignoring all the off-diagonal elements in the system matrix. BER performance of SIC-MAP and TE-MMSE-OND2 is very similar in the first iteration. Some of the existing symbol detection schemes (both iterative and non-iterative) under doubly dispersive channel conditions ignore the off-diagonal elements. From this plot we see that at relatively low Doppler frequencies, no much of performance is lost even if the off-diagonal elements are discarded. b) BER gains are relatively less even after six iterations for both schemes. This, again, can be attributed to the insignificant off-diagonal elements.

EXIT charts are briefly introduced in Fig 3.8. It depicts the EXIT charts for SIC-MAP and TE-MMSE-OND2 schemes. The EXIT curve for SIC-MAP, although starts at a lower point (corresponding to a higher BER curve at the first iteration), catches up with the TE-MMSE-OND2 at higher I_A which points to the asymptotic identical behavior of SIC-MAP with TE-MMSE-OND2. A more thorough treatment of EXIT chart based inference process is provided in Chapter 5 while dealing with MIMO systems.

3.8 Conclusion

We have proposed a low complexity detection scheme employing successive interference cancellation (SIC-MAP), to mitigate the effects of ICI in mobile OFDM systems. SIC-MAP, while having near identical performance to TE-MMSE-OND2 and TE-BLK2 can

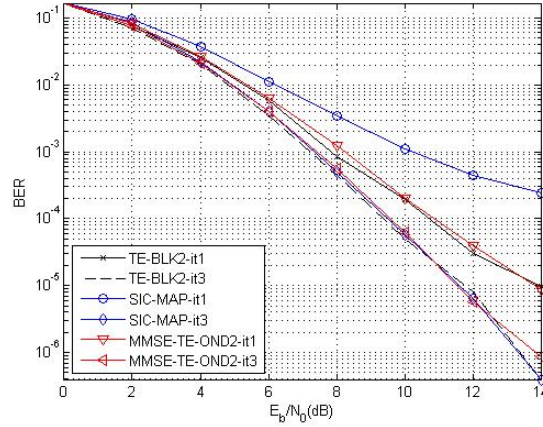


Figure 3.5: BER Plots- TE-MMSE-OND2, SIC-MAP and TE-BLK2 ($f_d T_s N = 0.2$, $N = 256$, $L = 1$, $\#iter = 1, 3$, $N_h = 30$).

be implemented respectively with only 33% and 30% of their computational burden. It was also found that performance and implementation complexity of SIC-MAP can effectively be traded for one another. EXIT charts are introduced briefly to analyze the convergence of TE-SIC while a more elaborate discussion on the topic is postponed for Chapter 5.

SIC-MAP deals with a coded system. However, the same scheme can be extended to uncoded systems as well. While using coded systems, we can have only a block implementation as opposed to a serial implementation for uncoded systems. This is because, for coded systems, we can update priors from one iteration to the next only at the end of decoding of the block as there is interleaving and decoding involved. However, the performance of iterative detection is considerably better in a coded system due to the coding gain of the decoder in the system.

3.9 Appendix

3.9.1 Derivation of (3.8)

Ref. to Table 3.2 for the QPSK symbol alphabet definition.

$$\text{LLR}_{\text{ext}}(c(2k)) = \ln \frac{p(\tilde{\mathbf{y}}_{\mathbf{k}}|x(k) = \eta_1)P(0) + p(\tilde{\mathbf{y}}_{\mathbf{k}}|x(k) = \eta_3)P(1)}{p(\tilde{\mathbf{y}}_{\mathbf{k}}|x(k) = \eta_2)P(0) + p(\tilde{\mathbf{y}}_{\mathbf{k}}|x(k) = \eta_4)P(1)} \quad (3.13)$$

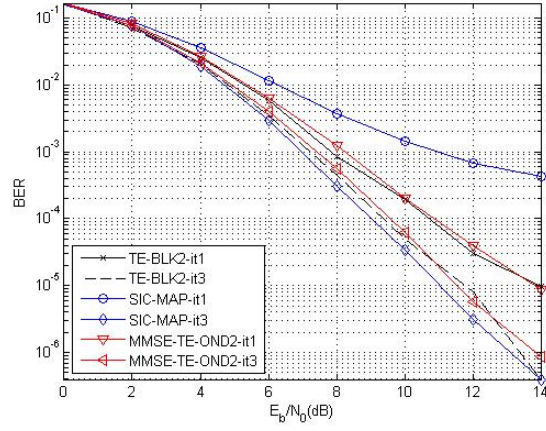


Figure 3.6: BER Plots - SIC-MAP ($L = 3$), TE-MMSE-OND2 ($L = 1$) and TE-BLK2 ($L = 1$). ($f_d T_s N = 0.2$, $N = 256$, $\#iter = 1, 3$, $N_h = 30$).

Here

$$\begin{aligned}
 p(\tilde{\mathbf{y}}_{\mathbf{k}} | x(k) = \eta_1) &= e^{-\frac{(\tilde{\mathbf{y}}_{\mathbf{k}} - \mathbf{h}_{\mathbf{k}} \eta_1)^H (\tilde{\mathbf{y}}_{\mathbf{k}} - \mathbf{h}_{\mathbf{k}} \eta_1)}{2\sigma^2}} \\
 &= e^{\frac{-1}{2\sigma^2} (a1 + a2 - 2Re(\mathbf{y}_{\mathbf{k}}^H \mathbf{h}_{\mathbf{k}} \eta_1))}
 \end{aligned} \tag{3.14}$$

where

$$a1 = \mathbf{y}_{\mathbf{k}}^H \mathbf{y}_{\mathbf{k}}$$

and

$$a2 = (\mathbf{h}_{\mathbf{k}} \eta_1)^H (\mathbf{h}_{\mathbf{k}} \eta_1).$$

Note that, for QPSK

$$(\mathbf{h}_{\mathbf{k}} \eta_1)^H (\mathbf{h}_{\mathbf{k}} \eta_1) = (\mathbf{h}_{\mathbf{k}} \eta_2)^H (\mathbf{h}_{\mathbf{k}} \eta_2) = (\mathbf{h}_{\mathbf{k}} \eta_3)^H (\mathbf{h}_{\mathbf{k}} \eta_3) = (\mathbf{h}_{\mathbf{k}} \eta_4)^H (\mathbf{h}_{\mathbf{k}} \eta_4).$$

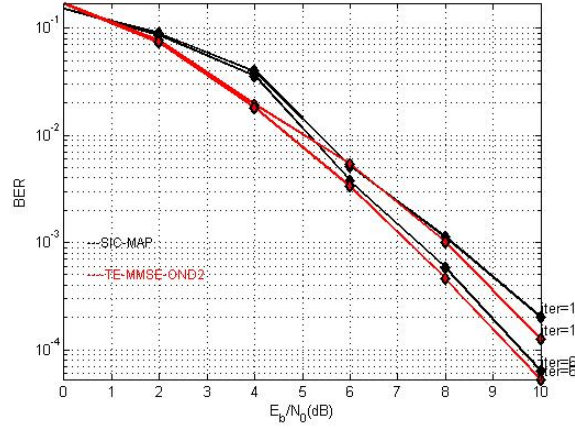


Figure 3.7: BER Plots - SIC-MAP, TE-MMSE-OND2 and SIC-MAP($f_d T_s N = 0.1$, $N = 256$, $L = 1$, $\#iter = 1, 6$, $N_h = 30$).

	1	2	3	4
$(m0, m1)$	$(0, 0)$	$(1, 0)$	$(0, 1)$	$(1, 1)$
η_i	$\frac{1+j1}{\sqrt{2}}$	$\frac{-1+j1}{\sqrt{2}}$	$\frac{1-j1}{\sqrt{2}}$	$\frac{-1-j1}{\sqrt{2}}$

Table 3.2: QPSK Alphabet

Substituting for all the terms from (3.14) in (3.13), defining $z := \tilde{\mathbf{y}}_{\mathbf{k}}^H \mathbf{h}_{\mathbf{k}}$ and removing the common terms, we get,

$$\begin{aligned}
 \text{LLR}_{\text{ext}}(c(2k)) &= \ln \frac{e^{Re(z\eta_1)/\sigma^2} P(0) + e^{Re(z\eta_3)/\sigma^2} P(1)}{e^{Re(z\eta_2)/\sigma^2} P(0) + e^{Re(z\eta_4)/\sigma^2} P(1)} \\
 &= \ln \frac{e^{\sqrt{2}Re(z(1+j))/\sigma^2} P(0) + e^{Re(z(1-j))/\sigma^2} P(1)}{e^{\sqrt{2}Re(z(-1+j))/\sigma^2} P(0) + e^{Re(z(-1-j))/\sigma^2} P(1)} \\
 &= \ln \frac{e^{\sqrt{2}(Re(z)-Im(z))/\sigma^2} P(0) + e^{\sqrt{2}(Re(z)+Im(z))/\sigma^2} P(1)}{e^{\sqrt{2}(-Re(z)-Im(z))/\sigma^2} P(0) + e^{\sqrt{2}(-Re(z)+Im(z))/\sigma^2} P(1)} \\
 &= \ln \left(\frac{e^{\frac{\sqrt{2}}{\sigma^2} Re(z)}}{e^{-\frac{\sqrt{2}}{\sigma^2} Re(z)}} \right) \\
 &= \frac{\sqrt{8}Re(\tilde{\mathbf{y}}_{\mathbf{k}}^H \mathbf{h}_{\mathbf{k}})}{\sigma^2}. \tag{3.15}
 \end{aligned}$$

Similarly we get $\text{LLR}_{\text{ext}}(c(2k+1)) = \frac{\sqrt{8}Im(\tilde{\mathbf{y}}_{\mathbf{k}}^H \mathbf{h}_{\mathbf{k}})}{\sigma^2}$

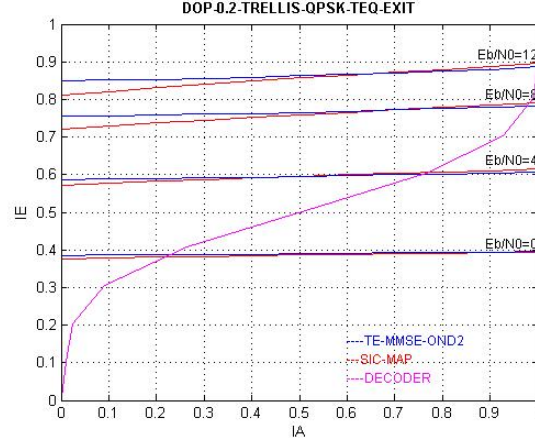


Figure 3.8: EXIT Charts - TE-MMSE-OND2 and SIC-MAP ($f_d T_s N = 0.2$, $N = 256$, $L = 1$, $\#iter = 3$, $N_h = 30$).

3.9.2 Detailed Complexity Computation

The computational complexity of various schemes used in our study are derived in this section [71, 73]. Tables 3.3 and 3.4 describe the implementation and complexity computation of TE-MMSE-OND2 scheme whereas tables 3.5 and 3.6 describe that of MMSE-OND2 scheme. The computational complexity of SIC-MAP is described in Table 3.7 while that of TE-BLK2 is taken from [1]

Table 3.3: TE-MMSE-OND2 – An Efficient Implementation

INPUT
extrinsic LLRs from decoder ($\text{LLR}'_{\text{ext}}(c(n))$)
INITIALIZATION
compute $\mu_x(k), \nu_x(k), \forall k$,
compute $\Sigma_{\mathbf{y}_0, \mathbf{y}_0}^{-1} = (\sigma^2 I_{(2L+1)} + \mathbf{H}_0 \Sigma_{\mathbf{x}_0, \mathbf{x}_0} \mathbf{H}_0^H)^{-1}$
LINEAR MMSE ESTIMATION
FOR $k = 0$ TO $N - 1$ DO
$\mathbf{f}_k = \Sigma_{\mathbf{y}_k, \mathbf{y}_k}^{-1} \mathbf{h}_k \nu_{x(k)}$
$\mathcal{Y}_k = (\mathbf{y}_k - \mathbf{H}_k \mu_{x(k)})$
$\hat{x}(k) = \mu_x(k) + \mathbf{f}_k^H \mathcal{Y}_k$
$\text{LLR}_{\text{ext}}(c(2k)) = \frac{\sqrt{8}}{1 - \nu_x(k) \mathbf{h}_k^H \mathbf{f}_k} \cdot \text{Re}(\hat{x}(k))$
$\text{LLR}_{\text{ext}}(c(2k+1)) = \frac{\sqrt{8}}{1 - \nu_x(k) \mathbf{h}_k^H \mathbf{f}_k} \cdot \text{Im}(\hat{x}(k))$
ITERATIVE UPDATE OF $\Sigma_{\mathbf{y}_k, \mathbf{y}_k}^{-1}$ (see below).
END
ITERATIVE UPDATE OF $\Sigma_{\mathbf{y}_k, \mathbf{y}_k}^{-1}$
(inversion with one row update at a time)
(complexity $O((2L+1)^2)$)
$\begin{bmatrix} \mathbf{a} & \mathbf{B}^H \\ \mathbf{B} & \mathbf{A} \end{bmatrix} := \Sigma_{\mathbf{y}_k, \mathbf{y}_k}^{-1}$ $\mathbf{A}_p = \mathbf{A} - \mathbf{B} \mathbf{B}^H / \mathbf{a}$ $\begin{bmatrix} \mathbf{B}_p \\ \mathbf{a}_p \end{bmatrix} := \begin{bmatrix} \mathbf{0}_{2L} \\ \sigma^2 \end{bmatrix} + \mathbf{H}_{k+1} \Sigma_{\mathbf{x}_{k+1}, \mathbf{x}_{k+1}} \mathbf{H}_{k+1}^H \begin{bmatrix} \mathbf{0}_{2L} \\ 1 \end{bmatrix}$ $\mathbf{B}_{pp} = -\mathbf{A}_p \mathbf{B}_p$ $\mathbf{a}_{\text{new}} = (\mathbf{a}_p + \mathbf{B}_p^H \mathbf{B}_{pp})^{-1}$ $\mathbf{B}_{\text{new}} = \mathbf{a}_{\text{new}} \mathbf{B}_{pp}$ $\mathbf{A}_{\text{new}} = \mathbf{A}_p + \mathbf{a}_{\text{new}} (\mathbf{B}_{pp} \mathbf{B}_{pp}^H)$ $\Sigma_{\mathbf{y}(k+1), \mathbf{y}(k+1)}^{-1} := \begin{bmatrix} \mathbf{A}_{\text{new}} & \mathbf{B}_{\text{new}} \\ \mathbf{B}_{\text{new}}^H & \mathbf{a}_{\text{new}} \end{bmatrix}$
OUTPUT
extrinsic LLRs to the decoder ($\text{LLR}_{\text{ext}}(c(n))$)

Table 3.4: Complexity - TE-MMSE-OND2
Ignore Complexity for Initialization
complexity for Linear MMSE Estimation

steps	operation	operand size	\times	\div
1	$\Sigma_{\mathbf{y}_k, \mathbf{y}_k}^{-1} \mathbf{h}_k$ \times $\nu_{x(k)}$	$(2L+1) \times (2L+1),$ $(2L+1) \times 1,$ 1×1	$(2L+1)^2 +$ $(2L+1)$	$-$ $-$
2	$\mathbf{H}_k \boldsymbol{\mu}_{\mathbf{x}_k}$	$(2L+1) \times (4L+1),$ $(4L+1) \times 1$	$(4L+1)(2L+1)$	$-$
3	$\mathbf{f}_k^H \mathcal{Y}_k$	$(2L+1) \times 1,$ $(2L+1) \times 1$	$(2L+1)$	$-$
4	$\mathcal{S} = \nu_{x(k)} \mathbf{h}_k^H \mathbf{f}_k$ $\frac{\sqrt{8}}{1-S} \hat{x}(k)$	$1 \times 1,$ $(2L+1) \times 1,$ $(2L+1) \times 1,$ $-$	$(2L+1) + 1$ 1	$-$ 1
5	$\mathbf{B}\mathbf{B}^H/\mathbf{a}$	$(2L) \times 1,$ 1×1	$(2L)^2$	$(2L)$
6	$\mathbf{H}_{k+1} \Sigma_{\mathbf{x}_{k+1}, \mathbf{x}_{k+1}} \mathbf{H}_{k+1}^H$ $\times \begin{bmatrix} \mathbf{0}_{2L} \\ 1 \end{bmatrix}$	$(2L+1) \times (4L+1)$ $(4L+1) \times (4L+1)$	$(2L+1) \times (4L+1) +$ $(4L+1) \times (2L+1)$	
7	$\mathbf{A}_p \mathbf{B}_p$	$(2L) \times (2L),$ $(2L) \times 1$	$(2L)^2$	
8	$(\mathbf{a}_p + \mathbf{B}_p^H \mathbf{B}_{pp})^{-1}$	$(2L) \times 1$	$(2L)$	1
9	$\mathbf{a}_{\text{new}} \mathbf{B}_{pp}$	$1 \times 1,$ $(2L) \times 1$	$2L$	
10	$\mathbf{a}_{\text{new}} (\mathbf{B}_{pp} \mathbf{B}_{pp}^H)$	$1 \times 1,$ $(2L) \times 1$	$2L +$ $(2L)^2$	

$$AM_t := \text{Total } \times \text{ from step1 + step2} = (2L+1)(2L+4L+1+1+1)$$

$$AD_t := \text{Total } \div \text{ from step1 + step2} = 0$$

$$BM_t := \text{Total } \times \text{ from step3 + step4} = 2[(2L+1)+1]$$

$$BD_t := \text{Total } \div \text{ from step3 + step4} = 1$$

$$CM := \text{Total } \times \text{ for matrix inversion} = \text{step5} + \text{step6} \dots + \text{step10} = (2L+1)(6L+8L+2)$$

$$CD := \text{Total } \div \text{ for matrix inversion} = \text{step5} + \text{step6} \dots + \text{step10} = 2L+1$$

$$\text{Total } \times \text{ per sample per iteration for TE-MMSE-OND2} = AM_t + BM_t + CM$$

$$\text{Total } \div \text{ per sample per iteration for TE-MMSE-OND2} = AD_t + BD_t + CD$$

Table 3.5: MMSE-OND2 – An Efficient Implementation
INITIALIZATION

compute $\Sigma_{\mathbf{y}_0, \mathbf{y}_0}^{-1} = (\sigma^2 I_{(2L+1)} + \mathbf{H}_0 \mathbf{H}_0^H)^{-1}$
LINEAR MMSE ESTIMATION
FOR $k = 0$ TO $N - 1$ DO
$\mathbf{f}_k = \mathbf{h}_k^H \Sigma_{\mathbf{y}_k, \mathbf{y}_k}^{-1}$
$\mathbf{x}(k) = \mathbf{f}_k \mathbf{y}_k$
ITERATIVE UPDATE OF $\Sigma_{\mathbf{y}_k, \mathbf{y}_k}^{-1}$ (Ref. Table 3.3).
END

Table 3.6: Complexity - MMSE-OND2
Ignore Complexity for Initialization
complexity for Linear MMSE Estimation

steps	operation	operand size	\times	\div
1	$\mathbf{h}_k^H \Sigma_{\mathbf{y}_k, \mathbf{y}_k}^{-1}$	$(2L+1) \times (2L+1),$ $(2L+1) \times 1$	$(2L+1)^2$	–
2	$\mathbf{f}_k \mathbf{y}_k$	$1 \times (2L+1),$ $(2L+1) \times 1$	$(2L+1)$	–
3	ITERATIVE UPDATE OF $\Sigma_{\mathbf{y}_k, \mathbf{y}_k}^{-1}$ (ref Table 3.4)			
$AM_s := \text{Total} \times \text{from step1 + step2}$		$2(2L+1)$		
$AD_s := \text{Total} \div \text{from step1 + step2}$		0		
$CM := \text{Total} \times \text{for matrix inversion (step3)}$		CM in Table 3.4		
$CD := \text{Total} \div \text{for matrix inversion (step 3)}$		CD in Table 3.4		
Total \times per sample for MMSE-OND2 = $AM_s + CM$				
Total \div per sample for MMSE-OND2 = $AD_s + CD$				

Table 3.7: Complexity - SIC-MAP
Ignore Complexity for Computing $\mu_x(k) \forall k$

steps	operation	operand size	\times	\div
1	$\tilde{\mathbf{y}}_k$ (computation of $\mathbf{H}_k \tilde{\mu}_{\mathbf{x}_k}$) (3.6)	$(2L+1) \times (4L+1),$ $(4L+1) \times 1$	$(2L+1)(4L+1)$	–
2	$\text{LLR}_{\text{ext}}(c(\cdot))$ (3.8),(3.9)	$2L+1$	$2L+1+1$	–
$AM_{sic} := \text{Total} \times \text{from step1}$				
$AD_{sic} := \text{Total} \div \text{from step1}$				
$BM_{sic} := \text{Total} \times \text{from step2}$				
$BD_{sic} := \text{Total} \div \text{from step2}$				
Total \times per sample per iteration for SIC-MAP = $AM_{sic} + BM_{sic}$				
Total \div per sample per iteration for SIC-MAP = $AD_{sic} + BD_{sic}$				

Chapter 4

Channel Estimation–SISO Systems

4.1 Introduction

Channel estimation and equalization are two crucial functions in any receiver. Performance of a receiver is largely determined by how well these two functions are performed. We have presented a novel low complexity iterative equalization scheme for SISO OFDM systems in Chapter 3. In this chapter we address the complementary part, namely a low complexity channel estimation that works well with the iterative equalization scheme addressed earlier. The scheme presented here can be extended to MIMO systems in a straight forward fashion; however, this is not addressed in this thesis.

It has been concluded in [74] that a piecewise linear, LS based channel estimator can be a good compromise between complexity and performance. Inspired by the channel estimation algorithm proposed in [59], we propose a soft decision feedback based low complexity LS channel estimation scheme. In the context of channel estimation, we iteratively compute the ICI interference and subtract it from the original system thus turning the modified system matrix into a diagonal matrix. Equi-spaced pilot pattern is well suited for channel estimation in the modified system. The proposed algorithm works satisfactorily even when the channel length is longer than the number of pilots in the system ($N_h > N_p$). A first order linear model is used here to characterize the channel time variations. Unlike parametric model based channel estimation schemes, our approach does not restrict the channel variation to closely follow the proposed model (commonly Jakes) for good accuracies. The proposed algorithm makes use of soft information to refine the channel estimates so that it is capable of handling the long channel scenarios such as the ones encountered in Single Frequency Networks (DVB deployment in Europe) where the number of significant channel taps can be higher than

the number of pilot subcarriers in a given OFDM symbol.

4.2 Related Work

Based on the estimation methodology employed, channel estimation techniques, whether it is pilot aided or decision directed, can be broadly categorized into five different groups for doubly selective channels: a) LS based schemes which are approximate but simple to implement, b) schemes that exploit the second order statistics of the channel- LMMSE, c) Adaptive schemes, d) Finite parameter model based and e) Iterative schemes.

Consider the system described by (2.11). Let \mathbf{x} be replaced with \mathbf{s}_p , the pilot/training vector. When \mathbf{H} is diagonal, (2.11) can be rewritten as,

$$\mathbf{y} = \text{diag}(\mathbf{s}_p)\mathbf{h}_d + \mathbf{w} \quad (4.1)$$

where \mathbf{h}_d is a column vector created from the diagonal elements of \mathbf{H} . i.e.,

$$\mathbf{h}_d = [\mathbf{H}(0, 0), \mathbf{H}(1, 1) \dots \mathbf{H}(k, k) \dots \mathbf{H}(N - 1, N - 1)]^t$$

When the channel statistics are unknown, channel state information (CSI) is treated as a deterministic parameter and LS estimation is employed. That is,

$$\hat{\mathbf{h}}_d = (\text{diag}(\mathbf{s}_p))^{-1}\mathbf{y} \quad (4.2)$$

and \mathbf{H}_{LS} is a matrix with elements from $\hat{\mathbf{h}}_d$ along the main diagonal.

To reduce the computational complexity, $(\text{diag}(\mathbf{s}_p))^{-1}$ can be computed offline. Estimation in this case do not exploit the information from channel statistics. By exploiting the channel statistics, channel estimation can be significantly improved. For e.g., if the correlation matrix of the channel frequency response vector, $\mathbf{R}_H = E\{\mathbf{H}\mathbf{H}^H\}$, is available, using the methods described in Sec. 2.2.4, LMMSE estimate of the channel can be obtained as below,

$$\begin{aligned} \hat{\mathbf{H}}_{LMMSE} &= \mathbf{R}_H (\mathbf{R}_H + \sigma^2(\mathbf{s}_p\mathbf{s}_p^H)^{-1})^{-1} (\text{diag}(\mathbf{s}_p))^{-1}\mathbf{y} \\ &= \mathbf{R}_H (\mathbf{R}_H + \sigma^2(\mathbf{s}_p\mathbf{s}_p^H)^{-1})^{-1} \hat{\mathbf{H}}_{LS} \end{aligned} \quad (4.3)$$

Compared with LS estimation, LMMSE estimation has better performance; however, it requires channel statistics and thus has higher computational complexity.

Various schemes have been proposed to bring down this complexity. A couple of them are briefly mentioned below. The coefficient vector for LMMSE estimation can be obtained from the significant Singular Values of the system [75] thus simplifying the computations (sub-space method). In another scheme, correlation matrix is determined from the power delay profile (PDP) of the wireless channel. Therefore if the PDP is known in advance, the coefficient matrix for LMMSE estimation can be computed off line. When the accurate PDP is unknown in advance, *robust channel estimation* method is employed [76]. Here a channel PDP such as uniform or exponential is assumed for the system under consideration. Estimation performance can further be improved by a 2D (two dimensional) LMMSE estimator that takes advantage of the time domain correlation of the channel in addition to the frequency domain correlation. Techniques such as in [77] have been proposed to reduce the computational complexity of a 2D LMMSE estimator. Different transform domain techniques such as Fourier transform [78] or Hadarmard transform [79] or Discrete Cosine Transform [80] were also proposed for reduced complexity LMMSE channel estimation of OFDM systems.

Channel estimated in the previous OFDM blocks can be used to predict the channel in the next block [81, 82]. Prediction algorithms can be applied either on the channel taps (time domain) or the channels at the subcarriers (frequency domain). The previous has the advantage that the number of variables to predict is much smaller but needs IFFT to get the channel at the subcarriers. The latter requires no transformation but it requires the prediction of more number of variables, that is, subcarriers. An instantaneous noisy channel estimate can be made by direct division of interference removed data $y'(k)$ and soft symbol estimate $\mu(k)$, $(y'(k)/\mu(k))$. Using this, an LMS based adaptive channel predictor can be implemented in principle in frequency domain. The main issue associated with this approach is that a separate predictor need to be running for each tone. Thus for 2K FFT, common in DVB-T systems, we would need 2K adaptive predictors running. The complexity and memory requirement for this approach is significant. On the other hand, consider the NLMS/RLS implementation for channel tap prediction given in [81] (time domain). Adaptive predictors that do not require any statistical prior knowledge and are able to track non-stationary channel

and noise statistics are proposed in the above work. N_h number of adaptive predictors are running in parallel to predict N_h channel coefficients in time domain. It requires a set of past M symbols for the prediction of the future tap. It can be observed that such predictors (time or frequency domain) work well when the Doppler frequency is low ($f_d T_s N$ in the range of 0.01). Even in such scenarios, the prediction error convergence is slow. At normalized Doppler frequencies as high as 0.05, NLMS and RLS error performance starts deteriorating considerably. Thus it can be said that adaptive prediction based iterative methods give good results in slowly varying channels but their performance becomes unacceptable, once the channel varies fast over time. ARMA modeling and Kalman filtering [83] can alleviate this deficiency to a great extent at the cost of additional computational complexity.

Parametric model based channel estimation schemes assume that the time variation of channel coefficients can be captured by a linear combination of a finite number of basis functions (Basis expansion model (BEM)) [84, 85, 61, 86, 87, 88]. Channel response over a time interval can, therefore, be obtained by estimating those coefficients. Various basis functions such as complex exponential [85], Slepian functions [86] etc. have been investigated in the literature. These methods, in general are computationally more complex and are generally used when the channel is fast varying. They suffer when the channel variations do not follow the assumed model. In [88], MMSE, LS and BLUE symbol estimates for doubly selective channel that is assumed to be banded has been calculated from a set of pilot clusters. This assumes a generic BEM model for the channel. These clusters are mandatory as otherwise the LS matrix could become ill conditioned. A detailed overview of channel estimation techniques employed in OFDM systems, their advantages and drawbacks and relation to one another are presented in [89, 3] and the references therein.

Iterative channel estimation algorithms can be exploited to minimize the channel estimation errors [90, 57, 56, 91, 92, 93]. In this approach, the soft information obtained from the decoding process is used to remodulate the detected signal which then is used to improve the channel estimation iteratively. For e.g., in [90], LS based iterative estimation of both pilot and data subcarriers, followed by frequency domain combining

is employed. Better performance is achieved at the expense of more computations. The Expectation Maximization (EM) algorithm based iterative channel estimation [91] falls in this category.

4.3 System Model

Here we adopt the OFDM transceiver model described in 3.3.

4.4 Channel Estimation Algorithm

In this section, we propose a low complexity channel estimation scheme in OFDM systems under severe Doppler conditions. Following aspects are of prime consideration, while suggesting a practical solution to channel estimation problem for DVB-T like scenario. a) Any of the commercial standards, let it be DVB-T, DVB-H or 802.11a,g,n,ac have been developed with either equi-spaced pilots or training symbols. As explained in Chapter 2, equi-spaced pilots are the best configuration for static channel scenarios. A practical channel estimator to the existing network should be based on equi-spaced pilot pattern. b) DVB-T or 802.11x systems often encounter channels that are longer than the number of pilots in a OFDM symbol ($N_h > N_p$). For DVB-T, the Nordig requirement [94] has specially built-in test cases to test this scenario. Similar tests are devised for 802.11x systems as well. c) For DVB-T and 802.11x transmissions, commonly encountered normalized maximum Doppler spread is 0.2Hz which is generally higher than that can be handled by ordinary predictive algorithms d) Channel variations need not closely follow a proposed model and finally e) The estimator should be low in complexity.

The proposed algorithm makes use of the feedback symbol mean value, $\mu_x(k)$. $\mu_x(k)$ is used a) to compute and remove the ICI from the received data and b) to keep the LS estimator coefficients constant as explained in the sequel. At high Doppler frequencies, all the channel estimates need to be done essentially from a single OFDM symbol as the correlations between adjacent OFDM symbols diminish considerably. It has been established in [95] that for normalized Doppler of up to about 20%, channel time

variations can be approximated by piece-wise linear model with a constant slope over one OFDM symbol duration. Let $h_{avg}^j(l)$ and $\alpha^j(l)$ denote the time average and slope of the l^{th} channel tap at the j^{th} OFDM symbol respectively. The linear model for the l^{th} channel tap at the i^{th} time instant within the j^{th} OFDM symbol, $h^j(i, l)$, therefore, can be written as,

$$\begin{aligned} h^j(i, l) &= h_{avg}^j(l) + \left(i - \frac{N-1}{2}\right) \alpha^j(l), \\ 0 \leq i \leq N-1, 0 \leq l \leq N_h-1 \end{aligned} \quad (4.4)$$

where

$$h_{avg}^j(l) = \frac{1}{N} \sum_{i=0}^{i=N-1} h^j(i, l).$$

$h_{avg}^j(l)$ is obtained from the IFFT of the channel estimates at the pilot subcarriers as explained in the sequel. Knowing $h_{avg}^j(l)$, the slope $\alpha^j(l)$ can be computed easily from geometrical considerations [96, 70].

Define

$$\alpha_{pre}^j(l) = \frac{h_{avg}^j(l) - h_{avg}^{(j-1)}(l)}{N}, (j > 0)$$

and

$$\alpha_{post}^j(l) = \frac{h_{avg}^{(j+1)}(l) - h_{avg}^j(l)}{N}, j < j_{last},$$

(Ref. Fig. 4.3) where j_{last} is the last received OFDM symbol. Now,

$$\begin{aligned} \alpha^0(l) &= \alpha_{post}^0(l) \\ \alpha^j(l) &= \alpha_{pre}^j(l), i < \frac{N-1}{2} \\ &= \alpha_{post}^j(l), i \geq \frac{N-1}{2} \\ \alpha^{j_{last}}(l) &= \alpha_{pre}^{j_{last}}(l). \end{aligned} \quad (4.5)$$

We drop the superscript j in the development below.

As in the case of symbol estimation, approximating $x(d)$ by $\mu_x(d)$, we get, $y(k)$ from

(3.3) as

$$\begin{aligned}
y(k) &= \mathbf{H}(k, k)x(k) + \sum_{d=k-2L, d \neq k}^{k+2L} \mathbf{H}(k, d)x(d) + w(k) \\
&\approx \mathbf{H}(k, k)x(k) + \sum_{d=k-2L, d \neq k}^{k+2L} \mathbf{H}(k, d)\mu_x(d) + w(k).
\end{aligned} \tag{4.6}$$

Piecewise linear channel model in time domain, given by (4.7), leads to the following frequency domain channel coefficients,

$$\mathbf{H}(k, k) = \sum_{l=0}^{l=N_h-1} h_{avg}(l)e^{-j2\pi lk/N}, 0 \leq k \leq N-1 \tag{4.7}$$

and

$$\begin{aligned}
\mathbf{H}(k, d) &= \frac{1}{N} \sum_{l=0}^{l=N_h-1} \sum_{i=0}^{N-1} \left(i - \frac{N-1}{2} \right) \times \\
&\quad \alpha(l)e^{-j2\pi i(k-d)/N} e^{-j2\pi ld/N}, \\
0 \leq k \leq N-1, -L \leq (k-d) \leq L, d \neq k.
\end{aligned} \tag{4.8}$$

Define

$$\begin{aligned}
\mathbf{h}_{avg} &:= [h_{avg}(0), h_{avg}(1), \dots, h_{avg}(N_h-1)]^t, \\
\boldsymbol{\alpha} &:= [\alpha(0), \alpha(1), \dots, \alpha(N_h-1)]^t, \\
\mathbf{b}_k &= [1, e^{-j2\pi k/N}, \dots, e^{-j2\pi k(N_h-1)/N}]^t
\end{aligned}$$

and

$$C_{k-d} = \frac{-1}{1 - e^{-j2\pi(k-d)/N}}.$$

(4.7) and (4.8) can now be written as,

$$\mathbf{H}(k, k) = \mathbf{b}_k^t \cdot \mathbf{h}_{avg} \tag{4.9}$$

$$\mathbf{H}(k, d) = C_{k-d} \mathbf{b}_d^t \boldsymbol{\alpha} \tag{4.10}$$

In [59], \mathbf{h}_{avg} and $\boldsymbol{\alpha}$ are jointly estimated from the same OFDM symbol. For a satisfactory performance of this scheme, pilot tones should be partitioned into equi-spaced groups on the FFT grid. This limits the use of this scheme in systems such as DVB [8] or IEEE802.16 [20] where equi-spaced pilot pattern (no grouping) is deployed.

In the proposed scheme, as in the case of equalization, we first remove the ICI from the received data using the channel estimates and feedback symbol mean values obtained from the previous iteration. The modified system matrix is diagonal with the elements given in (4.9). Equi-spaced pilot pattern is best suited for \mathbf{h}_{avg} estimation in the modified system. This enables the proposed scheme not to have the limitation cited above thus making it especially suitable for practical systems. A progressively improving estimate of \mathbf{h}_{avg} is computed as explained below. An improved estimate of $\boldsymbol{\alpha}$ can now be obtained from the new \mathbf{h}_{avg} (4.5). Note from (4.9) and (4.10) that the diagonal elements of \mathbf{H} can be computed from \mathbf{h}_{avg} whereas the off diagonal elements (which causes ICI) of \mathbf{H} can be computed from $\boldsymbol{\alpha}$.

The ICI removed received data,

$$y'(k) \approx y(k) - \sum_{d=k-2L, d \neq k}^{k+2L} C_{k-d} \mathbf{b}_d^t \boldsymbol{\alpha} \mu_x(d),$$

can be written in vector form as below,

$$\mathbf{y}' = \text{diag}(\boldsymbol{\mu}_x) \cdot (\mathbf{A} \mathbf{h}_{\text{avg}}) + \mathbf{w} \quad (4.11)$$

where the $N \times N_h$ matrix \mathbf{A} is given by

$$\mathbf{A} = [\mathbf{b}_0, \mathbf{b}_1, \dots, \mathbf{b}_{N-1}]^t.$$

Premultiplying (4.11) with $(\text{diag}(\boldsymbol{\mu}_x))^{-1}$, we get

$$\check{\mathbf{y}} = \mathbf{A} \mathbf{h}_{\text{avg}} + \check{\mathbf{w}} \quad (4.12)$$

where

$$\check{\mathbf{y}} = [\frac{y'(0)}{\mu(0)}, \dots, \frac{y'(N-1)}{\mu(N-1)}]^t$$

and

$$\check{\mathbf{w}} = [\frac{w(0)}{\mu(0)}, \dots, \frac{w(N-1)}{\mu(N-1)}]^t.$$

The LS estimate of \mathbf{h}_{avg} can be obtained from (4.12) as,

$$\mathbf{h}_{\text{avg}} = (\mathbf{A}^H \mathbf{A})^{-1} \mathbf{A}^H \check{\mathbf{y}}. \quad (4.13)$$

Observe that the LS coefficients, $(\mathbf{A}^H \mathbf{A})^{-1} \mathbf{A}^H$, are constants and can be pre-computed and stored thus avoiding costly matrix multiplication and inverse operations and making this estimation scheme low in complexity. We thus estimate each $h_{avg}(l)$ with only a vector multiplication. Our aim is to generate an initial estimate of \mathbf{h}_{avg} and $\boldsymbol{\alpha}$ using pilots and subsequently refine them in every iteration using the feedback mean values. Assume that there are P pilot tones and they are placed at subcarriers $\mathbb{P} = \{p(1), \dots, p(P)\}$. Transmit symbols at pilot tones $x_p(1), x_p(2), \dots, x_p(P)$ are known at the receiver. The initial estimate of \mathbf{h}_{avg} is computed using the LS solution,

$$\mathbf{h}_{avg} = (\mathbf{A}_p^H \mathbf{A}_p)^{-1} \mathbf{A}_p^H \check{\mathbf{y}}_p \quad (4.14)$$

where

$$\mathbf{A}_p = [\mathbf{b}_{p(1)}, \mathbf{b}_{p(2)}, \dots, \mathbf{b}_{p(P)}]^t$$

and

$$\check{\mathbf{y}}_p = [\check{y}_{p(1)}, \check{y}_{p(2)}, \dots, \check{y}_{p(P)}]^t.$$

For the first iteration only pilot subcarriers are used for channel estimation as no feedback information is available from the decoder. No ICI is removed from \mathbf{y} for the initial channel estimate. For subsequent iterations, compute \mathbf{h}_{avg} by setting $\check{y}(k) = 0$ or $\check{y}(k) = y'(k)/\mu_x(k)$ in (4.13), based on a threshold value of the conditional feedback variance $\nu_x(k)$ (3.12) obtained from the decoder at the end of the previous iteration. The threshold should be small enough so that $\mu_x(k)$ is close to the actual symbol value. Since $\nu_x(k)$ is small, hard slicing $\mu_x(k)$ to the nearest $x(k)$ also is found to be effective as the error propagation is largely absent. $\boldsymbol{\alpha}$ is computed from (4.5). As $\nu_x(k) \rightarrow 0$, $\mu_x(k) \rightarrow x(k)$. Thus the channel estimate progressively improves as the iterations proceed. If $N_h \leq N_p$, LS estimate can also be computed from a sub matrix \mathbf{A}_{CP} of \mathbf{A} , such that \mathbf{A}_{CP} is at least $N_p \times N$ in size and the chosen N_p rows should contain the rows corresponding to that of pilots in the system.

A distinct advantage of this iterative estimation method is that it does not set the lower limit, $(N_h \leq P)$, on the number of pilot subcarriers, as most of the data carriers act as pilots from the second iteration onwards. Operation of the proposed Iterative Receiver (IR) algorithm is enumerated in the next subsection.

4.4.1 The Proposed IR with SIC-MAP

1. Choose the maximum number of iterations. For each iteration and for each frequency bin k ,
2. Compute channel estimate $\mathbf{H}_{\mathbf{k}}$.
 - (a) Compute \mathbf{h}_{avg} ((4.13) or (4.14) as the case may be). $\mu_x(k) = 0$ for first iteration, use $\mu_x(k)$ from steps 11, 12 otherwise. For each frequency bin k , compute $\mathbf{H}(k, k)$ (4.9).
 - (b) Compute $\boldsymbol{\alpha}$ (4.5). Compute $\mathbf{H}(k, d)$ for all $d \neq k$ ($k - 2L \leq d \leq k + 2L$) (4.10).
3. Compute $\tilde{\mathbf{y}}_{\mathbf{k}}$ from \mathbf{y} (3.6). $\mu_x(k) = 0$ for first iteration, use $\mu_x(k)$ from steps 11,12 otherwise.
4. Perform symbol de-interleaving.
5. Compute $\text{LLR}_{\text{ext}}(c(\cdot))$ (3.8),(3.9).
6. Perform bit de-interleaving.
7. Compute $\text{LLR}_{\text{app}}(b(n))$ using BCJR/SOVA.
8. If $\text{LLR}_{\text{app}}(b(n))$ s are sufficiently converged or the maximum number of iterations are reached, hard-slice $\text{LLR}_{\text{app}}(b(n))$. Output the information bits $\hat{a}(n)$ and stop the iterations; otherwise,
9. Compute $\text{LLR}'_{\text{ext}}(b(n))$.
10. Perform bit interleaving.
11. Compute $\mu'_s(k)$ (3.11).
12. Perform symbol interleaving.
13. Go to step 2.

Table 4.1: Complexity Computation - Channel Estimation.

Initialize the LS coefficients $(\mathbf{A}^H \mathbf{A})^{-1} \mathbf{A}^H$ or $(\mathbf{A}_p^H \mathbf{A}_p)^{-1} \mathbf{A}_p^H$				
Initialize Look up table for $e^{\frac{-j2\pi lk}{N}}$				
Initialize Look up table for C_{k-d}				
step	Variable	Operation	MMSE-OND2 per sample	SIC-MAP per sample per iter.
1	\mathbf{y}' in (4.11)	\times \div	— —	$4L$ —
2	$\check{\mathbf{y}}$ in (4.12)	\times \div	— $\frac{P}{N}$	— 1
3	\mathbf{h}_{avg} (4.13)	\times \div	$N_h \frac{P}{N}$ —	N_h —
4	$\boldsymbol{\alpha}$ in (4.5)	\times \div	— $\frac{N_h}{N}$	— $\frac{N_h}{N}$
5	$\mathbf{H}(k, k)$ (4.9)	\times \div	N_h —	N_h —
6	$\mathbf{H}(k, d)$ (4.10)	\times \div	$(N_h + 1)4L$ —	$(N_h + 1)4L$ —
	Total	\times \div	$4L + (4L + 1 + P/N)N_h$ $\frac{N_h + P}{N}$	$(4L + 2)N_h + 8L$ $1 + \frac{N_h}{N}$

4.5 Computational Complexity

Channel estimation is performed in the time domain using frequency domain interference canceled observation vector. Matrix multiplication and inverse described in (4.13, 4.14) can be pre-computed and stored. This will let a vector multiplication to make a channel tap (average) estimate. The slope of the channel can be computed easily and thus the overall channel estimation is computationally less complex compared to its LS counterparts where matrix inversion has to be performed as well. The complexity of the proposed scheme is proportional to the number of significant channel taps. The scheme has approximately linear complexity per iteration. A more accurate account of the complexity computation is given in Table 4.1. Note that the adaptive algorithm described in [81] has comparable computational complexity.

4.6 Simulation Results

In this section we examine the results of numerical simulations of the proposed IR over doubly selective channels. We consider the same OFDM system from Chapter 3. Performance of MMSE-TE-OND2 and SIC-MAP based IRs that employ the aforementioned channel estimation scheme are compared. The non-iterative MMSC-OND2 receiver is also used in our study. Each channel path is Rayleigh fading characterized by Jakes Doppler Spectrum (exponentially decaying power delay profile) with a normalized Doppler frequency spread of 20% of the sub-carrier spacing. The receivers are assumed to have $N_p = 32$ equi-spaced pilots per OFDM symbol. The system has $N_h = 30$.

Performance of the IRs, as can be seen from Fig. 4.1, is significantly better than the non-iterative receiver at moderate to high SNR region. As will be seen later in Sec. 5.5, at low SNRs, mutual information does not tend to 1 over multiple iterations. In this case, $\mu_x(k) \not\rightarrow x(k)$. The inferior performance of the iterative scheme at low SNRs can be attributed to the insufficient convergence of the scheme at low SNRs over multiple iterations.

Both the iterative schemes perform near identically as expected. Fig. 4.2 depicts the behavior of the estimation scheme when the number of channel taps ($N_h = 40$) are more than the number of pilots ($N_p = 32$). Comparing Figures 4.1 and 4.2, it is clear that the iterative schemes perform identically in both the scenarios ($N_h \leq P$ and $N_h > P$), due to the availability of increased number of “pilots”, at SNRs of practical interest whereas the non-iterative scheme performance is considerably poor in the latter case.

At high SNRs the noise in the system due to imperfect channel estimation dominates and this causes the error floor. This loss in performance is justified because we employ a LS based channel estimator, which although is known to be a robust estimator (requiring no knowledge about the channel and noise statistics), performs inferior when the interference is prominent. Besides, In addition to the LS estimator inaccuracies, the piece-wise modeling of time domain channel taps is barely valid [95] at such high Doppler frequencies. More expensive estimators such as the one described in [88] could

provide more accurate channel values (and lower noise floors).

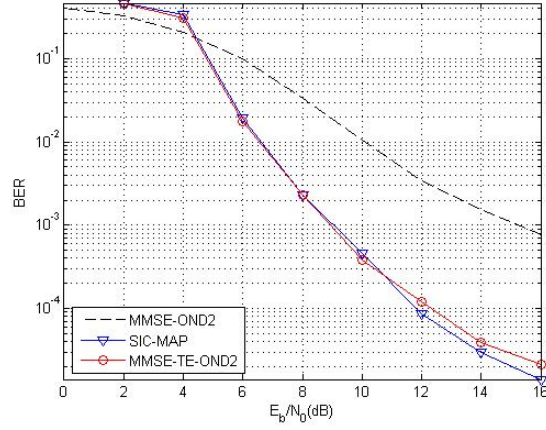


Figure 4.1: BER Plots - TE-MMSE-OND2 and SIC-MAP Based IRs With Channel Estimation ($N_h \leq P$). ($f_d T_s N = 0.2$, $N = 256$, $L = 1$, $\#iter = 3$, $P = 32$, $N_h = 30$).

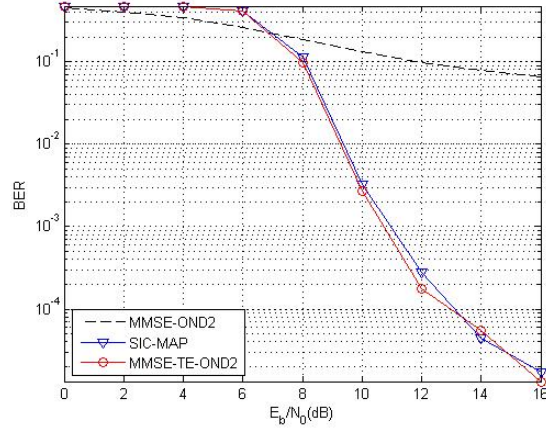


Figure 4.2: BER Plots - TE-MMSE-OND2 and SIC-MAP Based IRs With Channel Estimation ($N_h > P$). ($f_d T_s N = 0.2$, $N = 256$, $L = 1$, $\#iter = 3$, $P = 32$, $N_h = 40$).

4.7 Conclusion

A low complexity iterative LS channel estimation scheme, suitable for practical iterative receivers, is proposed in this chapter. Besides low complexity, another advantage of the iterative channel estimation scheme is that, unlike pilot-only based LS schemes,

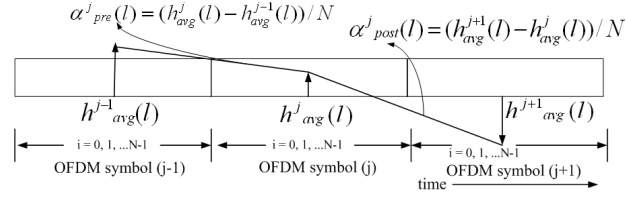


Figure 4.3: Slopes $\alpha^j_{pre}(l)$ and $\alpha^j_{post}(l)$ in Channel Estimation.

it works satisfactorily for systems that has higher number of channel taps than pilot subcarriers, a phenomenon that is commonly encountered in DVB systems deployed in single frequency networks.

Chapter 5

Low Complexity Turbo Equalization Scheme for Multi Antenna OFDM Systems

5.1 Introduction

We have discussed the advantages of OFDM systems and MIMO transmission in Chapter 1. MIMO-OFDM based transmission systems can provide very high data rates with a relatively simple receiver design and are now adopted in many recent wireless communication standards. For e.g., 802.11n [22] specifies a maximum of 600Mb/s using four independent spatial streams transmitted over a 40MHz channel whereas IEEE-802.11ac [23] specifies a data rate of up to 3.5Gb/sec using eight independent spatial streams (with eight transmit and eight receive antennas) in 80MHz channel. WiMAX [19, 21] specifies a limit of approximately 100 Mb/s using four spatial streams in a 5MHz channel and LTE suggests a peak data rate of 326.4 Mb/s using a 20 MHz downlink with four transmit antennas [16].

Under static multipath channel conditions (e.g., as assumed for WLAN systems [22, 23]), the received signal in the MIMO receiver is corrupted only by CAI. However, high transceiver mobility at high carrier frequency causes severe time-varying frequency-selective multipath fading at the receiver. This breaks the orthogonality of subcarriers and, hence, causes ICI in the received signal. As an example, in WiMAX and LTE, we generally encounter doubly dispersive channels such as the one described by Vehicular-A channel model [97]. At a transmission frequency of 5GHz and at vehicular speeds of 240kmh to 480kmh which are common in high speed trains, the expected maximum receiver Doppler spread in these systems is of the order of 12 to 23 percent of the inter-carrier spacing (ICS). It is believed that future wireless communications will adopt higher carrier frequencies and higher mobility requirements and, thus, further increasing

the maximum relative Doppler frequency and exacerbating the ICI. In such scenarios, efficient detector design for MIMO-OFDM systems is a challenging practical problem.

As we observed in Chapter 3, turbo iterative detection schemes have good performance; however they suffer from high computation complexity which makes their implementation expensive both in terms of silicon area and battery power. Motivated by the above challenges, in this chapter, we have extended the low complexity SISO detector design of Chapter 3, SIC-MAP, to OFDM MIMO systems (SIC-MAP-MIMO) and have analyzed its performance both in static and dynamic channel conditions [98, 99]. It has been found that SIC-MAP-MIMO provides a comparable performance to MMSE-OND2-MIMO (MMSE-OND2 from Chapter 3 extended to MIMO) and TE-BLK2-MIMO (TE-BLK2 from Chapter 3 extended to MIMO) but with significantly less computational complexity. Additionally, SIC-MAP-MIMO is specifically suited for channel equalization of mobile devices where available battery power in the receiver is limited, as it can very effectively trade the system performance against the available battery power.

SIC-MAP-MIMO leverages on the soft feedback symbol estimate to remove the intercarrier interference (ICI) and co-antenna interference (CAI) from the received data thus making the subsequent MAP decoding simple. As will be demonstrated later, CAI can be found to be a higher source of interference compared to ICI even at high Doppler frequencies. It has been found that SIC-MAP-MIMO performs equally as good as in SISO case even with CAI, but requires a few additional iterations. Significant computational savings are achieved even after considering the higher number of iterations.

5.2 Related Work

The Iterative Interference Cancellation scheme proposed in section 5.4 is related to, yet distinct from a number of published algorithms. The field of SIC is quite rich and so a comprehensive survey of the published SIC schemes is not within the scope of this thesis. However our work is briefly contrasted below with a few salient ones published in the last decade.

Some early MIMO equalization schemes proposed in the literature to cope with ICI and CAI are: a) block linear [100]; b) banded MMSE linear [70]; and c) banded MMSE decision-feedback [101]. More recently, various iterative equalization schemes based on successive cancellation of ICI and CAI [42, 102, 91, 103, 104] or MMSE TE [40, 105, 106, 57, 107, 108, 109, 110] were proposed. [102] is an extension of the scheme proposed in [42] (discussed in Chapter 3). However in [102], additional filtering is performed to suppress both the ISI and MAI residuals. These schemes require $O(N^2)$ operations. Ref. [91] describes EM based iterative receiver. [105] proposes TE for space-time-trellis coded (STTrC)MIMO systems. In [103], derived for MIMO systems, a new MMSE filter taking the decision errors into account is derived. MMSE estimate of each QAM symbol from each antenna (rather than a joint estimation of symbols from all antennas) is used successively to cancel the interference coming from other antennas. [111] proposes a similar SIC scheme for Time Reversal Space Time Block Coded (TR-STBC) systems. [104] deals with the design of a multi-user detector in a CDMA system. In a CDMA environment, unlike in a single user scenario, the interferers are many and the order in which the interference cancellation is performed can result in significant performance differences (If there are K users, there are $K!$ different cancellation orderings). Interference from each user is computed using the channel values and MMSE estimate (after slicing) (MMSE based Decision Feedback (DF) detector) of each transmitted symbol. The proposed design employs successive parallel cancellation of interferences from parallel arbitrated branches. The proposed architecture uses different orders of cancellation and selects the most likely estimate. [106] describes a technique similar to the one in [40], but for static channel MIMO systems working in a hostile jamming environment. In [57] the received signal is split into small segments such that the channel remain approximately static during each small segment. Suitable signal processing is performed on each of these segments such that the resulting channel matrix is made diagonal. TE, such as the one described in [40], is performed on the modified system to recover the received bits. Ref. [91, 106, 57] has one aspect in common. They try to obtain a modified system with only diagonal entries using different techniques. Ref. [108] proposes a TE for static channel MIMO

OFDM systems with higher order modulation where the soft information as in [40] is derived from the equalizer output. Ref. [112, 110] and [113] propose TEs where ISI and CAI are treated separately to bring down the computational complexity. Scheme proposed in [107] is similar to [2] (discussed in Chapter 3), but extended to OFDM MIMO. It proposes a new window for received signal. SIC-MAP-MIMO does not perform windowing, but better performance can be expected with any of the windowing proposed above. In [109] an OFDM MIMO detection based on successive cancellation of interference is proposed. Using a novel LLR criteria, the layers with least MSE error are successively identified and MMSE based TE is then applied iteratively to estimate the symbols from the selected layer. The contributions of these estimated symbols are then subtracted from the observation before making a new MMSE estimate. This is unlike in a typical V-BLAST scheme where no distinction is made between layers while computing the interference. In general [109, 103, 104] deal with co-antenna interference in MIMO systems in static channels. In this scenario, as is demonstrated in the works above, optimal ordering of the interference cancellation can improve the performance significantly as the SNRs on each channel can vary significantly.

In SIC-MAP-MIMO, copies of the received signal on the same and adjacent subcarriers of all receive antennas are carefully separated out to obtain frequency diversity. The resulting system matrix is a column matrix. It has been identified through simulations that the banded sparse structure of the system matrix, as in the case of doubly selective MIMO channels, allows this simplification without sacrificing the performance. MAP decoding is performed on this simplified system. SIC-MAP-MIMO is perhaps close to the inter symbol interference cancellation stage of [42]. However, unlike [42] and [102], SIC-MAP-MIMO requires only $O(N)$ operations. It leverages the banded sparse structure (as shown in Fig 5.2) of the single user LTV MIMO system matrix to reorder ICI cancellation to obtain frequency diversity.

5.3 System Model

The MIMO OFDM transceiver system with n_T transmit and n_R receive antennas is shown in Fig. 5.1. We assume that $n_T \leq n_R$. Information bits ($\{a\}$) are convolution-

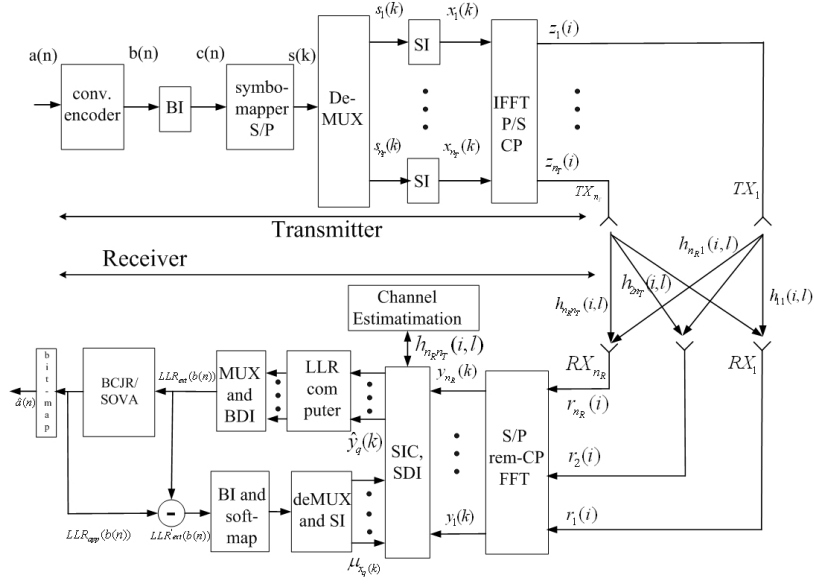


Figure 5.1: MIMO OFDM Transceiver.

ally encoded ($\{b\}$) and passed through a bit interleaver (BI) ($\{c\}$). The symbol mapper modulates them into QAM symbols ($\{s\}$). A set of N of these coded QAM “frequency domain” symbols is collected to form an OFDM symbol. The demultiplexer collects n_T OFDM symbols (an OFDM symbol frame) and sends each symbol ($\{s_q\}$) to one of the n_T transmit paths. Symbol interleaver (SI) in each path interleaves them ($\{x_q\}$). As discussed in 3.3, IFFT is performed, CP is added ($\{z_q\}$) and these samples are then simultaneously transmitted from n_T transmit antennas. At the receiver, the CP removed OFDM data from each receive antenna is converted back to the “frequency domain” by performing N point DFT and passed to the Successive Interference Canceller (SIC) and Symbol deinterleaver (SDI). LLR (Log Likelihood Ratio) Computer computes the LLRs of the received bits from the interference removed observation. This is appropriately multiplexed, bit de-interleaved (BDI) and passed to a BCJR or SOVA based decoder. We assume perfect carrier, symbol and sample synchronization at the receiver. Besides it is assumed that the channel is known at the receiver. If channel is unknown, it can be estimated using the methods described in [89, 95, 90, 114, 93]. Mathematical modeling of this system has been described in Sec. 2.2.3.

In this chapter, since we deal only with MIMO systems, the superscript (m) can be

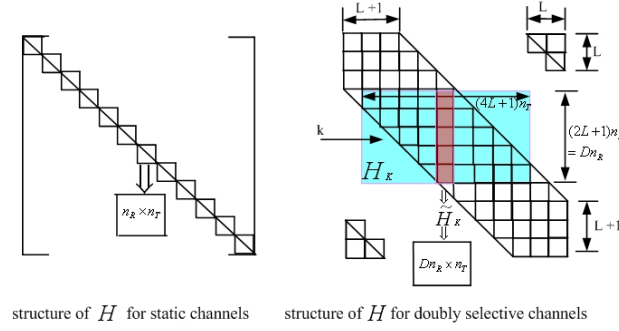


Figure 5.2: MIMO OFDM Channel Structure.

dropped without ambiguity from the formulation in Sec. 2.2.3. Thus $\mathbf{H}^{(\mathbf{m})}$ from Sec. 2.2.3, for example, is denoted simply as \mathbf{H} in this chapter.

In the case of MIMO systems in Rayleigh fading channels, as was in the case of SISO systems, it has been shown that \mathbf{H} in (2.16) will be a block-banded matrix with significant block coefficients concentrated in a banded structure, with width D along the diagonal [100, 101]. The value of D is chosen as in the case of SISO. If the channel is static, Ξ will be a block circulant matrix and \mathbf{H} will be a block diagonal matrix. Different structures of \mathbf{H} are shown in Fig. 5.2.

5.4 Successive Interference Cancellation Based MAP Receiver: MIMO (SIC-MAP-MIMO)

5.4.1 Formulation of the Proposed MAP Receiver

In this section, we redesign SIC-MAP from Sec. 3.4 for MIMO systems. The proposed scheme, as in the case of SISO, simplify the system matrix to a single column matrix by selectively removing the ICI and CAI interference from the received symbols which are computed using the feedback symbol mean values. Soft information is computed directly from this modified model and is fed to a MAP bit decoder.

Observations from Sec. 3.4, are modified as below in the context of MIMO systems.

1. The relative magnitude of each subblock and superblock diagonal element of the doubly selective Rayleigh fading channel matrix \mathbf{H} decreases significantly as we

move away from the main diagonal (Fig. 5.2). We ignore all elements that are far away from the main diagonal.

2. As the *extrinsic* information becomes more accurate over multiple turbo iterations, the conditional mean, $\underline{\boldsymbol{\mu}_{\mathbf{x}}(k)} \rightarrow \mathbf{x}(k)$, which is the true symbol value and the conditional variance, $\underline{\boldsymbol{\nu}_{\mathbf{x}}(k)} \rightarrow \mathbf{0}_{n_T \times 1}$. Therefore, in each new iteration, we can use $\boldsymbol{\mu}_{\mathbf{x}}(k)$ from the previous iteration to selectively remove CAI and ICI from the received symbol in such a manner that the resulting system matrix is a column vector. MAP decoding of the modified system is computationally efficient to implement.

Based on observation one, (2.16) can be approximated as,

$$\begin{aligned} \mathbf{y}_{\mathbf{k}} &:= [\mathbf{y}(\langle k-L \rangle_N), \dots, \mathbf{y}(\langle k+L \rangle_N)]^t \\ &= \mathbf{H}_{\mathbf{k}} \mathbf{x}_{\mathbf{k}} + \mathbf{w}_{\mathbf{k}}, \end{aligned} \quad (5.1)$$

where

$$\begin{aligned} \mathbf{x}_{\mathbf{k}} &:= [\mathbf{x}(\langle k-2L \rangle_N), \dots, \mathbf{x}(\langle k+2L \rangle_N)]^t, \\ \mathbf{w}_{\mathbf{k}} &:= [\mathbf{w}(\langle k-L \rangle_N), \dots, \mathbf{w}(\langle k+L \rangle_N)]^t \end{aligned}$$

and $\mathbf{H}_{\mathbf{k}}$ is the shaded (green) section of \mathbf{H} in Fig. 5.2 (right) given by (5.2). Note that modulo-N ($\langle \rangle_N$) operation is used in the equation above; thanks to the CP in the system.

$$\mathbf{H}_{\mathbf{k}} := \begin{bmatrix} \mathbf{H}(\langle k-L \rangle_N, \langle k-2L \rangle_N) & \dots & \mathbf{H}(\langle k-L \rangle_N, \langle k+2L \rangle_N) \\ \mathbf{H}(\langle k-L+1 \rangle_N, \langle k-2L \rangle_N) & \dots & \mathbf{H}(\langle k-L+1 \rangle_N, \langle k+2L \rangle_N) \\ \dots & \dots & \dots \\ \mathbf{H}(\langle k+L \rangle_N, \langle k-2L \rangle_N) & \dots & \mathbf{H}(\langle k+L \rangle_N, \langle k+2L \rangle_N) \end{bmatrix} \quad (5.2)$$

Each element $\mathbf{H}(m, n)$ in (5.2) (one small grid in Fig. 5.2) is itself a matrix of size $n_R \times n_T$ given as

$$\mathbf{H}(m, n) := \begin{bmatrix} H_{11}(m, n) & \dots & H_{1n_T}(m, n) \\ \dots & \dots & \dots \\ H_{n_R 1}(m, n) & \dots & H_{n_R n_T}(m, n) \end{bmatrix}. \quad (5.3)$$

For simplicity of notation, the modulo operation ($\langle \rangle_N$) is omitted in the sequel.

Now,

$$\mathbf{x}_k = \boldsymbol{\mu}_{\mathbf{x}_k} + \boldsymbol{\delta}_{\mathbf{x}_k}$$

where $\boldsymbol{\delta}_{\mathbf{x}_k}$ is the residual error, which approaches $\mathbf{0}_{(4L+1)n_T}$ as the extrinsic LLR becomes more reliable over multiple iterations. Substituting for \mathbf{x}_k in (5.1) and rearranging yields (5.4). $\tilde{\mathbf{w}}_k$, the new noise, contains the ICI from the residual error $\boldsymbol{\delta}_{\mathbf{x}_k}$. $\tilde{\boldsymbol{\mu}}_{\mathbf{x}_k}$ is as defined in (5.4).

$$\mathbf{y}_k = \mathbf{H}_k[\mathbf{i}_{2L \cdot n_T}, \dots, \mathbf{i}_{(2L+1) \cdot n_T - 1}] \mathbf{x}(k) + \underbrace{\mathbf{H}_k \begin{bmatrix} \mu_{\mathbf{x}}(k-2L) \\ \vdots \\ \mathbf{0}_{n_T} \\ \vdots \\ \mu_{\mathbf{x}}(k+2L) \end{bmatrix}}_{\tilde{\boldsymbol{\mu}}_{\mathbf{x}_k}} + \underbrace{\mathbf{H}_k \begin{bmatrix} \delta_{\mathbf{x}}(k-2L) \\ \vdots \\ \mathbf{0}_{n_T} \\ \vdots \\ \delta_{\mathbf{x}}(k+2L) \end{bmatrix}}_{\tilde{\mathbf{w}}_k} + \mathbf{w}_k \quad (5.4)$$

Let

$$\begin{aligned} \tilde{\mathbf{y}}_k &:= \mathbf{y}_k - \mathbf{H}_k \tilde{\boldsymbol{\mu}}_{\mathbf{x}_k} \\ &= \mathbf{H}_k[\mathbf{i}_{2L \cdot n_T}, \dots, \mathbf{i}_{(2L+1) \cdot n_T - 1}] \mathbf{x}(k) + \tilde{\mathbf{w}}_k \\ &= \tilde{\mathbf{H}}_k \mathbf{x}(k) + \tilde{\mathbf{w}}_k. \end{aligned} \quad (5.5)$$

Notice that $\tilde{\mathbf{y}}_k \in \mathcal{C}^{D \cdot n_R}$ and $\mathbf{x}(k) \in \mathcal{C}^{n_T}$ and $\tilde{\mathbf{H}}_k$ is shown in red in Fig. 5.2 (right). It is a matrix of size $D \cdot n_R \times n_T$. For static channels where $L = 0$, $\tilde{\mathbf{y}}_k$ will only have n_R nonzero elements at the center. While dealing with the reception of $x_q(k)$, the k^{th} symbol from the q^{th} transmit antenna, k^{th} symbols from all other transmit antennas ($\{x_l(k)_{l \neq q}\}$) are causing CAI on the received samples \mathbf{y}_k . Using similar techniques as above, the CAI can be estimated and removed from the system as well. The resulting system equation is

$$\mathbf{y}'_{\mathbf{q}_k} = \mathbf{h}_{\mathbf{q}_k} x_q(k) + \mathbf{w}'_{\mathbf{q}_k}, \quad (5.6)$$

where

$$\mathbf{y}'_{\mathbf{q}_k} := \tilde{\mathbf{y}}_k - \tilde{\mathbf{H}}_k \tilde{\boldsymbol{\mu}}_{\mathbf{x}_q}(k),$$

$$\mathbf{h}_{\mathbf{qk}} := \tilde{\mathbf{H}}_{\mathbf{k}} i_q,$$

$$\tilde{\mu}_{\mathbf{xq}}(k) := [\mu_{x_1}(k), \dots, \mu_{x_{q-1}}(k), 0, \mu_{x_{q+1}}(k), \dots, \mu_{x_{n_T}}(k)]^t$$

and

$$\mathbf{w}'_{\mathbf{qk}} := \tilde{\mathbf{w}}_{\mathbf{k}} + \tilde{\mathbf{H}}_{\mathbf{k}} \tilde{\delta}_{\mathbf{xq}}(k),$$

where

$$\tilde{\delta}_{\mathbf{xq}}(k) := [\delta_{x_1}(k), \dots, \delta_{x_{q-1}}(k), 0, \delta_{x_{q+1}}(k), \dots, \delta_{x_{n_T}}(k)]^t.$$

We assume $\mathbf{w}'_{\mathbf{qk}}$ has a variance of $\sigma'^2 I_{(2L+1)n_R}$. As noted earlier and as will be shown later, the combined contributions of residual ICI and CAI to the noise variance σ'^2 is small and decreasing over multiple iterations as the reliability in the feedback information increases. We thus approximate $\sigma'^2 \mathbf{I}_{n_R(2L+1)} \approx \sigma^2 \mathbf{I}_{n_R(2L+1)}$. This is further analyzed in sec. 5.4.4.

LLR Computer calculates, $\text{LLR}_{\text{ext}}(c_q(n))$, the *extrinsic* LLR. It represents information about $c_q(n)$ contained in $\mathbf{y}'_{\mathbf{qk}}$ and $P(c_q(l))$ for all $l \neq n$. These are passed to a MAP decoder where they are used as *a priory* LLRs. $\text{LLR}_{\text{ext}}(c_q(n))$ is calculated from the modified system using (5.7), where $0 \leq i \leq Q-1$, $\mathcal{S} = [m_0, m_1, \dots, m_{Q-1}]^t \in F_2$, $\{\eta\} = \text{map}(\mathcal{S})$, is the signal constellation and F_2 is binary Galois Field. Q denotes the number of bits per symbol. For e.g., $Q = 1$ for BPSK, $Q = 2$ for QPSK and so on.

$$\begin{aligned} \text{LLR}_{\text{ext}}(c_q(Qk+i)) &= \text{LLR}_{\text{app}}(c_q(Qk+i)) - \text{LLR}(c_q(Qk+i)) \\ &= \ln \frac{P((c_q(Qk+i)=0)|\mathbf{y}'_{\mathbf{qk}})}{P((c_q(Qk+i)=1)|\mathbf{y}'_{\mathbf{qk}})} - \text{LLR}(c_q(Qk+i)) \\ &= \ln \frac{p(\mathbf{y}'_{\mathbf{qk}}|(c_q(Qk+i)=0))P(c_q(Qk+i)=0)}{p(\mathbf{y}'_{\mathbf{qk}}|(c_q(Qk+i)=1))P(c_q(Qk+i)=1)} - \text{LLR}(c_q(Qk+i)) \\ &= \ln \frac{p(\mathbf{y}'_{\mathbf{qk}}|(c_q(Qk+i)=0))}{p(\mathbf{y}'_{\mathbf{qk}}|(c_q(Qk+i)=1))} + \text{LLR}(P(c_q(Qk+i))) \\ &\quad - \text{LLR}(c_q(Qk+i)) \\ &= \ln \frac{\sum_{\mathcal{S} \in F_2: \mathcal{S}_i=0} p(\mathbf{y}'_{\mathbf{qk}}|(x_q(k) = \text{map}(\mathcal{S}))) \prod_{j=0: j \neq i}^{Q-1} P(m_j)}{\sum_{\mathcal{S} \in F_2: \mathcal{S}_i=1} p(\mathbf{y}'_{\mathbf{qk}}|(x_q(k) = \text{map}(\mathcal{S}))) \prod_{j=0: j \neq i}^{Q-1} P(m_j)} \end{aligned} \quad (5.7)$$

As shown in Appendix, 5.9, for QPSK, the above expression can be simplified as

$$\text{LLR}_{\text{ext}}(c_q(2k)) = \frac{\sqrt{8} \text{Re}(\mathbf{y}'_{\mathbf{qk}}{}^H \mathbf{h}_{\mathbf{qk}})}{n_T \sigma^2} \quad (5.8)$$

$$\text{LLR}_{\text{ext}}(c_q(2k+1)) = \frac{\sqrt{8} \text{Im}(\mathbf{y}'_{\mathbf{qk}}{}^H \mathbf{h}_{\mathbf{qk}})}{n_T \sigma^2}. \quad (5.9)$$

5.4.2 Example

Consider an OFDM system with $N = 64$, $CP = N/8$, sample duration $T_s = 7/64 \mu\text{sec}$, $n_T = 2$ and $n_R = 3$. Also consider a time varying channel with a Doppler frequency f_d of 900 Hz. In this case, $L = \lceil f_d T_s N \rceil = 1$. For illustration purposes, $\mathbf{h}_{\mathbf{q}\mathbf{k}}$ is given below for different values of q and k . For $q = 1, k = 9$,

$$\mathbf{h}_{\mathbf{1}_9} := [H_{11}(8, 9) \ H_{21}(8, 9) \ H_{31}(8, 9) \ H_{11}(9, 9) \\ H_{21}(9, 9) \ H_{31}(9, 9) \ H_{11}(10, 9) \ H_{21}(10, 9) \ H_{31}(10, 9)]^t.$$

If the channel is static,

$$\mathbf{h}_{\mathbf{1}_9} := [0 \ 0 \ 0 \ H_{11}(9, 9) \ H_{21}(9, 9) \ H_{31}(9, 9) \ 0 \ 0 \ 0]^t.$$

For $q = 2, k = 9$,

$$\mathbf{h}_{\mathbf{2}_9} := [H_{12}(8, 9) \ H_{22}(8, 9) \ H_{32}(8, 9) \ H_{12}(9, 9) \\ H_{22}(9, 9) \ H_{32}(9, 9) \ H_{12}(10, 9) \ H_{22}(10, 9) \ H_{32}(10, 9)]^t.$$

For $q = 1, k = 1$,

$$\mathbf{h}_{\mathbf{1}_1} := [H_{11}(63, 1) \ H_{21}(63, 1) \ H_{31}(63, 1) \ H_{11}(1, 1) \\ H_{21}(1, 1) \ H_{31}(1, 1) \ H_{11}(2, 1) \ H_{21}(2, 1) \ H_{31}(2, 1)]^t.$$

5.4.3 Receiver Operation

The SIC-MAP-MIMO system block diagram is shown in Fig. 5.1. Elements of $\mathbf{H}_{\mathbf{k}}$ are obtained from the channel estimation block [89, 95, 90, 114, 93]. BCJR or SOVA [35] based decoders compute $\text{LLR}_{\text{app}}(b(n))$ —the a posteriori reliability information of each coded bit—in the log likelihood ratio (LLR) form. The input *a priori* LLR to the decoder is subtracted from $\text{LLR}_{\text{app}}(b(n))$ to obtain the *extrinsic* reliability information $\text{LLR}'_{\text{ext}}(b(n))$. It is passed through a bit interleaver and is used in the soft-mapper to compute mean $\mu'_{\mathbf{s}}$. This is demultiplexed appropriately to obtain $\mu'_{\mathbf{s}_1}, \mu'_{\mathbf{s}_2}, \dots, \mu'_{\mathbf{s}_{n_T}}$. These are symbol interleaved to produce $\mu_{\mathbf{x}_1}, \mu_{\mathbf{x}_2}, \dots, \mu_{\mathbf{x}_{n_T}}$ which, in turn, are used in SIC-MAP-MIMO to remove the ICI and CAI interference as described in (5.4) and (5.6). The ICI and CAI removed data is fed to the LLR Computer to generate more

reliable LLRs to further improve the output bit estimate. This process is repeated until further gains are insignificant. $\text{LLR}_{\text{app}(b(n))}$ are then hard-sliced at the bit-map block and information bit estimates $\hat{a}(n)$ are retrieved from the received data bit estimates $\hat{b}(n)$. Mapping $\text{LLR}'_{\text{ext}}(b(n))$ s to $\mu'_s(k)$ and conditional variance, $\nu'_s(k)$, is described in [40]. For QPSK modulation,

$$\begin{aligned}\mu'_s(k) &= \tanh(\text{LLR}'_{\text{ext}}(c(2n))/2) \\ &\quad + i \tanh(\text{LLR}'_{\text{ext}}(c(2n+1))/2)\end{aligned}\tag{5.10}$$

$$\nu'_s(k) = 1 - |\mu'_s(k)|^2\tag{5.11}$$

5.4.4 Computation of Residual ICI and CAI

Neglecting the terms in \mathbf{H} that are beyond the band (shaded area in Fig. 5.2), the interference canceled signal $y_p(k)$ at the l^{th} iteration can be represented as,

$$\begin{aligned}y_p(k) &= H_{p,q}(k, k)x_p(k) + \sum_{i=-2L, i \neq 0}^{i=2L} \sum_{q=1}^{q=n_T} H_{p,q}(k, k+i)(x_q(k+i) - \mu_{x_q}^{(l-1)}(k+i)) \\ &\quad + \sum_{q=1, q \neq p}^{q=n_T} H_{p,q}(k, k)(x_q(k) - \mu_{x_q}^{(l-1)}(k)) + w(k)\end{aligned}\tag{5.12}$$

In (5.12), first term is the desired signal while second and third terms are the ICI and CAI respectively. Average power of ICI, P_{ICI}^{pk} , at the k^{th} subcarrier on the p^{th} receive antenna can be expressed as,

$$\begin{aligned}P_{ICI}^{pk} &= \sum_{i=-2L, i \neq 0}^{i=2L} \sum_{q=1}^{q=n_T} E\{\|H_{p,q}(k, k+i)(x_q(k+i) - \mu_{x_q}^{(l-1)}(k+i))\|^2\} \\ &= \sum_{i=-2L, i \neq 0}^{i=2L} \sum_{q=1}^{q=n_T} \|H_{p,q}(k, k+i)\|^2 E\{\|(x_q(k+i) - \mu_{x_q}^{(l-1)}(k+i))\|^2\} \\ &= \sum_{i=-2L, i \neq 0}^{i=2L} \sum_{q=1}^{q=n_T} \|H_{p,q}(k, k+i)\|^2 \nu_q^{(l-1)}(k+i)\end{aligned}\tag{5.13}$$

Where $E\{\|(x_q(k) - \mu_{x_q}^{(l-1)}(k))\|^2\}$ is the conditional variance at the $(l-1)^{\text{th}}$ iteration, $\nu_q^{(l-1)}(k)$ is given in (5.11). Average ICI power, therefore, on the p^{th} receive antenna is obtained by averaging P_{ICI}^{pk} across k , i.e., $P_{ICI}^p = \frac{1}{N} \sum_{k=0}^{k=N-1} P_{ICI}^{pk}$. Average power of

CAI on the k^{th} subcarrier on the p^{th} receive antenna, P_{CAI}^{pk} can similarly be written as,

$$\begin{aligned}
P_{CAI}^{pk} &= \sum_{q=1, q \neq p}^{q=n_T} E \left\{ \|H_{p,q}(k, k)(x_q(k) - \mu_{x_q}^{l-1}(k))\|^2 \right\} \\
&= \sum_{q=1, q \neq p}^{q=n_T} \|H_{p,q}(k, k)\|^2 E \left\{ \|(x_q(k) - \mu_{x_q}^{l-1}(k))\|^2 \right\} \\
&= \sum_{q=1, q \neq p}^{q=n_T} \|H_{p,q}(k, k)\|^2 \nu_q^{l-1}(k)
\end{aligned} \tag{5.14}$$

Average CAI power, on the p^{th} receive antenna is obtained by averaging P_{CAI}^{pk} across k , i.e., $P_{CAI}^p = \frac{1}{N} \sum_{k=0}^{k=N-1} P_{CAI}^{pk}$. The signal to interference ratio (SIR) at the k^{th} sub-carrier after l iterations can be computed as,

$$SIR = \frac{E(\|H_{p,q}(k, k)x_q(k)\|^2)}{P_{ICI}^p + P_{CAI}^p} \tag{5.15}$$

Another low complexity MIMO detector has been proposed in [115]. However, its performance is inferior compared to the proposed scheme above. Ref. [115] is based on the diagonalization of channel matrix.

5.5 Convergence Analysis Using EXIT Charts

As was described in Chapters 2 and 3, in EXIT Charts, the flow of extrinsic information between the equalizer and decoder is traced using simulation. Extrinsic information is computed from the mutual information between the transmit bits and their received LLR values. Detection schemes that may have low computational complexity per iteration might take more iterations to converge and vice versa. Thus comparing the complexity per iteration for different schemes is not fair unless the convergence speed is also taken into account. EXIT Charts are thus used in section 5.7 to investigate the convergence behavior of the iterative schemes [47, 48, 49].

EXIT charts for SIC-MAP-MIMO is obtained as described below. Frames of MIMO symbols generated from iid input bits ($b(n)$) are passed through the transmitter, channel and receiver front end. The received data, \mathbf{y} , is fed to the SIC-MAP-MIMO. Other inputs to the system are the *a priori* LLRs, $\text{LLR}'_{\text{ext}}(b(n))$, and the channel matrix, \mathbf{H} . *A priori* LLRs are generated as described in Sec. 3.5. Symbol mean values are

computed and processed within the system. The extrinsic LLRs are computed using (5.18) and (5.19). Generating EXIT Charts for decoder are described in Sec. 3.5.

5.6 Computational Complexity

Computational complexity of SIC-MAP-MIMO is compared with two iterative equalization schemes used in our study. These schemes were proposed in [2] and [1] and are respectively called TE-MMSE-OND2-MIMO and TE-BLK2-MIMO (the second equalizer. It is the best performer among three proposed equalizers) in this paper. These schemes were originally proposed for SISO channels. In this study we have extended the above schemes to MIMO systems. Complexity of the non-iterative MMSE scheme, referred to as MMSE-OND2-MIMO, is also computed. TE-BLK2-MIMO is a low complexity block TE scheme. TE-MMSE-OND2-MIMO is a serial TE scheme based on a section of \mathbf{H} (\mathbf{H}_k in Fig. 5.2 (right)) whereas MMSE-OND2-MIMO is the non-iterative version of TE-MMSE-OND2-MIMO. [70].

MMSE-OND2-MIMO schemes, turbo or not, involve the inversion of a matrix of size $D \cdot n_R$. Matrix inversion, generally, has cubic complexity. However, it has been shown that MMSE-OND2-MIMO or TE-MMSE-OND2-MIMO can be performed with approximately $O(N(n_R \cdot D)^2)$ operations [71]. Table 5.1 tabulates the approximate total number of arithmetic operations (\times, \div) for symbol estimation required per sample (sample per iteration in the case of iterative systems). Computations involved in BCJR are identical to all schemes and so are not considered. Cost of adders is significantly lower than that of multipliers. \tanh operation can be performed using a small look-up table. These operations are thus not considered in the comparison.

For a typical set of parameters ($n_T = n_R = 2, L = 1$), it is clear from Table 5.1 that TE-BLK2-MIMO and TE-MMSE-OND2-MIMO require approximately 4.3 and 4.5 times more computations than SIC-MAP-MIMO per iteration. A fair evaluation of the computational complexity can be undertaken only after studying their convergence behavior in the next subsection. The non-iterative scheme, MMSE-OND2-MIMO, requires 4 times more computations than SIC-MAP-MIMO per iteration.

Additionally, in mobile applications where battery power is limited, SIC-MAP-MIMO scheme has another advantage. The number of iterations can be adapted as a function of the available power and BER, so that a better trade-off between performance and power consumption can be achieved.

	TE-BLK2 -MIMO per sample per iter	MMSE-OND2 -MIMO per sample per iter	TE-MMSE-OND2 -MIMO per sample per iter.	SIC-MAP -MIMO per sample per iter.
Total \times	$48L^2n_Tn_R$ $+48Ln_R + 17$ (approx)	$2[(2L + 1)n_R]^2 +$ $n_R(2L + 1)(6Ln_R$ $+8Ln_T$ $+3n_R + 2n_T - 3)$	$(2L + 1)n_R \times$ $(8Ln_R + 12Ln_T +$ $4n_R + 3n_T) + 2$	$(2L + 1)n_R \times$ $[(4L + 1)n_T + 2] + 2$
Total \div	$4Ln_R + 7$	$(2L + 1)n_R$	$(2L + 1)n_R + 2$	—
Normalized complexity $L = 1$ $n_T = n_R = 2$	4.3	3.9	4.5	1

Table 5.1: Complexity Comparison

5.7 Simulation Results

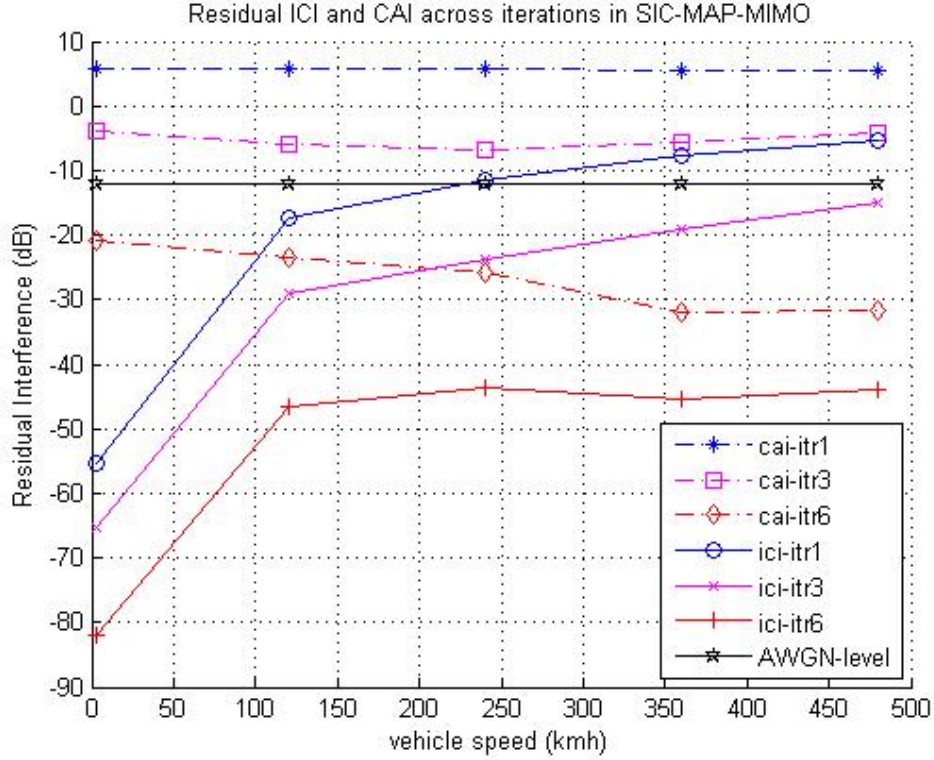


Figure 5.3: Interference Power (ICI and CAI) across Iterations.

Here we present the simulation results of the proposed scheme and compare it with two other similar iterative schemes described in section 5.6. We consider WiMAX like transmission at different vehicular speeds at a transmission frequency of 5GHz over vehicular-A channel [97] which is the customary channel model for WiMAX and LTE systems. We thus choose an OFDM-MIMO system with $N = 256$, $N_h = 6$, $N_p = N/8$ and $n_T = n_R = 2$. the transmission bandwidth is 5MHz. Speeds considered are 3kmh, 120kmh, 240kmh, 360kmh and 480kmh which corresponds to normalized Doppler frequency of 0.07%, 5.8%, 11.7%, 17.6% and 23.3% respectively. Results are shown for a rate 1/2 convolutional code having the generator polynomial (7,5). Symbols are QPSK modulated with average power = $1/n_T$. Both time and frequency interleaving are performed with S-random interleavers [72], with $S = 31$ and $S = 7$, respectively.

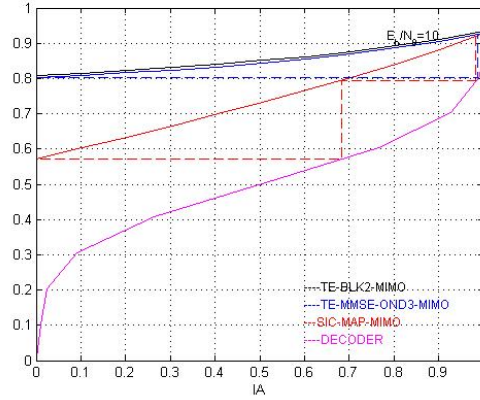


Figure 5.4: EXIT Curves - I_E vs I_A . ($E_b/N_0 = 10$, $n_T = 2$, $n_R = 2$, $N = 256$, $N_h = 6$, $f_d T_s N = 0.12$, QPSK).

In the case of static channels, the $n_T \cdot n_R$ channels are independent and constant over one OFDM symbol. In the case of doubly selective channels, The $n_T \cdot n_R$ channels are independent and Rayleigh fading, characterized by Jakes Doppler spectrum [25], with an exponentially decaying power delay profile. Simulations are run approximately for 10^7 bits.

Fig. 5.3 shows the average residual ICI and CAI interference in SIC-MAP-MIMO at different vehicular speeds over multiple iterations. This figure gives good insight into the proposed algorithm. At iteration one, there is no ICI or CAI cancellation and so it represents the relative ICI and CAI powers in the uncompensated system. CAI is a bigger source of interference than ICI even at very high vehicular speeds. It significantly dominates the AWGN level in the system at moderate to high SNRs (AWGN at 12 dB below the signal power is shown in the figure). At high vehicular speeds the ICI interference becomes significant if left uncompensated. At each iteration, both CAI and ICI reduces by several dBs. After about 6 iterations the CAI and ICI interference reduces so much that they are well below the AWGN level in the system, neglecting which, as is done in sections 3.4 and 5.4.1, is a valid approximation at all practical vehicular speeds. The approximation in (5.6) and the proposed decoding scheme in general, may not be valid for a generic system matrix $\mathbf{H}_{\mathbf{k}}$. As shown through simulations in Sec. 5.4.4 and in Fig. 5.3, the banded sparse structure of the system

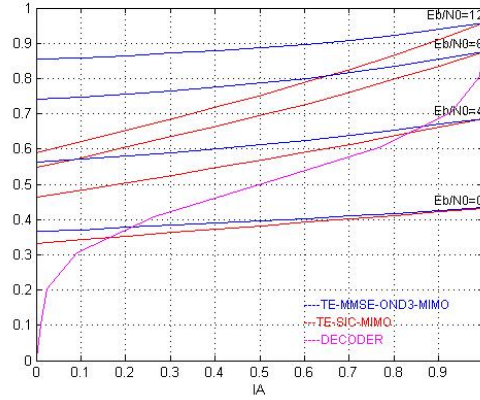


Figure 5.5: EXIT Curves for Different E_b/N_0 . ($n_T = 2$, $n_R = 2$, $N = 256$, $N_h = 9$, $f_d T_s N = 0.1$, QPSK)

matrix, lets the residual ICI and CAI interference to reduce considerably upon multiple iterations. This is the principal reason for this simplification to work. Note also that as we go up in vehicular speed, the proposed scheme is more effective in canceling the interference. This is due to the higher frequency diversity in the system due to Doppler spread.

Performance of SIC-MAP-MIMO is numerically analyzed with the help of EXIT Charts next. In Fig.5.4, EXIT charts for all the three iterative schemes used in our study, namely SIC-MAP-MIMO , TE-MMSE-OND2-MIMO and TE-BLK2-MIMO at 12% normalized Doppler, is plotted for $E_b/N_0 = 10dB$. Decoder EXIT chart is also shown.

A few general observations can be made from the equalizer EXIT chart. The range of both I_E and I_A is from 0 to 1, corresponding to “no knowledge” to “perfect *a priori* knowledge” about input bits $b(n)$. Consider the curve corresponding to SIC-MAP-MIMO at $E_b/N_0 = 10$. In the first iteration , there is no *a priori* information (corresponding to $I_A = 0$), and the equalizer output LLR has $I_E = 0.57$. This corresponds to a vertical line in the iterative receiver system trajectory. This mutual information is used as input to the decoder. The decoder, in turn, outputs LLRs with $I_D = 0.68$, which corresponds to a horizontal line. A vertical-horizontal trajectory pair

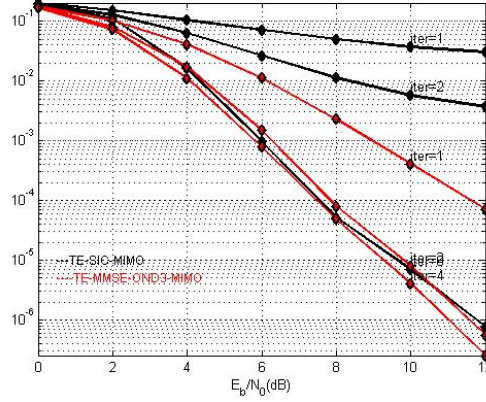


Figure 5.6: BER Plots - Different # Iterations. SIC-MAP-MIMO (# iter 3, 6), TE-MMSE-OND2-MIMO (# iter 1, 2) and TE-BLK2-MIMO (# iter 1, 2). ($n_T = 2$, $n_R = 2$, $N = 256$, $N_h = 6$, $f_d T_s N = 0.12$, QPSK).

completes one equalizer-decoder iteration. Such a trajectory demonstrates the mutual information buildup in the iterative receiver. Although an accurate BER performance may not always be possible to derive from an EXIT chart, it can be used as a useful tool to compare the convergence behavior of two different iterative schemes. In reality, the actual trajectory may not exactly follow the predicted trajectory. This is because the S-random interleaver has finite length, and the LLRs are no more random after a few initial iterations.

EXIT curve for TE-MMSE-OND2-MIMO and TE-BLK2-MIMO are quite close, however the exit curve for TE-BLK2-MIMO is consistently above the former showing the slight performance superiority of TE-BLK2-MIMO. Although SIC-MAP-MIMO EXIT chart starts at a lower point, it has higher slope and ends up very close to that of the other two. Such behavior is found to be true for different values of E_b/N_0 (Fig. 5.5). This is because the overall noise in the SIC-MAP-MIMO system during the initial iterations is higher than that of MMSE-OND2-MIMO, owing to ICI and CAI contributions from the residual error terms. However, as the estimator becomes more accurate with multiple iterations, these terms and, in turn, the system noise, gradually come down as seen in Fig. 5.3. All three schemes have very close end points corresponding to $I_A = 1$, indicating identical asymptotic behavior of these schemes.

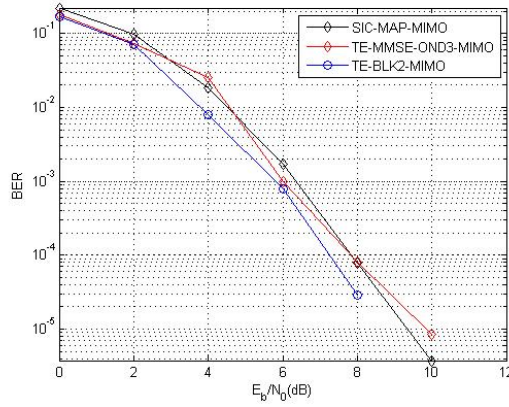


Figure 5.7: BER Plots. ($f_d T_s N = 0.23$, $n_T = 2$, $n_R = 2$, $N = 256$, $N_h = 6$, $\# \text{ iter} = 6$, QPSK).

The higher the EXIT curve slope, the better the BER gain per iteration. BER gain per iteration is, thus, higher for SIC-MAP-MIMO. At higher E_b/N_0 , the gap between the starting points of the two schemes is larger because at high E_b/N_0 , noise due to residual ICI and CAI starts dominating. It is clear from Fig. 5.4 that, SIC-MAP-MIMO needs more number of iterations compared to the other two schemes for the same level of convergence. When Doppler frequency goes up, ICI becomes more severe. EXIT charts, in this case, will start lower corresponding to a high BER for the first iteration. For static channels, EXIT curves start relatively.

The above postulations from the EXIT charts have been verified using simulations. Fig. 5.6 depicts the BER performance of these three iterative schemes for different numbers of iterations for 12% normalized Doppler frequency. It can be observed that SIC-MAP-MIMO requires three iterations for the same level of convergence per iteration of the other two schemes. The conventional MMSE symbol estimation scheme around the sub-diagonal matrix, MMSE-OND2-MIMO, is equivalent to the first iteration of TE-MMSE-OND2-MIMO in Fig. 5.6. From these observations and Table 5.1 it can be said that TE-MMSE-OND2-MIMO, TE-BLK2-MIMO and MMSE-OND2-MIMO are respectively 50%, 43% and 30% more expensive than the proposed algorithm.

Refer Fig. 5.5. If E_b/N_0 is below a threshold, we see that the decoder and equalizer

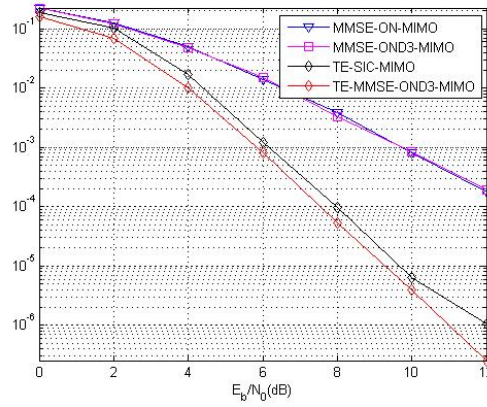


Figure 5.8: BER Plots. ($f_d T_s N = 0$ (static) $n_T = 2$, $n_R = 2$, $N = 256$, $N_h = 9$, # iter = 8 (SIC-MAP-MIMO), # iter = 4 (TE-MMSE-OND2-MIMO), QPSK).

EXIT charts intersect at a fairly low value of (I_D, I_E) . Under such circumstances (pinch off region) any number of iterations will not provide a near error free operation. The inferior performance of the channel estimator in Chapter 4, at low SNRs can be attributed to this behavior. Note that the pinch off region can be brought down if the decoder has an EXIT curve that “matches” (runs parallel) with the equalizer or vice versa. Another useful observation is that the y axis with $I_A = 1$, corresponds to the match filter operation for the turbo schemes. This is because when the equalizer has perfect knowledge of the input bits, $\boldsymbol{\mu}_s(k) = \mathbf{s}(k)$ and $\boldsymbol{\Sigma}_s$ is an all zero matrix with a single entry of 1 in the middle.

Fig. 5.7 shows the final BER performance of all three iterative schemes considered in our study for 23% normalized Doppler frequency after 6 iterations. SIC-MAP-MIMO and TE-MMSE-OND2-MIMO has approximately the same *steady-state* performance at high SNRs whereas TE-BLK2-MIMO performs slightly better than the other two.

Performance comparison of MMSE-OND2-MIMO, TE-MMSE-OND2-MIMO and SIC-MAP-MIMO under static channel conditions is provided in Fig. 5.8. The joint estimation of transmit symbols, as is done in TE-MMSE-OND2-MIMO, performs slightly better than SIC-MAP-MIMO. This is because SIC-MAP-MIMO essentially leverages

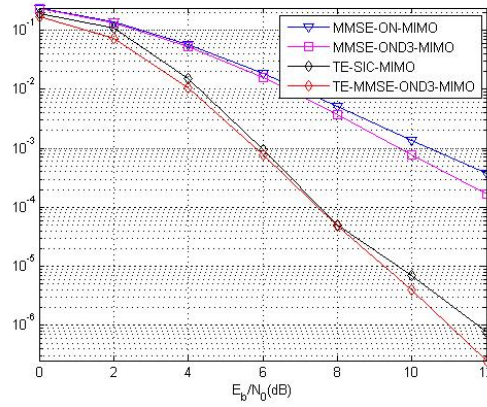


Figure 5.9: BER Plots. ($f_d T_s N = 0.1$, $n_T = 2$, $n_R = 2$, $N = 256$, $N_h = 9$, # iter = 8 (SIC-MAP-MIMO), # iter = 4 (TE-MMSE-OND2-MIMO), QPSK).

the frequency diversity due to Doppler spread. This does not exist in static channel conditions. As can be seen, SIC-MAP-MIMO has a gain of approximately 4 dBs compared to the non-iterative scheme MMSE-OND2-MIMO at the high SNR region.

By observing Figs. 5.8, 5.9 and 5.7, we can conclude that, as we move from static to moderate to high doubly selective channel conditions, the performance gap between SIC-MAP-MIMO and the two other schemes (which primarily perform the joint estimation of transmit symbols) narrows due to the increasing frequency diversity gain that the SIC-MAP-MIMO is taking advantage of. Thus, SIC-MAP-MIMO puts the Doppler induced “diversity gain” to effective use. Note also that the performance gap between iterative and noniterative schemes increase progressively as Doppler frequency increases.

Simulation results for 3 transmit 3 receive antenna system are given in Fig. 5.10. At low SNRs, SIC-MAP is less effective but it catches up with other schemes as the receiver SNR improves. All the previous observations can be seen to be valid independent of the number of antennas in the system.

It has been shown that the maximum rate of an outer code that stays underneath the EXIT curve of the equalizer so that the iterative equalization can converge is equal to

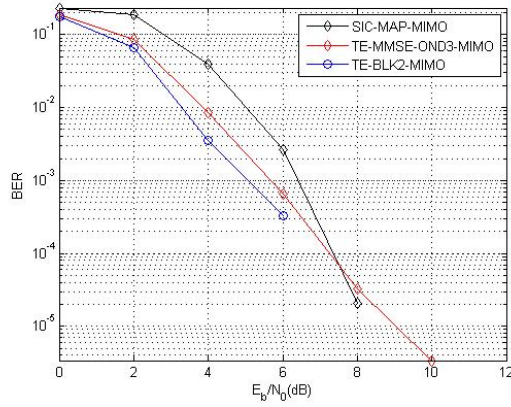


Figure 5.10: BER Plots. ($f_d T_s N = 0.23$, $n_T = 3$, $n_R = 3$, $N = 256$, $N_h = 6$, $\# \text{ iter} = 6$, QPSK).

the area under the EXIT curve of the equalizer [45]. Since the effective area under SIC-MAP-MIMO is lesser than that under the other two schemes, it is possible, at least in theory, to find codes that will work for the latter scheme but not for SIC-MAP-MIMO.

EXIT charts give a glimpse on the requirements of the channel estimation scheme. If the channel estimate is inaccurate, ICI and CAI will be left inadequately compensated in the detection process. This will act as additional noise in the system and will lower the start and end points of the EXIT curve. This would result in equalizer-decoder EXIT curves to intersect at a lower point in the chart causing a higher error floor. For SIC-MAP-MIMO, it is sufficient to come up with a channel estimation scheme that will become more accurate as we progress in iteration. This is because, unlike in TE-MMSE-OND2-MIMO, no full knowledge of the channel is required for the first iteration since only the main diagonal elements are made use of in the initial detector iteration.

Useful hints on the length of training sequence for TE-MMSE-OND2-MIMO and SIC-MAP-MIMO can also be obtained from the EXIT chart [44]. The longer the training sequence (equivalently higher the *detector code rate*), the more accurate the initial channel estimation is. This will cause the starting point of the EXIT chart to move relatively higher. This fact could be used in the training sequence design.

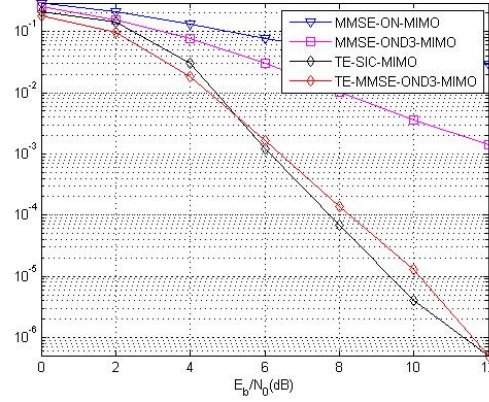


Figure 5.11: BER Plots. ($f_d T_s N = 0.3$, $n_T = 2$, $n_R = 2$, $N = 256$, $N_h = 9$, # iter = 8 (SIC-MAP-MIMO), # iter = 4 (TE-MMSE-OND2-MIMO), QPSK).

5.8 Conclusion

In this chapter, we have extended SIC-MAP from Chapter 3 to MIMO systems. We demonstrated through interference power, EXIT chart analysis and BER simulations that SIC-MAP-MIMO performance under time varying multipath conditions is on par with MMSE based TE schemes, TE-MMSE-OND2-MIMO, which is based on a sub-matrix of the system matrix and the block turbo equalization scheme, TE-BLK2-MIMO, based on the full system matrix. It was also found that TE-MMSE-OND2-MIMO, TE-BLK2-MIMO and the non-iterative MMSE-OND2-MIMO are respectively 50%, 43% and 30% more expensive than the proposed algorithm. It was demonstrated that SIC-MAP-MIMO performance progressively improves as the channel time variation increases due to the increasing frequency diversity gain that SIC-MAP-MIMO is taking advantage of. Another distinctive advantage of the proposed algorithm is its high scalability (power vs. performance) in practical receivers.

	1	2	3	4
$(m0, m1)$	$(0, 0)$	$(1, 0)$	$(0, 1)$	$(1, 1)$
η_i	$\frac{1+j1}{\sqrt{2n_T}}$	$\frac{-1+j1}{\sqrt{2n_T}}$	$\frac{1-j1}{\sqrt{2n_T}}$	$\frac{-1-j1}{\sqrt{2n_T}}$

Table 5.2: QPSK Alphabet

5.9 Appendix

5.9.1 Derivation of (5.8)

Ref. to Table 5.2 for the QPSK symbol alphabet definition.

$$\text{LLR}_{\text{ext}}(c_q(2k)) = \ln \frac{p(\tilde{\mathbf{y}}_{\mathbf{q}_k}|x_q(k) = \eta_1)P(0) + p(\tilde{\mathbf{y}}_{\mathbf{q}_k}|x_q(k) = \eta_3)P(1)}{p(\tilde{\mathbf{y}}_{\mathbf{q}_k}|x_q(k) = \eta_2)P(0) + p(\tilde{\mathbf{y}}_{\mathbf{q}_k}|x_q(k) = \eta_4)P(1)} \quad (5.16)$$

Here

$$\begin{aligned} p(\tilde{\mathbf{y}}_{\mathbf{q}_k}|x_q(k) = \eta_1) &= e^{-\frac{(\tilde{\mathbf{y}}_{\mathbf{q}_k} - \mathbf{h}_{\mathbf{q}_k} \eta_1)^H (\tilde{\mathbf{y}}_{\mathbf{q}_k} - \mathbf{h}_{\mathbf{q}_k} \eta_1)}{2\sigma^2}} \\ &= e^{\frac{-1}{2\sigma^2} (a1 + a2 - 2\text{Re}(\tilde{\mathbf{y}}_{\mathbf{q}_k}^H \mathbf{h}_{\mathbf{q}_k} \eta_1))} \end{aligned} \quad (5.17)$$

where

$$a1 = \tilde{\mathbf{y}}_{\mathbf{q}_k}^H \tilde{\mathbf{y}}_{\mathbf{q}_k}$$

and

$$a2 = (\mathbf{h}_{\mathbf{q}_k} \eta_1)^H (\mathbf{h}_{\mathbf{q}_k} \eta_1).$$

Note that, for QPSK

$$(\mathbf{h}_{\mathbf{q}_k} \eta_1)^H (\mathbf{h}_{\mathbf{q}_k} \eta_1) = (\mathbf{h}_{\mathbf{q}_k} \eta_2)^H (\mathbf{h}_{\mathbf{q}_k} \eta_2) = (\mathbf{h}_{\mathbf{q}_k} \eta_3)^H (\mathbf{h}_{\mathbf{q}_k} \eta_3) = (\mathbf{h}_{\mathbf{q}_k} \eta_4)^H (\mathbf{h}_{\mathbf{q}_k} \eta_4).$$

Substituting for all the terms from 5.17 in 5.16, defining $z := \tilde{\mathbf{y}}_{\mathbf{q}_k}^H \mathbf{h}_{\mathbf{q}_k}$ and removing the common terms, we get,

$$\begin{aligned}
\text{LLR}_{\text{ext}}(c_q(2k)) &= \ln \frac{e^{Re(z\eta_1)/\sigma^2} P(0) + e^{Re(z\eta_3)/\sigma^2} P(1)}{e^{Re(z\eta_2)/\sigma^2} P(0) + e^{Re(z\eta_4)/\sigma^2} P(1)} \\
&= \ln \frac{e^{\sqrt{2}Re(z(1+j))/(n_T\sigma^2)} P(0) + e^{Re(z(1-j))/(n_T\sigma^2)} P(1)}{e^{\sqrt{2}Re(z(-1+j))/(n_T\sigma^2)} P(0) + e^{Re(z(-1-j))/(n_T\sigma^2)} P(1)} \\
&= \ln \frac{e^{\sqrt{2}(Re(z)-Im(z))/(n_T\sigma^2)} P(0) + e^{\sqrt{2}(Re(z)+Im(z))/(n_T\sigma^2)} P(1)}{e^{\sqrt{2}(-Re(z)-Im(z))/(n_T\sigma^2)} P(0) + e^{\sqrt{2}(-Re(z)+Im(z))/(n_T\sigma^2)} P(1)} \\
&= \ln \left(\frac{e^{\frac{\sqrt{2}}{(n_T\sigma^2)} Re(z)}}{e^{\frac{-\sqrt{2}}{(n_T\sigma^2)} Re(z)}} \right) \\
&= \frac{\sqrt{8}Re(\tilde{\mathbf{y}}_{\mathbf{q}_k}^H \mathbf{h}_{\mathbf{q}_k})}{(n_T\sigma^2)} \tag{5.18}
\end{aligned}$$

Similarly we get

$$\text{LLR}_{\text{ext}}(c_q(2k+1)) = \frac{\sqrt{8}Im(\tilde{\mathbf{y}}_{\mathbf{q}_k}^H \mathbf{h}_{\mathbf{q}_k})}{(n_T\sigma^2)} \tag{5.19}$$

5.9.2 Detailed Complexity Computation

The computational complexity of various schemes used in our study are derived in this section [116, 73]. Tables 5.3 and 5.5 describe the efficient implementations of TE-MMSE-OND2-MIMO and MMSE-OND2-MIMO. The number of computations required for each step for the above implementation are derived [71] in Tables 5.4 and 5.6. The complexity of SIC-MAP-MIMO is derived in 5.7.

Table 5.3: TE-MMSE-OND2-MIMO - An Efficient Implementation

INPUT
extrinsic LLRs from decoder ($\text{LLR}'_{\text{ext}}(c(n))$)
INITIALIZATION
compute $\mu_{x_q}(k), \forall k, q,$ compute $\Sigma_{\mathbf{y}_0, \mathbf{y}_0}^{-1} = (\sigma^2 I_{(2L+1) \cdot n_R} + \frac{1}{n_T} \mathbf{H}_0 \Sigma_{\mathbf{x}_0, \mathbf{x}_0} \mathbf{H}_0^H)^{-1}$
LINEAR MMSE ESTIMATION
FOR $K = 0$ TO $N - 1$ DO
$\mathbf{F}_{\mathbf{k}} = \Sigma_{\mathbf{y}_{\mathbf{k}}, \mathbf{y}_{\mathbf{k}}}^{-1} \tilde{\mathbf{H}}_{\mathbf{k}} \left(\frac{1}{n_T} \nu_{\mathbf{x}(\mathbf{k})} \right)$
$\mathcal{Y}_{\mathbf{k}} = (\mathbf{y}_{\mathbf{k}} - \mathbf{H}_{\mathbf{k}} \mu_{\mathbf{x}_{\mathbf{k}}})$
for $q = 0$ to $q = n_T$
$\mathbf{f}_{\mathbf{q}_{\mathbf{k}}} := \mathbf{F}_{\mathbf{k}}(:, q)$
$\mathbf{h}_{\mathbf{q}_{\mathbf{k}}} := \tilde{\mathbf{H}}_{\mathbf{k}}(:, q)$
$\nu_{x_q}(k) = \nu_{\mathbf{x}(\mathbf{k})}(q, q)$
$\hat{x}_q(k) = \mu_{x_q}(k) + \mathbf{f}_{\mathbf{q}_{\mathbf{k}}}^H \mathcal{Y}_{\mathbf{k}}(:, q)$
$\text{LLR}_{\text{ext}}(c_q(2k)) = \frac{\sqrt{8}}{1 - \nu_{x_q}(k) \mathbf{h}_{\mathbf{q}_{\mathbf{k}}}^H \mathbf{f}_{\mathbf{q}_{\mathbf{k}}}} \cdot \text{Re}(\hat{x}_q(k))$
$\text{LLR}_{\text{ext}}(c_q(2k+1)) = \frac{\sqrt{8}}{1 - \nu_{x_q}(k) \mathbf{h}_{\mathbf{q}_{\mathbf{k}}}^H \mathbf{f}_{\mathbf{q}_{\mathbf{k}}}} \cdot \text{Im}(\hat{x}_q(k))$
end
ITERATIVE UPDATE OF $\Sigma_{\mathbf{y}_{\mathbf{k}}, \mathbf{y}_{\mathbf{k}}}^{-1}$ (MIMO) (see below).
END
ITERATIVE UPDATE OF $\Sigma_{\mathbf{y}_{\mathbf{k}}, \mathbf{y}_{\mathbf{k}}}^{-1}$ (MIMO).
for $q = 0$ to $q = n_T$
ITERATIVE UPDATE OF $\Sigma_{\mathbf{y}_{\mathbf{k}}, \mathbf{y}_{\mathbf{k}}}^{-1}$ (SISO) (see below).
end
ITERATIVE UPDATE OF $\Sigma_{\mathbf{y}_{\mathbf{k}}, \mathbf{y}_{\mathbf{k}}}^{-1}$ (SISO).
(inversion with one row update at a time)
(complexity $O(((2L+1)n_R)^2)$)
$\begin{bmatrix} \mathbf{a} & \mathbf{B}^H \\ \mathbf{B} & \mathbf{A} \end{bmatrix} := \Sigma_{\mathbf{y}_{\mathbf{k}}, \mathbf{y}_{\mathbf{k}}}^{-1}$ $\mathbf{A}_{\mathbf{p}} = \mathbf{A} - \mathbf{B} \mathbf{B}^H / \mathbf{a}$ $\begin{bmatrix} \mathbf{B}_{\mathbf{p}} \\ \mathbf{a}_{\mathbf{p}} \end{bmatrix} := \begin{bmatrix} \mathbf{0}_{(2L+1) \cdot n_R} & -1 \\ \sigma^2 & \end{bmatrix} + \mathbf{H}_{k+1} \Sigma_{\mathbf{x}_{k+1}, \mathbf{x}_{k+1}} \mathbf{H}_{k+1}^H \begin{bmatrix} \mathbf{0}_{(2L+1) \cdot n_R - 1} \\ 1 \end{bmatrix}$ $\mathbf{B}_{\mathbf{pp}} = -\mathbf{A}_{\mathbf{p}} \mathbf{B}_{\mathbf{p}}$ $\mathbf{a}_{\text{new}} = (\mathbf{a}_{\mathbf{p}} + \mathbf{B}_{\mathbf{p}}^H \mathbf{B}_{\mathbf{pp}})^{-1}$ $\mathbf{B}_{\text{new}} = \mathbf{a}_{\text{new}} \mathbf{B}_{\mathbf{pp}}$ $\mathbf{A}_{\text{new}} = \mathbf{A}_{\mathbf{p}} + \mathbf{a}_{\text{new}} (\mathbf{B}_{\mathbf{pp}} \mathbf{B}_{\mathbf{pp}}^H)$ $\Sigma_{\mathbf{y}(\mathbf{k}+1), \mathbf{y}(\mathbf{k}+1)}^{-1} := \begin{bmatrix} \mathbf{A}_{\text{new}} & \mathbf{B}_{\text{new}} \\ \mathbf{B}_{\text{new}}^H & \mathbf{a}_{\text{new}} \end{bmatrix}$
OUTPUT
extrinsic LLRs to the decoder ($\text{LLR}_{\text{ext}}(c(n))$)

Table 5.4: Complexity - TE-MMSE-OND2-MIMO

Ignore Complexity for Initialization
complexity for Linear MMSE Estimation

no	operation	operand size	\times	\div
1	$\Sigma_{\mathbf{y}_k, \mathbf{y}_k}^{-1} \tilde{\mathbf{H}}_k$ \times $\left(\frac{1}{n_T} \nu_{\mathbf{x}(k)}\right)$	$(2L+1)n_R \times (2L+1)n_R,$ $(2L+1)n_R \times n_T,$ $n_T \times n_T$	$((2L+1)n_R)^2 n_T +$ $(2L+1)n_R n_T$	$-$ n_T
2	$\mathbf{H}_k \mu_{\mathbf{x}_k}$	$(2L+1)n_R \times (4L+1)n_T,$ $(4L+1)n_T \times n_T$	$(4L+1)n_T (2L+1)n_R n_T$	$-$
3	$\mathbf{f}_{\mathbf{q}_k}^H \mathcal{Y}_k(:, q)$	$(2L+1)n_R \times 1,$ $(2L+1)n_R \times 1$	$(2L+1)n_R$	$-$
4	$\mathcal{S} = \nu_{x_q}(k) \mathbf{h}_{\mathbf{q}_k}^H \mathbf{f}_{\mathbf{q}_k}$ $\frac{\sqrt{8}}{1-\mathcal{S}} \hat{x}_q(k)$	$1 \times 1,$ $(2L+1)n_R \times 1,$ $(2L+1)n_R \times 1,$ $-$	$(2L+1)n_R + 1$ 1	$-$ 1
5	$\mathbf{B}\mathbf{B}^H/\mathbf{a}$	$((2L+1)n_R - 1) \times 1$ 1×1	$((2L+1)n_R - 1)^2$	$(2L+1)n_R$ -1
6	$\mathbf{H}_{k+1} \Sigma_{\mathbf{x}_{k+1}, \mathbf{x}_{k+1}}$ $\times \mathbf{H}_{k+1}^H \begin{bmatrix} \mathbf{0}_{(2L+1) \cdot n_R - 1} \\ 1 \end{bmatrix}$	$(2L+1)n_R \times (4L+1)n_T$ $(4L+1)n_T \times (4L+1)n_T$	$(2L+1)n_R \times (4L+1)n_T +$ $(4L+1)n_T \times (2L+1)n_R$	
7	$\mathbf{A}_p \mathbf{B}_p$	$((2L+1)n_R - 1) \times$ $((2L+1)n_R - 1),$ $((2L+1)n_R - 1) \times 1$	$((2L+1)n_R - 1)^2$	
8	$(\mathbf{a}_p + \mathbf{B}_p^H \mathbf{B}_{pp})^{-1}$	$((2L+1)n_R - 1) \times 1$	$((2L+1)n_R - 1)$	1
9	$\mathbf{a}_{\text{new}} \mathbf{B}_{pp}$	$1 \times 1,$ $((2L+1)n_R - 1) \times 1$	$(2L+1)n_R - 1$	
10	$\mathbf{a}_{\text{new}} (\mathbf{B}_{pp} \mathbf{B}_{pp}^H)$	$1 \times 1,$ $((2L+1)n_R - 1) \times 1$	$(2L+1)n_R - 1 +$ $((2L+1)n_R - 1)^2$	

$$AM_t := \text{Total } \times \text{ from step1 + step2} = (2L+1)n_R n_T (2Ln_R + 4Ln_T + n_R + n_T + 1)$$

$$AD_t := \text{Total } \div \text{ from step1 + step2} = n_T$$

$$BM_t := \text{Total } \times \text{ from step3 + step4} = 2[(2L+1)n_R + 1]$$

$$BD_t := \text{Total } \div \text{ from step3 + step4} = 1$$

$$CM := \text{Total } \times \text{ for mat. inv.} = \text{step5} + \dots \text{step10} = n_R(2L+1)(6Ln_R + 8Ln_T + 3n_R + 2n_T - 3)$$

$$CD := \text{Total } \div \text{ for mat. inv.} = \text{step5} + \dots \text{step10} = (2L+1)n_R$$

$$\text{Total } \times \text{ per sample per iteration for TE-MMSE-OND2-MIMO} = AM_t/n_T + BM_t + CM$$

$$\text{Total } \div \text{ per sample per iteration for TE-MMSE-OND2-MIMO} = AD_t/n_T + BD_t + CD$$

Table 5.5: MMSE-OND2-MIMO - An Efficient Implementation

INITIALIZATION

 compute $\Sigma_{\mathbf{y}_0, \mathbf{y}_0}^{-1} = (\sigma^2 I_{(2L+1) \cdot n_R} + \frac{1}{n_T} \mathbf{H}_0 \mathbf{H}_0^H)^{-1}$

LINEAR MMSE ESTIMATION

 FOR $K = 0$ TO $N - 1$ DO

$$\mathbf{F}_k = (\frac{1}{n_T}) \tilde{\mathbf{H}}_k^H \Sigma_{\mathbf{y}_k, \mathbf{y}_k}^{-1}$$

$$\mathbf{x}(k) = \mathbf{F}_k \mathbf{y}_k$$

ITERATIVE UPDATE OF $\Sigma_{\mathbf{y}_k, \mathbf{y}_k}^{-1}$ (MIMO) (Ref. Table 5.3).

 END

Table 5.6: Complexity - MMSE-OND2-MIMO

Ignore Complexity for Initialization				
complexity for Linear MMSE Estimation				
steps	operation	operand size	\times	\div
1	$\frac{1}{n_T} \tilde{\mathbf{H}}_k^H \Sigma_{\mathbf{y}_k, \mathbf{y}_k}^{-1}$	$(2L+1)n_R \times n_T$, $(2L+1)n_R \times (2L+1)n_R$	$((2L+1)n_R)^2 n_T$	$-$ $n_T \times (2L+1)n_R$
2	$\mathbf{F}_k \mathbf{y}_k$	$n_T \times (2L+1)n_R$, $(2L+1)n_R \times n_T$	$((2L+1)n_R)^2 n_T$	$-$
3	ITERATIVE UPDATE OF $\Sigma_{\mathbf{y}_k, \mathbf{y}_k}^{-1}$ (MIMO) (Ref. Table 5.4)			
$AM_s := \text{Total} \times \text{from step1} + \text{step2}$ $AD_s := \text{Total} \div \text{from step1} + \text{step2}$ $CM := \text{Total} \times \text{for matrix inversion (step3)}$ $CD := \text{Total} \div \text{for matrix inversion (step 3)}$				
			$2[(2L+1)n_R]^2 n_T$	
			$n_T \times (2L+1)n_R$	
			CM in Table 5.4	
			CD in Table 5.4	
Total \times per sample per iteration for MMSE-OND2-MIMO = $AM_s/n_T + CM$				
Total \div per sample per iteration for MMSE-OND2-MIMO = $AD_s/n_T + CD$				

Table 5.7: Complexity - SIC-MAP-MIMO

Ignore Complexity for Computing $\mu_{x_q}(k) \forall k, q$				
steps	operation	operand size	\times	\div
1	$\tilde{\mathbf{y}}_{\mathbf{k}}$ (computation of $\mathbf{H}_{\mathbf{k}}\tilde{\mu}_{\mathbf{x}_{\mathbf{k}}}$) (5.5)	$(2L+1)n_R \times (4L+1)n_T$, $(4L+1)n_T \times n_T$	$(2L+1)n_R(4L+1)n_T^2$	—
2	computation of $\mathbf{y}'_{\mathbf{q}_{\mathbf{k}}}$ (5.6)	—	$(2L+1)n_R$	—
3	LLR _{ext} ($c_q(2k)$) (5.8), (5.9)	—	$(2L+1)n_R+1$	1

$$AM_{sic} := \text{Total} \times \text{from step1}$$

$$AD_{sic} := \text{Total} \div \text{from step1}$$

$$BM_{sic} := \text{Total} \times \text{from step2} + \text{step3}$$

$$BD_{sic} := \text{Total} \div \text{from step2} + \text{step3}$$

$$\text{Total} \times \text{per sample per iteration for SIC-MAP-MIMO} = AM_{sic}/n_T + BM_{sic}$$

$$\text{Total} \div \text{per sample per iteration for TE-MMSE-OND2-MIMO} = AD_{sic}/n_T + BD_{sic}$$

Chapter 6

Conclusion and Possible Future Work

A low complexity iterative receiver for SISO (Chapters 3 and Chapter 4) and MIMO (Chapter 5) systems in doubly selective channel conditions has been described in this dissertation. The proposed receiver design makes several assumptions about the system. This includes base band transmission, perfect synchronization and no impairments such as phase noise or impulse noise present in the system. With these idealized assumptions, the proposed design is far from a practical low complexity IR in a commercial application. The above IR, instead, has to be taken as a first step towards the design of a ‘real’ receiver. However, it gives good insights into the practical benefits in terms of performance and power savings possible with low complexity iterative receivers. Some of the following aspects require future work:

1. Delay Mitigation

Besides the computation complexity, another, perhaps more limiting aspect, in turbo like IR is the delay associated with turbo iterations. The detector has to wait until the soft information from the decoder is available before it can perform the second iteration. This is a source of big delay in processing for two reasons: a) The classical BCJR decoder would make the soft information available at the end of a convolutionally coded block and b) more importantly, the interleaver in the path would require the entire block of data to be available before the equalizer can start processing the soft information. Iterative schemes such as the ones proposed in [2, 108] address this issue by excluding the decoder from the path. But the performance gain will be modest in such systems as they do not take advantage of the coding gain of the decoder. A carefully designed interleaver which randomize

the bits sufficiently, yet do not incorporate long delays (conflicting requirements) may solve this issue. Such a practical interleaver is another interesting problem to consider. Sliding Window BCJR decoding or Tail biting trellis decoding [117, 118] can be definitely considered as well.

2. A Complete Receiver

As mentioned earlier, a complete receiver design would encompass the carrier and sampling clock recovery mechanisms and additional signal processing to suppress phase noise, impulse noise adjacent channel interference and similar other impairments. The newly available conditional mean and variance at the end of each iteration can be thought of as additional pilots and their confidence level respectively. As in the case of channel estimation, if this data is put to use in a suitable manner for SIC-MAP, it can improve the iterative receiver described in this dissertation to a more complete commercial receiver. Some of the available literature in this regard can be found in [119, 120, 121, 122].

3. EXIT Chart Modifications

As we saw earlier, EXIT chart is a simulation based technique to analyze the convergence behavior of iterative systems. We have made use of this tool extensively in analyzing various TE schemes and comparing our proposed equalization scheme with competing other schemes. This technique has been proposed originally by coding theorists where AWGN channel is assumed. No work, to our knowledge, has been done to enhance this technique to a turbo-equalizer scenario in a Rayleigh fading channel where apart from the BER (or Mutual Info) performance, outage probability is another important performance measure to consider. This is especially true for MIMO channels. The SNR vs. BER curve in Rayleigh fading channels (averaged for long) reveal only part of the receiver performance. What is more revealing is the BER for a given SNR and outage probability. Currently by sufficiently averaging the mutual Information from the

iterative equalizer, we make the results look like that for an AWGN Channel. So the exit curves for TE-MIMO systems should be modified to exit condors or surfaces in 3D space with I_A , I_E and outage probability as three quantities of interest.

4. MIMO Channel Estimation

We have dealt with SISO channel estimation in doubly selective channel conditions. Lastly, it is straight forward to extend the SISO channel estimation scheme proposed in this dissertation to MIMO systems in doubly selective channel conditions. However, it need to be done and performance need to be analyzed.

References

- [1] Kun Fang, Luca Rugini, and Geert Leus. Low-complexity block turbo equalization for OFDM systems in time - varying channels. *IEEE Transactions on Signal Processing*, pages 5555–5566, Nov. 2008.
- [2] Philip Schniter. Low-complexity equalization of OFDM in doubly selective channels. *IEEE Transactions on Signal Processing*, 52(4):1002–1011, 2004.
- [3] Taewon Hwang, Chenyang Yang, Gang Wu, Shaoqian Li, and Geoffrey Ye Li. OFDM and its wireless applications: A survey. *IEEE Transactions on Vehicular Technology*, 58(4):1673 – 1694, May 2009.
- [4] John A C Bingham. Multicarrier modulation for data transmission: An idea whose time has come. *IEEE Communication Magazine*, 28(5):5–14, May 1990.
- [5] Z. Wang and G. B. Giannakis. Wireless multicarrier communications: where fourier meets shannon,. *IEEE Signal Processing Mag*, 17:29–48, May 2000.
- [6] Michael Speth, Stefan. A. Fechtel, Gunnar Fock, and Heinrich Meyr. Optimum receiver design for wireless broad-band systems using OFDM-part 1. *IEEE Trans. Commun*, 47:1668–1677, Nov 1999.
- [7] Thomas M Cover and Joy A Thomas. *Elements of Information Theory*. Wiley-Interscience, 2005.
- [8] Digital video broadcasting (DVB): Framing structure, channel coding and modulation for digital terrestrial television. *ETSI Standard. ETS 300 744*, July 1999.
- [9] Transmission system for digital terrestrial television broadcasting. *ARIB Standard STD-B31 Ver.1.5*, July 2003.
- [10] Vahid Tarokh, Nambirajan Seshadri, and A. Robert Calderbank. Space-time codes for high data rate wireless communication: Performance criteria and code construction. *IEEE Transactions on Information Theory*, 44(2):744–764, March 1998.
- [11] S. M. Alamouti. A simple transmit diversity technique for wireless communications. *IEEE J. Sel. Areas Commun*, 16(8):1438–1451, Oct 1998.
- [12] V. Tarokh, H. Jafarkhani, and A.R.Calderbank. Space-time block codes from orthogonal designs. *IEEE J. Inform. Theory*, 45:1456–1467, Jul. 1999.
- [13] Ayman F. Naguib, Vahid Tarokh, Nambirajan Seshadri, and A. Robert Calderbank. A space-time coding modem for high-data-rate wireless communications. *IEEE Journal on Selected Areas in Communications*, 16(8):1459–1478, October 1998.

- [14] G. J. Foschini. Layered space-time architecture for wireless communication in a fading environment when using multi-element antennas. *Bell Labs Tech. J.*, pages 41–59, Autumn 1996.
- [15] Alcatel Shanghai Bell Co. Ltd. Hongwei Yang. A road to future broadband wireless access: MIMO-OFDM-based air interface. *IEEE Communications Magazine*, pages 53–60, January 2005.
- [16] D. Astély, E. Dahlman, P. Frenger, R. Ludwig, M. Meyer, S. Parkvall, P. Skillermark, and N. Wiberg. A future radio-access framework. *IEEE Journal on Selected Areas in Communications*, 24(3):693–706, March 2006.
- [17] Amitava Ghosh, Rapeepat Ratasuk, Bishwarup Mondal, Nitin Mangalvedhe, and Motorola Inc. Tim Thomas. LTE-advanced: Next-generation wireless broadband technology. *IEEE Wireless Communications*, 17(3):10–22, June 2010.
- [18] 3GPP tr 36.913. requirements for further advancements for evolved universal terrestrial radio access (EUTRA). 8.0.1:1046–1061, March 2009.
- [19] IEEE. Standard for local and metropolitan area networks part 16. std. IEEE802.16E-2005. 2005.
- [20] Air interface for fixed broadband wireless access systems: Part A: Systems between 2 - 11GHz. *IEEE Stand. 802.16, 01/01r1*, July 2001.
- [21] IEEE. 802.16m-08/003r6. IEEE 802.16m system description document [draft].
- [22] IEEE. P802.11n/D10.0. May 2009.
- [23] IEEE. P802.11ac. May 2011.
- [24] Arogyaswami J. Paulraj and Dhananjay A. Gore. An overview of MIMO communications – a key to gigabit wireless. *Proceedings of the IEEE*, 92(2):1459–1478, February 2004.
- [25] W. C. Jakes. *Microwave Mobile Communications*. Wiley, 1974.
- [26] Theodore S. Rappaport. *Wireless Communications Principles and Practice*. Prentice Hall, 2002.
- [27] P.F.Driessen and G.J.Foschini. On the capacity formula for multiple-input multiple output wireless channels: A geometric interpretation. *IEEE Transaction on Communications*, 47(2):173–176, Feb. 1999.
- [28] H. V. Poor. *An introduction to Signal Detection and Estimation, 2nd ed.* New York: Springer, 1994.
- [29] Ali. H. Sayed. *Fundamentals of Adaptive Filtering*. A John Wiley and Sons, 2003.
- [30] I. Barhumi, G. Leus, and M. Moonen. Optimal training design for MIMO-OFDM systems in mobile wireless channels. *IEEE Trans. Signal Processing*, 51(6):1615–1624, June 2003.

- [31] R. Negi and J. Cioffi. Pilot tone selection for channel estimation in a mobile OFDM system. *IEEE Transactions on Consumer Electronics*, 44:1122–8, 1998.
- [32] X. Ma, G. B. Giannakis, and S. Ohno. Optimal training for block transmissions over doubly selective wireless fading channels. *IEEE Trans. Signal Processing*, 51(5):1351–1366, May 2003.
- [33] M. Dong and L. Tong. Optimal design and placement of pilot symbols for channel estimation. *IEEE Trans. Signal Processing*, 50(12):3055–3069, Dec 2002.
- [34] W. T. Ng and V. K. Dubey. On coded pilot based channel estimation for OFDM in very fast multipath fading channel. *Proc. IEEE Pacific Rim Conf. Commun., Computers and Signal Processing, Honolulu, HI*, 2:859–863, Dec 2003.
- [35] Shu Lin and Daniel J. Costello. *Error control coding*. Prentice Hall, 2004.
- [36] L. R. Bahl, J. Cocke, F. Jelinek, and J. Raviv. Optimal decoding of linear codes for minimizing symbol error rate. *IEEE Trans. Inform. Theory*, pages 284–287, March 1974.
- [37] John L. Fan. *Constrained Coding and Soft Iterative Decoding*. Kluwer Academic Publishers, 2001.
- [38] Ralf Koetter, Andrew. C. Singer, and Michael Tüchler. Turbo equalization. *IEEE signal processing Magazine*, Jan 2001.
- [39] C. Douillard, M. Jezequel, C. Berrou, A. Picart, P. Didier, and A. Glavieux. Iterative correction of inter-symbol interference: Turbo equalization. *European Trans. Telecomm*, 6:507–511, Sept.-Oct 1995.
- [40] M. Tüchler, A. Singer, and R. Kotter. Minimum mean squared error (MMSE) equalization using a priori information,. *IEEE Trans. Signal processing*, 50:673–683, Mar 2002.
- [41] M. Tüchler, R. Kotter, and A. Singer. Turbo equalization: Principles and new results. *IEEE Trans. Commun*, 50:754–767, May 2002.
- [42] Xiaodong Wang and H. Vincent Poor. Iterative (turbo) soft interference cancellation and decoding for coded CDMA. *IEEE Transactions on Communications*, 47(7):1046–1061, July 1999.
- [43] Stephan ten Brink. Convergence behavior of iteratively decoded parallel concatenated codes. *IEEE Transactions on Communications*, 49(10):1727–1737, October 2001.
- [44] Rold Otnes and Michael Tüchler. EXIT chart analysis applied to adaptive turbo equalization. *presented at the Nordic Signal Processing Symp, Trondheim, Norway*, October 2002.
- [45] Joachim Hagenauer. The EXIT chart - introduction to extrinsic information transfer in iterative processing. <http://scholar.google.co.uk/scholar?cluster=9622901384089680641&hl=en>.

- [46] David. P. Shepherd, Matt Ruan, Mark. C. Reed, and Zhenning Shi. An analytical comparison of EXIT and variance transfer (VT) tools for iterative decodedr analysis. *Conference Record of The Thirty-Ninth Asilomar Conference on Signals, Systems and Computers*, pages 956–960, 2005.
- [47] S. Ahmed, T. Ratnarajah, M. Sellathurai, and Colin. F. N. Cowan. EXIT chart analysis of a reduced complexity iterative MIMO-OFDM receiver. *Vehicular Technology Conference*, pages 2430–2434, Spring 2007.
- [48] Seok-Jun Lee and Andrew C. Singer. Convergence analysis for linear turbo equalization. *Thirty-Seventh Asilomar Conference on Signals, Systems and Computers*, pages 667–671, 2003.
- [49] Stephan Sand, Simon Plass, and Armin Dammann. EXIT chart analysis of iterative receivers for space-time-frequency coded OFDM systems. *Vehicular Technology Conference*, pages 725–729, Fall 2007.
- [50] Todd K. Moon. *Error correction coding Mathematical Methods and Algorithms*. A John Wiley and Sons, 2005.
- [51] Vamadevan Namboodiri, Hong Liu, and Predrag Spasojević. Low complexity iterative receiver design for mobile OFDM systems. *accepted for publication in EURASIP Journal on Advances in Signal Processing*, 2012.
- [52] Won Gi Jeon, Kyung Hi Chang, and Yong Soo Cho. An equalization technique for orthogonal frequency-division multiplexing systems in time-variant multipath channels. *IEEE Transactions on Communications*, 47:27–31, January 1999.
- [53] J. P. M. G. Linnartz and A Gorokhov. New equalization approach for OFDM over dispersive and rapidly time varying channel. *Proc. IEEE Int. Symposium Personal Indoor Mobile Radio Commun*, 2:1375–1379, 2000.
- [54] Y. S. Choi, P. J. Voltz, and F. A. Cassara. On channel estimation and detection for multicarrier signals in fast and selective rayleigh fading channels. *IEEE Trans. Commun*, 49:1375–1387, Aug 2001.
- [55] Paolo Baracca, Stefano Tomasin, Lorenzo Vangelista, Nevio Benvenuto, and Alberto Morello. Per sub-block equalization of very long OFDM blocks in mobile communications. *IEEE Transactions on Communications*, 59(2):363–368, February 2011.
- [56] Stefano Tomasin, Alexei Gorokhov, Haibing Yang, and Jean-Paul Linnartz. Iterative interference cancellation and channel estimation for mobile OFDM. *IEEE Transactions on Wireless Communications*, 4(1):238–245, January 2005.
- [57] Qinghua Guo and Li Ping and Defeng Huang. A low complexity iterative channel estimation and detection technique for doubly selective channels. *IEEE Transactions on Wireless Communications*, 8(1):4340–4349, 2009.
- [58] Shaoping Chen and Cuitao Zhu. ICI and ISI analysis and mitigation for OFDM systems with insufficient cyclic prefix in time-varying channels. *IEEE Transactions on Consumer Electronics*, 50:78–83, 2004.

- [59] Shaoping Chen and Tianren Yao. Intercarrier interference suppression and channel estimation for OFDM systems in time-varying frequency-selective fading channels. *IEEE Transactions on Consumer Electronics*, 50(2):429–435, May 2004.
- [60] Soon Up Hwang, Jeong Hoon Lee, and Jongsoo Seo. Low complexity iterative ICI cancellation and equalization for OFDM systems over doubly selective channels. *IEEE Transactions on Broadcasting*, 55(1):132–139, March 2009.
- [61] Jianzhong Huang, Shengli Zhou, Jie Huang, Christian R Berger, and Peter Willett. Progressive inter-carrier interference equalization for OFDM transmission over time-varying underwater acoustic channels. *IEEE Journal of Selected Topics in Signal Processing*, 5(8):1524 – 1536, December 2011.
- [62] Erdal Panayirci, Hakan Dogan, and H Vincent Poor. Low-complexity MAP-based successive data detection for coded OFDM systems over highly mobile wireless channels. *IEEE Transactions on Vehicular Technology*, 60(6):2849 – 2857, July 2011.
- [63] Andreas F. Molisch, Martin Toeltsch, and Sameer Vermani. Iterative methods for cancellation of intercarrier interference in OFDM systems. *IEEE Transactions on Vehicular Technology*, 56(4):2158–2167, July 2007.
- [64] Sen Jiang, Li Ping, Hong Sun, and Chi Sing Leung. Modified LMMSE turbo equalization. *IEEE Communications Letters*, 8:173–176, March 2004.
- [65] Fabian Vogelbruch, Roland Zukunft, and Sven Haar. 16-QAM turbo equalization based on minimum mean squared error linear equalization. *Conference Record of the Thirty-Sixth Asilomar Conference on Signals, Systems and Computers*, 2:1943 – 1947, 2002.
- [66] Vamadevan Namboodiri, Hong Liu, and Predrag Spasojević. Low complexity turbo equalization for mobile OFDM systems with application to DVB-H. *Globe-com 2010*.
- [67] S. Ahmed, M. Sellathurai, and J. A. Chambers. Low complexity iterative method of equalization for OFDM in doubly selective channels. *Proc. Asilomar Conf. on Signals, Systems and Computers*, pages 687–691, 2005.
- [68] Luca Rugini, Paolo Banelli, and Geert Leus. Simple equalization of time-varying channels for OFDM. *IEEE Communications Letters*, 9:619–621, July 2005.
- [69] Rob Maunder. Rob maunders research pages. <http://users.ecs.soton.ac.uk/rm/resources/matlabexit/>.
- [70] Sili Lu, Balachander Narasimhan, and Naofal Al-Dhahir. A novel SFBC-OFDM scheme for doubly selective channels. *IEEE Transactions on Vehicular Technology*, 58(5):2573–2578, June 2009.
- [71] Liu Hong. *Frequency domain equalization of single carrier transmissions over doubly selective channels*. PhD thesis, The Ohio State University, 2007.
- [72] C. Heegard and S. Wicker. *Turbo Coding*. Kluwer, Boston, MA, 1999.

- [73] Carl D. Meyer. *Matrix Analysis and Applied Linear Algebra*. SIAM, 2000.
- [74] Seog Geun Kang, Yong Min Ha, and Eon Kyeong Joo. A comparative investigation on channel estimation algorithms for OFDM in mobile communications. *IEEE Transactions on Broadcasting*, 49(2):142–149, June 2003.
- [75] Ove Edfors, Magnus Sandell, Jan-Jaap van de Beek, Sarah Kate Wilson, and Per Ola Börjesson. OFDM channel estimation by singular value decomposition. *IEEE Transactions on Communications*, 46(7):931–939, July 1998.
- [76] Y. (G.) Li, L. Cimini, and N. R. Sollenberger. Robust channel estimation for OFDM systems with rapid dispersive fading channels. *IEEE Trans. Commun.*, 46(7):902–915, July 1998.
- [77] P. Hoeher, S. Kaiser, and P. Robertson. Two-dimensional pilot symbol-aided channel estimation by wiener filtering. *Proc. IEEE Int. Conf. Acoustic. Speech Signal Process.*, 3:1845–1848, April 1997.
- [78] S. Coleri, M. Ergen, A. Puri, and A. Bahai. Channel estimation techniques based on pilot arrangement in OFDM systems. *IEEE Transactions on Broadcasting*, 48(3):223 – 229, Sep 2002.
- [79] Y. Li and N. R. Sollenberger. Clustered OFDM with channel estimation for high rate wireless data. *IEEE Trans. Commun.*, 49(12):2071–2076, Dec 2001.
- [80] Y. H. Yeh and S. G. Chen. Efficient channel estimation based on discrete cosine transform. *Proc. IEEE Int. Conf. Acoustic. Speech Signal Process., Hong Kong, China* , pages=676-679, year=April 2000.
- [81] D. Schafhuber and G. Matz. MMSE and adaptive prediction of time-varying channels for OFDM systems. *IEEE Transactions on Wireless Communications*, 4(2):593 – 602, March 2005.
- [82] Z. Yuanjin. A novel channel estimation and tracking method for wireless OFDM systems based on pilots and kalman filtering. *IEEE Trans. Consumer Electronics*, 49(2):275–83, May 2003.
- [83] S. B. Bulumulla, S. A. Kassam, and S. S. Venkatesh. A systematic approach in detecting OFDM signals in a fading channel. *IEEE Trans. Commun.*, 48(5):725–728, May 2000.
- [84] E. P. Simon, L. Ros, H. Hijazi, and M. Ghogho. Joint carrier frequency offset and channel estimation for OFDM systems via the EM algorithm in the presence of very high mobility. *IEEE Transactions on Signal Processing*, 60(2):754 – 765, Feb. 2012.
- [85] N. M. Idrees, W. Haselmayr, D. Schellander, and A. Springer. Time variant channel estimation using a modified complex exponential basis expansion model in LTE-OFDM systems. *IEEE 21st International Symposium on Personal Indoor and Mobile Radio Communications (PIMRC)*, pages 603 – 607, Sept. 2010.

- [86] Jinho Kim, Chih-Wei Wang, and W. E. Stark. Frequency domain channel estimation for OFDM based on slepian basis expansion. *IEEE International Conference on Communications, 2007. ICC '07*, pages 3011 – 3015, June 2007.
- [87] Hyosung Kim and Jitendra. K. Tugnait. Turbo equalization for doubly-selective MIMO fading channels using exponential basis models. *IEEE 10th Workshop on Signal Processing Advances in Wireless Communications*, pages 21–25, 2009.
- [88] Zijian Tang, Rocco Claudio Cannizzaro, Geert Leus, and Paolo Banelli. Pilot-assisted time-varying channel estimation for OFDM systems. *IEEE Transactions on Signal Processing*, 55(5):2226–2238, May 2007.
- [89] Mehmet Kemal Ozdemir and Huseyin Arslan. Channel estimation for wireless OFDM systems. *IEEE Communications Surveys and Tutorials*, 2nd quarter 2005.
- [90] Ming Zhao, Zhenning Shi, and Mark C. Reed. Iterative turbo channel estimation for OFDM system over rapid dispersive fading channel. *IEEE International Conference on Communications*, pages 4849–4854, June 2007.
- [91] Meng-Lin Ku, Wen-Chuan Chen, and Chia-Chi Huang. EM-based iterative receivers for OFDM and BICM/OFDM systems in doubly selective channels. *IEEE Transactions on Wireless Communications*, 10(5):1405–1415, May 2011.
- [92] Rui Li, Yonghui Li, and Branka Vucetic. Iterative receiver for MIMO-OFDM systems with joint ICI cancellation and channel estimation. *Wireless Communications and Networking Conference*, March 2008.
- [93] Y. Sun, M. Yee, and M. Sandell. Iterative channel estimation with MIMO MMSE - Turbo equalization. *Vehicular Technology Conference*, 2, Fall 2003.
- [94] Nordig unified test specifications for integrated receiver decoders for use in cable, satellite, terrestrial and ip-based networks. *NorDig Unified Test specification, ver 2.2*.
- [95] Yasamin Mostofi and Donald C. Cox. ICI mitigation for pilot-aided OFDM mobile systems. *IEEE Transactions on Wireless Communications*, 4(2):765–774, March 2005.
- [96] Sili Lu, Reza Kalbasi, and Naofal Al-Dhahir. OFDM interference mitigation algorithms for doubly-selective channels. *IEEE Vech. Tech Conf*, 2006.
- [97] ITU-T. Guidelines for evaluation of radio transmission technologies for IMT-2000, ITU-T Std. M. 1225. 1997.
- [98] Vamadevan Namboodiri, Hong Liu, and Predrag Spasojević. Successive interference cancellation based turbo equalization for MIMO OFDM systems. *Proc. Conference on Information Sciences and Systems, Baltimore, MA*, March 2011.
- [99] Vamadevan Namboodiri, Hong Liu, and Predrag Spasojević. Successive interference cancellation and MAP decoding for mobile MIMO OFDM systems and their convergence behavior. *Submitted to the special issue on Broadband Mobile Communications at Very High Speeds - EURASIP Journal on Wireless Communications and Networking*, 2012.

- [100] Anastasios Stamoulis, Suhas N. Diggavi, and Naofal Al-Dhahir. Intercarrier interference in MIMO OFDM. *IEEE Transactions on Signal Processing*, 50(10):2451–2464, October 2002.
- [101] Luca Rugini and Banelli. Banded equalizers for MIMO-OFDM in fast time varying channels. *EUSIPCO 2006, Florence, Italy*, Sept 2006.
- [102] Tetsushi Abe and Tadashi Matsumoto. Space-time turbo equalization in frequency-selective MIMO channels. *IEEE Transactions on Vehicular Technology*, 52(3):469–475, May 2003.
- [103] Heunchul Lee, Byeongsi Lee, and Inkyu Lee. Iterative detection and decoding with an improved V-BLAST for MIMO-OFDM systems. *IEEE Journal on Selected Areas in Communications*, 24(3):504–513, March 2006.
- [104] R.C. de Lamare and R. Sampaio-Neto. Minimum mean-squared error iterative successive parallel arbitrated decision feedback detectors for DS-CDMA systems. *IEEE Transactions on Communications*, 56(5):778 – 789, May 2008.
- [105] Nenad Veselinovic and Tad Matsumoto. Reduced complexity MIMO turbo equalization for STTRC-Codes. *15th IEEE International Symposium on Personal, Indoor and Mobile Radio Communications*, 1:269–273, 2004.
- [106] Celal Esli, Mutu Koca, and Hakan Delic. Iterative joint tone-interference cancellation and decoding for MIMO-OFDM. *IEEE Transactions on Vehicular Technology*, 57(5):2843–2855, September 2008.
- [107] Luca Rugini, Paolo Banelli, Kun Fang, and Geert Leus. Enhanced turbo MMSE equalization for MIMO-OFDM over rapidly time-varying frequency-selective channels. *IEEE 10th Workshop on Signal Processing Advances in Wireless Communications*, pages 36–40, 2009.
- [108] S. Ahmed, T. Ratnarajah, M. Sellathurai, and Colin. F. N. Cowan. Iterative receivers for MIMO-OFDM and their convergence behavior. *IEEE Transactions on Vehicular Technology*, 58(1):461–468, January 2009.
- [109] Jun Won Choi, Andrew C Singer, Jungwoo Lee, and Nam Ik Cho. Improved linear soft-input soft-output detection via soft feedback successive interference cancellation. *IEEE Transactions on Communications*, 58(3):986–996, March 2010.
- [110] Sami Chtourou, A.O.Berthet, and Raphael Visoz. Efficient doubly-iterative frequency domain turbo-equalization for single-carrier transmission over MIMO ISI channel. *IEEE International Conference on Wireless and Mobile Computing, Networking and Communications*, pages 254–261, 2006.
- [111] Lingyang Song, Rodrigo. C. de Lamare, and Alister. G. Burr. Successive interference cancellation schemes for time-reversal space-time block codes. *IEEE Transactions on Vehicular Technology*, 57(1):642–648, January 2008.
- [112] R. Visoz, A. O. Berthet, and S. Chtourou. A new class of iterative equalizers for space-time BICM over MIMO block fading ISI AWGN channel. *IEEE Transactions on Communications*, 53:2076–2091, Dec. 2005.

- [113] Tarik Ait-Idir, Samir Saoudi, and Najib Naja. Space-time turbo equalization with successive interference cancellation for frequency-selective MIMO channels. *IEEE Transactions on Vehicular Technology*, 57(5):2766–2778, September 2008.
- [114] W. G. Song and J. T. Lim. Channel estimation and signal detection for MIMO-OFDM with time varying channels. *IEEE Commun. Lett.*, 10:540–542, Jul. 2006.
- [115] Vamadevan Namboodiri, Hong Liu, and Predrag Spasojević. Low complexity turbo equalization for mobile MIMO OFDM systems. *Proc. IEEE International Conference on Communications and Signal Processing, NIT Calicut, India*, 2011.
- [116] Michael Tüchler. *Turbo Equalization*. PhD thesis, University of Illinois at Urbana-Champaign, 2004.
- [117] H. Ma and J. Wolf. On tail biting convolutional codes. *IEEE Trans. Commun.*, 34(2):104–111, 1986.
- [118] I.F. Afikel. Implementation issues for high rate turbo codes on BPSK/QPSK channels. *GLOBECOM'99*, 1.
- [119] X. Wu and H. Xiang. Iterative carrier phase recovery methods in turbo receivers. *IEEE Commun. Lett.*, 9:735–737, Aug. 2005.
- [120] N. Noels, H. Steendam, and M. Moeneclaey. Carrier phase tracking from turbo and LDPC coded signals affected by a frequency offset. *IEEE Commun. Lett.*, 9:915–917, Oct. 2005.
- [121] L. Zhang and A. Burr. Iterative carrier phase recovery suited to turbocoded systems. *IEEE Trans. Wireless Commun.*, 3:2267–2276, Nov. 2004.
- [122] A. Burr and L. Zhang. A novel carrier phase recovery method for turbo-coded QPSK system. *Proc. EW2002, Florence, Italy*, Feb. 2002.

Curriculum Vitae

Vamadevan Namboodiri

EDUCATION

- 2012** Ph.D. (Electrical & Computer Engineering), Rutgers – The State University of New Jersey, USA
- 2006** M.S. (Electrical & Computer Engineering), University of Texas at Dallas – TX, USA
- 1992** M.E. (Systems Science and Automation), Indian Institute of Science, Bangalore, India
- 1990** B.Tech. (Electrical and Electronics), Regional Engineering College, Calicut, Kerala, India

EMPLOYMENT/CAREER

- 2011–2012** Broadcom Corporation, Bangalore, India
- 2005–2011** Broadcom Corporation, Yardley, PA, USA
- 2000–2005** STMicroelectronics, Carrollton, Dallas, TX, USA
- 1995 - 2000** STMicroelectronics, Singapore
- 1994 - 1995** NCORE Technologies, Bangalore, India
- 1992 - 1994** Indian Telephone Industries, Bangalore, India

PUBLICATIONS

- 2012** Vamadevan Namboodiri, Hong Liu and Predrag Spasojević, “Low Complexity Iterative Receiver Design for Mobile OFDM Systems,” *accepted for publication in EURASIP Journal on Advances in Signal Processing*.
- 2012** Vamadevan Namboodiri, Hong Liu and Predrag Spasojević, “Successive Interference Cancellation and MAP decoding for Mobile MIMO OFDM systems and their convergence behavior,” *Submitted to the special issue on Broadband Mobile Communications at Very High Speeds - EURASIP Journal on Wireless Communications and Networking*.

- 2011** Vamadevan Namboodiri, Hong Liu and Predrag Spasojević, “Successive Interference Cancellation Based Turbo Equalization for MIMO OFDM Systems,” in *Proc. Conference on Information Sciences and Systems March 2011*, Baltimore, MA.
- 2010** Vamadevan Namboodiri, Hong Liu and Predrag Spasojević, “Low Complexity Turbo Equalization for Mobile OFDM Systems with Application to DVB-H,” in *Globecom 2010*, Miami FL, USA.
- 2009** Vamadevan Namboodiri, Hong Liu and Predrag Spasojević, “Low Complexity Turbo Equalization for Mobile MIMO OFDM Systems,” in *Proc. IEEE International Conference on Communications and Signal Processing 2011*, NIT Calicut, India.

PATENTS

- 2012** Casas, Raul A; Hryszko, Mark; Namboodiri, Devan (Vamadevan); Wongwirawat, Wongwirawat Supat, “METHOD AND APPARATUS FOR DETECTING AND CORRECTING MODULATED SIGNAL IMPAIRMENTS,” *Patent Pending: Under Final Process. Filed in 2007.*
- 2011** Liu, Vince (Wensheng), Namboodiri, Devan (Vamadevan), “METHOD AND APPARATUS FOR DETECTING AND CORRECTING MODULATED SIGNAL IMPAIRMENTS,” *US patent 8,014,478.*